ULTIMATE LOAD BEHAVIOUR OF INTERNALLY PRESSURIZED 'CUT-AND-COVER' ORTHOTROPIC REACTOR CONTAINMENT

MOHAMED FOUAD ABDEL MENEIM AHMAD


CENTRE FOR NFLD. STUDIES
OCT 6 1981
MEMORIAL UNIVERSITY
OF NEWFOUNDLAND

NOTICE

The quality of this microfiche is heavily dependent upon the quality of the original thesis submitted for microfilming. Every effort has been made to ensure the highest quality of reproduction possible.

If pages are missing, contact the university which granted the degree.

Some pages may have indistinct print especially if the original pages were typed with a poor typewriter ribbon or if the university sent us a poor photocopy.

Previously copyrighted materials (journal articles, published tests, etc.) are not filmed.

Reproduction in full or in part of this film is governed by the Canadian Copyright Act, R.S.C. 1970, c. C-30. Please read the authorization forms which accompany this thesis.

THIS DISSERTATION HAS BEEN MICROFILMED EXACTLY AS RECEIVED

AVIS

La qualité de cette microfiche dépend grandement de la qualité de la thèse soumise au microfilmage. Nous avons tout fait pour assurer une qualité supérieure de reproduction.

S'il manque des pages, veuillez communiquer avec l'université qui a conféré le grade.

La qualité d'impression de certaines pages peut laisser à désirer, surtout si les pages originales ont été dactylographiées à l'aide d'un ruban usé ou si l'université nous a fait parvenir une photocopie de mauvaise qualité.

Les documents qui font déjà l'objet d'un droit d'auteur (articles de revue, examens publiés, etc.) ne sont pas microfilmés.

La reproduction, même partielle, de ce microfilm est soumise à la Loi canadienne sur le droit d'auteur, SRC 1970, c. C-30. Veuillez prendre connaissance des formules d'autorisation qui accompagnent cette thèse.

LA THÈSE A ÉTÉ MICROFILMÉE TELLE QUE NOUS L'AVONS REÇUE

ULTIMATE LOAD BEHAVIOUR OF INTERNALLY PRESSURIZED 'CUT-AND-COVER' ORTHOTROPIC REACTOR CONTAINMENT

by

© Mohamed Fouad Abdel Meneim Ahmad, B.Sc.

A Thesis submitted in partial fulfillment
of the requirements for the degree of
Master of Engineering

Faculty of Engineering and Applied Science
Memorial University of Newfoundland

December 1979

St. John's Newfoundland, Canada

To My Family

ABSTRACT

Nonlinear static and dynamic analyses are presented for 'cut-and-cover' type underground reinforced concrete nuclear reactor containments subjected to internal pressurization. A nonlinear anisotropic model has been adapted and incorporated into a general linear and nonlinear, static and dynamic finite element analysis programme, NONSAP, to account for the orthotropic behaviour of reinforced concrete. The load increment required in elastoplastic static analysis, and the time interval, as well as the boundary simulation of infinite or semi-infinite continuum in dynamic analysis, are adequately taken into account in this study. Numerical investigations of the stability of equilibrium iteration procedure to reduce the divergence of the incremental solution from the true solution, are also presented.

Parametric studies for the static response of the containment are carried out for: 1) stiffness of backfill (original and stabilized sandy loam fill with different cement ratios, 2%, 6%, and 10%); 2) thickness of backfill (2.5, 7.5, 12.5, and 18.5m); 3) percentage of reinforcing steel (#18 bars @ .25m, #18 bars @ .35m, #14 bars @ .35m, and plain concrete); 4) thickness of containment (1.25, 1.5, 2, and 2.5m) and; 5) different types of surrounding medium (sandy loam, clay, sand stone, and silty clay). The response values determined are: i) maximum positive vertical displacement, ii) maximum negative vertical displacement, iii) vertical and horizontal displacement, iv) stress-displacement relation at the point of maximum stress concentration. The results confirm the effect of the different

parameters on the response of the containment. The stiffness of backfill and the containment thickness have the greatest effect. The reinforcement effect is amplified when plastic flow commences.

Dynamic analysis is carried out to study the response of a containment to a typical pressure-time function following a Loss-of-Coolant-Accident (LOCA). A distrubance in displacements and stresses is observed immediately after pressure decreases for two seconds after which the response becomes steadystate.

ACKNOWLEDGEMENTS

The author wishes to gratefully acknowledge the guidance and encouragement offered by his supervisor, Professor D.V. Reddy, without whose continued personal interest and critical evaluation this thesis could not have been successfully completed.

Deepest gratitude is extended to Dean F. Aldrich, Dean of the Graduate Studies, who will always be remembered for his constant encouragement and advice.

Appreciation is also expressed to Dr. W. Bobby for his valuable ideas and references and many fruitful discussions. The author is grateful to Professor H.N. Ahuja for his help during the absence of Professor Reddy.

The author would like to thank Memorial University of Newfoundland for the award of a Graduate Fellowship. Thanks are due to Dean R.T. Dempster, Dean of Engineering, and Dr. T.R. Chari, Chairman of the Graduate Committee, for their encouragement and support. Sincere thanks are also extended to N.L.C.S. (Newfoundland and Labrador Computer Services) staff, especially Mr. G. Somerton and Mr. G. Bennet.

Appreciation and gratitude are extended to the author's parents, Mr. and Mrs. Abdel Meneim, for their encouragement, inspiration and guidance. The author is most fortunate in having a very understanding wife who has contributed in many ways to the successful completion of this thesis.

Special thanks go to Mrs. Gwendolyn Kerri for her dedicated work in typing the final manuscript.

Thanks are due to the author's fellow graduate students, for many simulating discussions, helpful suggestions and constructive criticism.

The work was supported in part by the National Research Council of Canada under Grant No. A8119.

TABLE OF CONTENTS

LIST OF TABLES

LIST OF FIGURES

NOTATION

a, b, c	Material axes of anisotropy
A_i^c	Effective concrete ratio in direction i
A_i^s	Effective steel ratio in direction i
{b}	Body force vector
[B]	Transformation relating strains and displacements
c	Damping coefficient
C	Cohesion
C_a	Unconfined compressive strength referred to axis a
[C]	Viscous damping matrix
$[C^E]$, [C]	Constitutive (stress-strain) matrix
$[C^{EP}]$	Elastic plastic material matrix
[D]	Constitutive (strain-stress) matrix
E	Young's modulus of elasticity
f_{cu}	Uniaxial compressive strength
f( )	Yield function
{F}	Vector of nodal actions (forces) for assemblage
$\{F_t^r\}$	Residual nodal forces at the end of time t
g( )	Plastic potential function
G	Shear modulus
I_1	First stress invariant
J_2	Second deviatoric stress invariant
[J]	Jacobian matrix
K	Hardening parameter
[K]	Stiffness matrix
$[K_o]$	Initial elastic stiffness matrix

$[M]$	Mass matrix
N	Displacement shape function
$\{N\}$	Coefficient vector for interpolation displacement model
p	Superscript indicating plastic
$\{P_i\}$	Nodal force vector
$[Q]$	Transformation matrix from global to local system
r, s	Curivlinear coordinates for quadrilateral elements
R, S, T	Unconfined torsional strength referred to axes a, b, c.
S	Surface area
t	Time
T	Natural period, superscript indicating transpose
T_a	Unconfined tensile strength referred to axis a
u, v, w	Displacements in Cartesian coordinates
$\{U\}$	Displacement vector
$\{\dot{U}\}$	Velocity vector
$\{\ddot{U}\}$	Acceleration vector
V	Volume
x, y, z	Cartesian coordinates
α	Variable, mass proportional damping coefficient
β	Parameter, stiffness proportional damping coefficient
γ	Shear strain
δ	Variational operator
Δt	Time increment
ε	Normal strain
ε_o, σ_o	Initial strain or stress
$\varepsilon_x, \gamma_{xy}, \sigma_x, \tau_{xy}$	x-components of direct and shear strain or stress

$\{\varepsilon\}$	Vector of strains
ν	Poisson's ratio
ζ	Damping ratio
ρ	Mass density
σ	Normal stress
σ_y	Yield stress in simple tension
σ_1	Major principal stress
σ_2	Intermediate principal stress
σ_3	Minor principal stress
$\{\sigma\}$	Stress vector
$\{\sigma_t\}$	Stresses at time t
τ	Shear stress
ϕ	Angle of friction
ω	Natural frequency

CHAPTER I

INTRODUCTION

1.1 General

More money is being spent on research into nuclear power than on any of the other alternatives to fossil fuel, as it appears technologically the most feasible of them. Its importance is, therefore, beyond question.

One of the drawbacks to nuclear power generation is the potential direness of the consequences of the escape of radioactive material. Public awareness of this has meant that not only must such installations be safe, but they must also be seen to be safe. The location of a nuclear plant can both contribute to the safety of the operation and determine to what extent such a plant may be considered safe by outsiders. Safety can be defined in several ways:

a) the risk of damage to the integrity of the system from any cause;

b) the risk of harm to operating personnel from normal or abnormal functioning of the plant; and

c) the risk or hazard from any cause, mechanical, biological or radioactive, to the surrounding population.

The first two safety criteria are usually met by suitable plant design and layout, and are affected by the selected site only in as far as unfavorable geological or meteorlogical phenomena, such as earthquakes, subsiding ground, flooding or high winds might interfere with the proper functioning of the facility. It is the third

criterion that is uppermost in the minds of most 'environmentalists' and the general public when they raise objections to the location of a nuclear plant in a given locality. Most objectors bear in mind that there is no such thing as a 'foolproof' system and any system can only be designed to reduce the consequences of human error and instrument failure to a certain extent.

To alleviate or remove the increased environmental objections to the surface plants, technical and economical feasibility studies have been carried out to decide if there are other solutions to siting of nuclear plants. Two of these prominently discussed at present are the underground and the offshore plants. It is postulated that the advantages of underground siting in some situations may more than compensate for added costs so that such facilities could be preferred even where surface sites are available. The feasibility of constructing large underground power plants is indicated by the partial burial of certain small European plants and the large underground excavations for hydroelectric facilities.

From a structural point of view, a nuclear power plant has a two-stage barrier against the escape of contained material. The reactor vessel itself is designed to withstand temperatures and stresses of normal operation with a generous margin of safety. Surrounding it, and at the same time containing the steam generation equipment, is a huge leak-tight barrier, referred to as a containment vessel. The following definition of containment is provided in the report of the ACI Committee 349 'Criteria for Reinforced Concrete Nuclear Power Containment Structures':

> ".... nuclear containment is defined as the functional capability of a system to control and limit the spread of radioisotopes in the event that these radioisotopes are released from the primary nuclear system".

To satisfy this function, the containment structure needs the capability of assured leakage control under accident conditions, adequate strength to withstand the adversities of nature in combination with possible nuclear accidents, and the assurance of protection of these properties against deterioration over the lifetime of the nuclear plant. The ability to verify the capability of the containment with respect to these properties is the central consideration in the public acceptance of nuclear installations. Consequently, most of the engineering treatment of containment is focused on providing these properties. Substantial improvement in containment is a reasonable expectation by underground siting.

The use of concrete structures, both conventionally reinforced and prestressed, for containment has become the prevalent structural approach for large nuclear power applications. However, the high degree of safety required for a nuclear containment is the cause of main problems and difficulties. Despite all the problems and difficulties, the technology of concrete containments has been developing very rapidly. This is largely due to the continuous growth - in both size and number - of nuclear power plants and the large amount of research effort.

Significant progress has recently been made in analytical methods for reinforced concrete structures. The finite element method has provided the basis for most of the new methods. The

analysis of structures - especially the underground structures - by formal analytical techniques have been restricted to linearly elastic bodies of idealized geometry and subjected to restricted forms of loading. Therefore, for the analysis of practical structures including realistic material properties and loading, approximate numerical methods must be employed. Both soil and concrete exhibit a complex structural response mainly due to the nonlinear stress-strain behaviour. So, a nonlinear analysis seems to be a logical need for an important structure like underground containment.

1.2 Statement of the Problem

In this thesis, a constitutive model for reinforced concrete has been adapted for use with a general purpose computer code. This nonlinear model takes into account anisotropy (different effective moduli in different directions) due to the reinforcement. The NONSAP nonlinear structural analysis programme was selected for the ease with which it can be modified to accept nonlinear material models not currently included in the material model library.

The programme is used to study the nonlinear structure medium interaction for the static and dynamic response of a 'cut-and-cover' type nuclear reactor containment to internal pressurization following an accident. Effect of reinforcement and thickness of the containment, filling material stiffness and thickness, and medium properties are studied.

1.3 Layout

Chapter II reviews the literature on underground containments

with emphasis on the 'cut-and-cover' concept, nonlinear analysis using the finite element method, and different reinforced concrete models suggested for finite element analysis.

Chapter III presents the nonlinear orthotropic yield condition, flow rules, and their incorporation into the NONSAP code.

Chapter IV describes the analysis procedure. Determination of the values of all parameters needed for analysis and details of the finite element model are discussed in detail.

Chapter V presents parametric studies and the results obtained for different cases of containment thickness, filling material stiffness, filling material thickness and different kinds of medium.

Chapter VI compares the results obtained in Chapters IV and V. The conclusions from this investigation and recommendations for further research are outlined at the end of the chapter.

Appendix A gives the listing of the subroutines incorporated into the NONSAP code.

CHAPTER II

REVIEW OF LITERATURE

2.1 General

The underground nuclear containment concept will be reviewed with emphasis on the 'cut-and-cover' type and nonlinear structural analysis using the finite element method. The different finite element models for reinforced concrete will be discussed in detail.

2.2 Underground Nuclear Reactor Containments With Emphasis on the 'Cut-and-Cover' Type.

The placement of a nuclear plant underground has been suggested as an alternative to present siting practice. Europe has pioneered the construction of underground nuclear plants (Norway, Sweden, France, and Switzerland). Watson, Kammer, Langley, Selzer, and Beck [99], and Kröger, Altes, and Schwarzer [51] presented a summary of the significant features of these plants.

In general, two types of underground plants are considered feasible:

a) "Subterranean cavities" and

b) "Cut-and-Cover" [3].

The former refers to the excavation of a cavity in good to excellent quality of rock with lined or unlined galleries. The latter refers to the excavation of the site, construction of the plant, and the subsequent backfilling to ground-level. In both concepts, the part of the plant that is underground (the turbine building for example, could be built at ground)can be laid out to occupy a single cavity

or a single all-inclusive structure, or can be made up of separate structures or cavities interconnected with access tunnels and shafts. Fig. 2.1 shows a possible layout of an underground nuclear power plant.

Feasibility studies carried out by different investigators have shown the potential capabilities for the underground siting of nuclear power plants. United Engineers Inc. [95] have summarized the feasibility studies carried out by different investigators. The advantages of underground containments were discussed by Reddy and Kierans [75], Kröger et al [61], and Lindbo [55]. It is a basic disadvantage that no uniform concept for large power reactors has yet been developed past the study stage to the ready-for-construction phase, and that the state of the art is not yet at the same level as that to be found in above-ground siting [51]. However, this gap can be closed quickly by using techniques and experience acquired in other fields.

The containment represents the most effective barrier to the atmospheric diffusion of fission products after hypothetical incidents involving the release of considerable quantities of fission products. For above-ground containments, Tan [94] reported that for the existing and proposed Boiling Water Reactor (BWR) and Pressurized Water Reactor (PWR) above-ground plants, there were about equal numbers of Reinforced Concrete Containment Vessels (RCCV's) and Prestressed Concrete Containment Vessels (PCCV's) with no overwhelming advantages for either system. RCCV's tend to use thicker walls, but the circumferential prestressing in PCCV's is awkward and time-consuming. Stevenson [91] presented a historical summary of the engi-

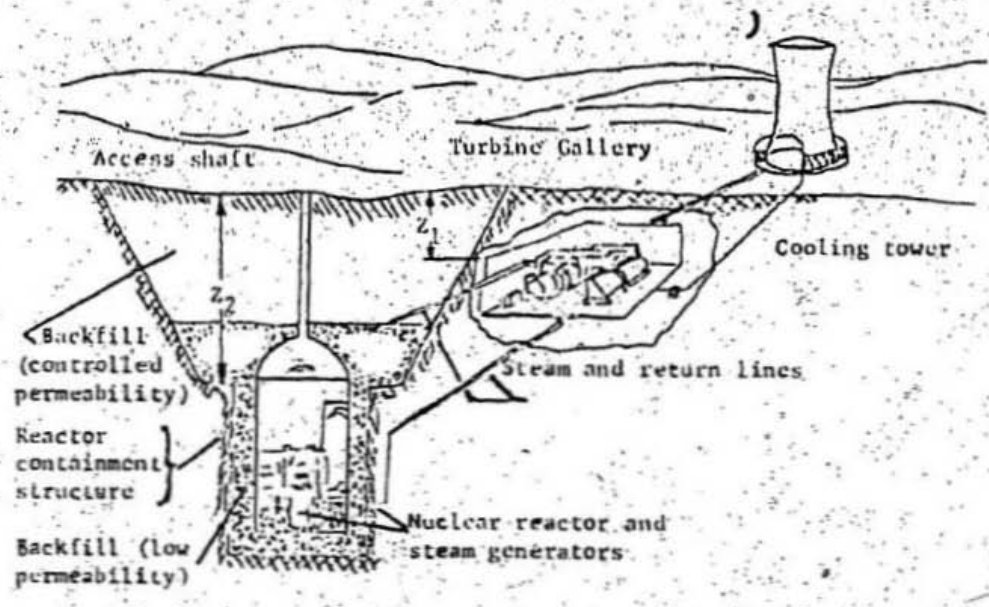

Fig. 2,1 Possible Layout of an Underground Nuclear Power Plant (Reproduced from Ref. 34)

neering practice and their evolution applied to the design of concrete containment structures in the U.S.A.. A discussion of safety considerations, current practices and reinforcement techniques were reported by Bender and Whitman [19]. A typical containment can be seen in Fig. 2.2, and details of reinforcement of a typical nuclear containment are given in Fig. 2.3.

Dynamic finite element analysis of underground containments subjected to blast excitation was reported by Moselhi [67], Sheha [85], and Reddy, Moselhi and Sheha [77], while dynamic analysis of 'cut-and-cover' type subjected to earthquake excitation was carried out by El-Tahan [35], and El-Tahan and Reddy [36]. The state-of-the-art of earthquake engineering for nuclear power facilities was given by Hadjian [40]. He also reviewed several alternatives to above-ground facilities which included the 'cut-and-cover' type.

Kröger et al [51] pointed out that the 'cut-and-cover' technique is the only configuration which can contribute toward a solution of the siting problems under the natural environmental conditions prevailing in Germany. The assessment of technical feasibility, costs, and the potential protection from extreme accident of large (1300 MWe) 'cut-and-cover' type nuclear plant was reported by Kröger, Altes, and Escherich [50].

Reddy, Bobby, and Mahrenholtz [76] carried out nonlinear static and dynamic analyses of a 'cut-and-cover' type nuclear reactor containment with reinforced earth backfill subjected to internal pressurization. Mahrenholtz, Reddy, and Bobby [59] studied the

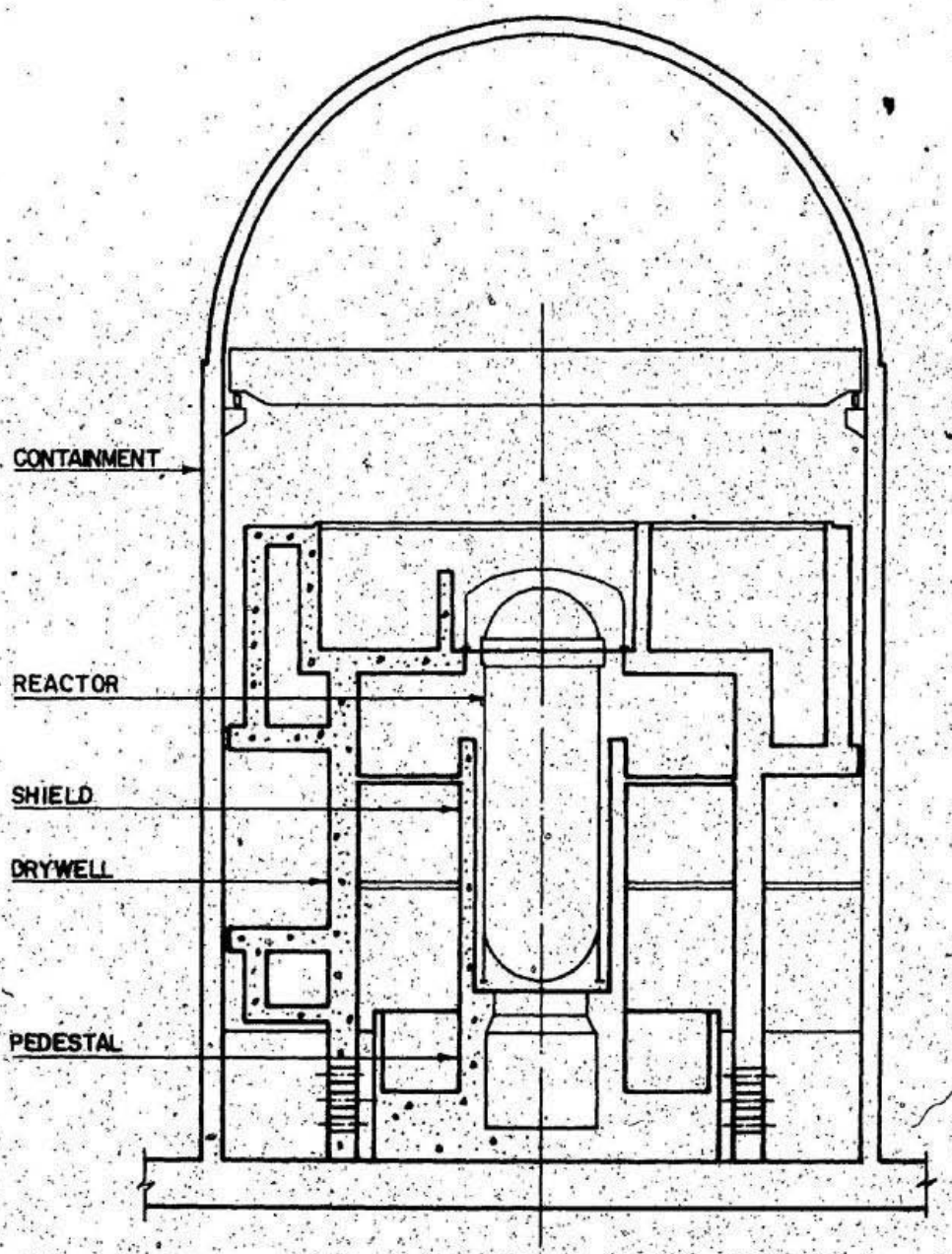

Fig. 2.2 Mark III Containment
(Reproduced from Ref. 3)

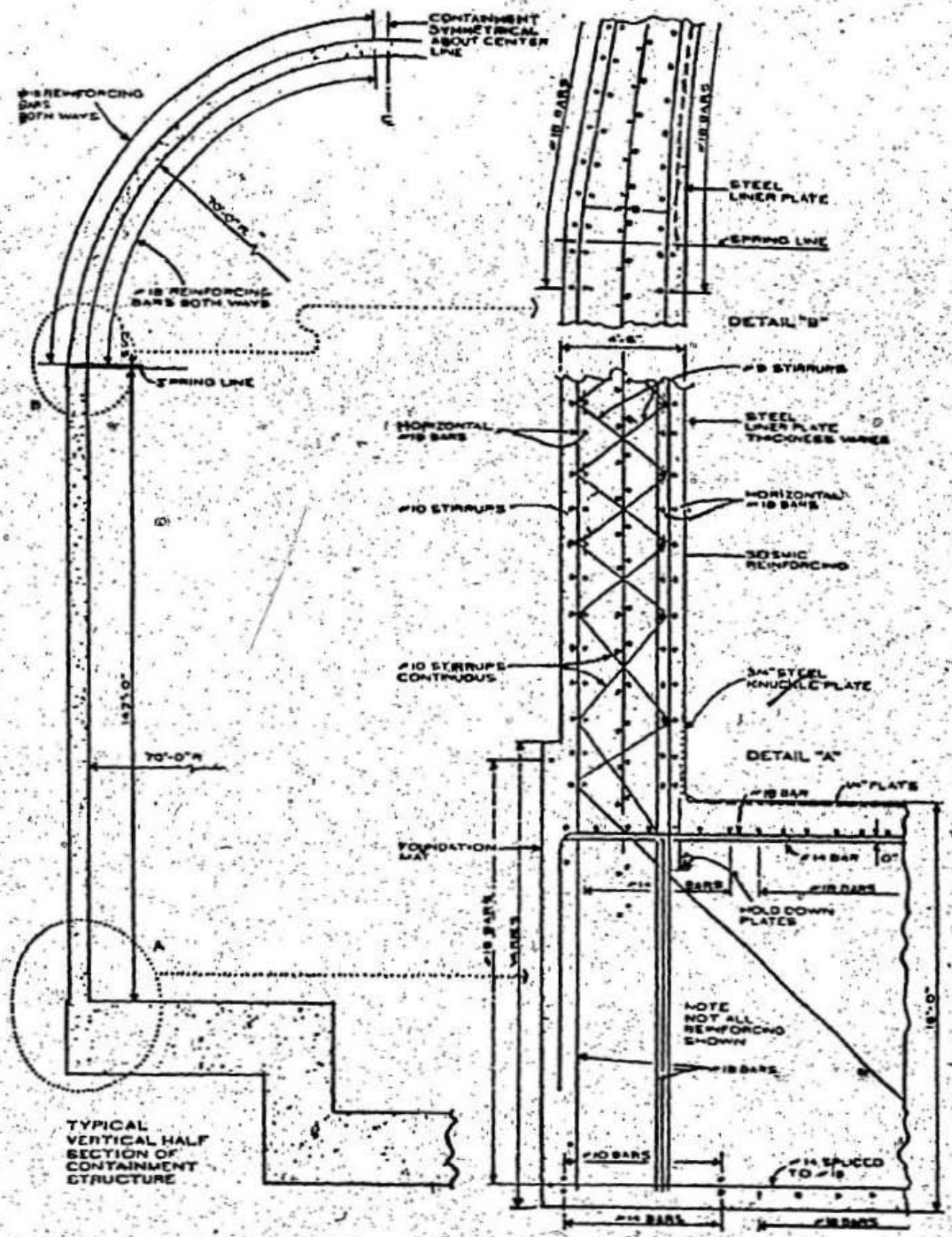

Fig. 2.3 Salem (N.J.) Plant (Reproduced from Ref. 90)

ultimate load behaviour of an underground 'cut-and-cover' type prestressed concrete nuclear containment buried in clay medium. The loading conditions which were considered are:

a) sustained prestress only and

b) sustained prestress and static/dynamic internal pressure.

2.3 Finite Element Analysis of Nonlinear Structures

No structure ever built behaves linearly. All deformations need not be small, nor need they be reversible. Few materials are truly elastic and even fewer behave linearly. The descriptions of nonlinear phenomena lead to nonlinear equations which immediately render classical methods of mathematical analysis inapplicable. The complexities of nonlinear analysis have created a "nonlinear barrier" which, only in very recent times, has begun to be penetrated through the efficient use of modern high-speed computers. The unparalleled success of the now well-known finite element method in connection with complex linear problems was also one of the main factors in breaking that nonlinear barrier. Now, many applications of the finite element method to nonlinear problems can be found in the books of Zienkiewicz [104], Desai and Abel [33], and Oden [72].

Nonlinear behaviour in structural systems can be classified as follows:

1) geometric nonlinearity, arising from nonlinear terms in the kinematical equations,

2) material nonlinearity, due to nonlinearities in the constitutive equations, and

3) combined geometric and material nonlinearities.

Computationally, these categories are somewhat superficial since the mathematical techniques that can be used successfully to treat one type of nonlinearity are, with modifications, generally applicable to other types of nonlinearity.

Hundreds of papers have appeared dealing with nonlinear static and dynamic analyses with material and geometric nonlinearities. A review of such papers is beyond the scope of this study. The review here will be confined to work applicable to the present study. A review of finite element applications to materially nonlinear problems and to problems involving combined geometric and material nonlinearities was reported by Oden [71]. He also presented an incremental stiffness relation for geometrically nonlinear elastoplastic structures.

In 1963, a finite element analysis of a class of two-dimensional nonlinear problems was treated in the dissertation of Wilson [101]. His analysis dealt with materially nonlinear structures. Subsequent applications and investigations have used more sophisticated formulations of the nonlinear problems. Two-dimensional problems were considered by Felippa [38], and Reyes and Deere [78]. A comparative study of various numerical schemes for handling elastoplastic problems was given by Marcal [60].

Zienkiewicz, Valliappan, and King [105], and Ref. 60 pointed out that two main approaches have been used successfully in analysing elastoplastic problems. One of these, the so-called "initial strain" approach, involves computing an increase in plastic strain during a

load increment, and then treating the plastic strain as an initial strain for which the stress distribution is adjusted. This approach fails in the case of ideal perfectly plastic materials. The second approach is basically a "tangent stiffness" approach in the sense that incremental stiffness relations are derived from incremental stress-strain laws for the material. These stiffness matrices are modified after each load increment in the case of elastoplastic, work hardening materials. This approach has been used most frequently in finite element applications (e.g., [31] and [78]). Zienkiewicz et al [105] used a third method for elastoplastic problems, termed an "initial stress" approach, wherein total incremental stress-strain relations are used to correct the total value of stress at the end of each load increment.

Farhoomand [37] presented an incremental expression of virtual work for the nonlinear dynamic analysis of structures. The finite element method was employed to reduce the integrals of the expression of virtual work to a system of nonlinear second order time-dependent differential equations. He also introduced a special incremental constitutive relation for soil materials which was used in the expression of virtual work. Marr and Christian [61] investigated the behaviour of finite element models employing different constitutive relations to describe the stress-strain behaviour of soils. Suitable methods of treating tension stresses and stresses which exceed the yield criteria were also discussed.

The theoretical and computational procedures which have been applied in the design of the general purpose computer codes, NONSAP

[13], ADINA [8], and ANSR-I [66], were presented by Bathe, Özdemir, and Wilson [10], Bathe, Bolourchi, Ramaswamy, and Snyder [9], and Mondkar and Powell [65] respectively. A survey of the integration methods and programmes used in reactor safety analysis was reported by Belytschko [18].

2.4 Finite Element Models for Reinforced Concrete

2.4.1 Introduction

An accurate analytical determination of the displacements and the internal stresses and deformations in a reinforced concrete structure throughout its load history is complicated by a number of factors:

1) The structural system is composed of two materials, concrete and steel.

2) The structural system has a continuously changing topology due to the cracking of the concrete under increasing load.

3) The stress-strain relationship for concrete is nonlinear and is a function of many variables.

4) Concrete deformations are influenced by creep and shrinkage and are time-dependent on load and environmental history.

5) Effects of dowel action in the steel reinforcement, bond between the steel reinforcement and the concrete, bond slip, and aggregate interlock at cracks are difficult to incorporate into a general analytical model.

However, significant progress has recently been made in developing analytical methods to examine reinforced concrete structures. The finite element method has provided the basis for most of the new

analytical methods. A comprehensive survey of the literature on application of the finite element method to the analysis of reinforced concrete structures was made by Scordelis [83] and Wegner [100].

Recently Bergan and Holand [20] presented an outline of a large number of proposed mathematical models for the material behaviour of concrete and reinforcement and for the interactive behaviour between them. They also classified the important mechanisms of reinforcement-concrete interaction. This classification is shown in Fig. 2.4.

2.4.2 Different Finite Element Models for Reinforced Concrete

One of the first applications of the finite element method to concrete was reported by Clough [28], and Sims, Rhodes, and Clough [86] who studied the behaviour of a gravity dam in which deep cracking had been observed. The crack was simulated in the finite element system by separation of the elements along the crack line; independent nodal points were assumed for the elements on each side of the crack. The concrete was supposed to behave elastically under all applied loads.

Three different models describing reinforced concrete, reported in Ref. 100, are shown in Fig. 2.5. The first one takes into account the components, concrete and steel-reinforcement, separately with different elements. Bond between both materials may be regarded as rigid, Fig. 2.5a, or may be represented by links, Figs. 2.5b and 2.5c respectively, by special bond elements, Fig. 2.5d.

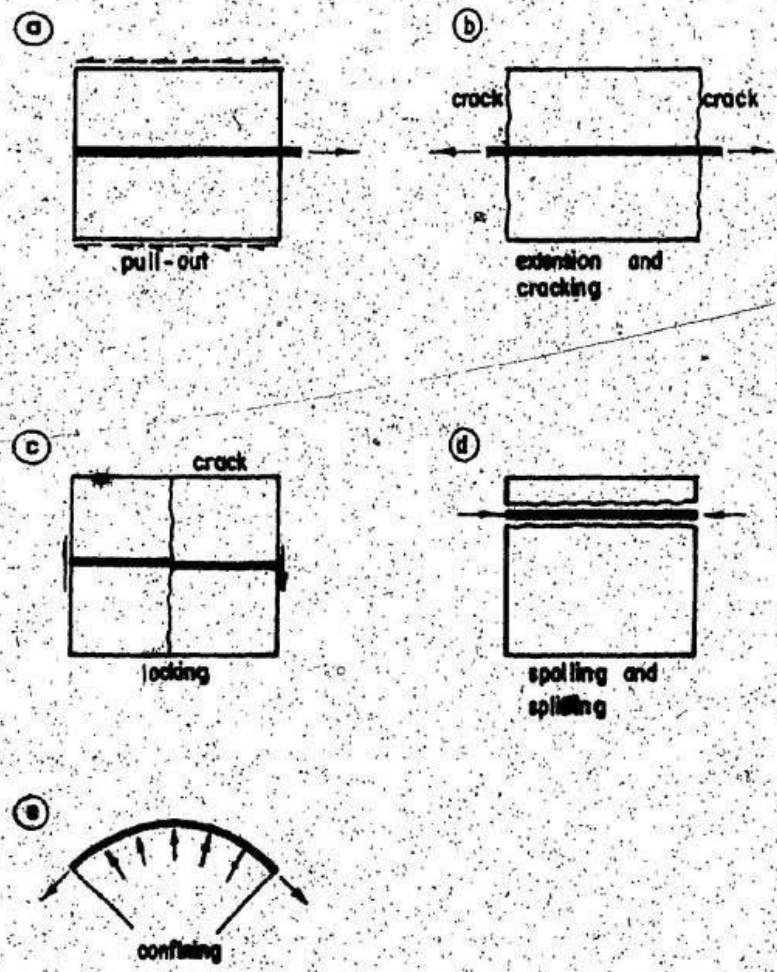

Fig. 2.4 Interactive Effects Between Concrete and Reinforcement (Reproduced from Ref. 20)

A. concrete and steel, different elements

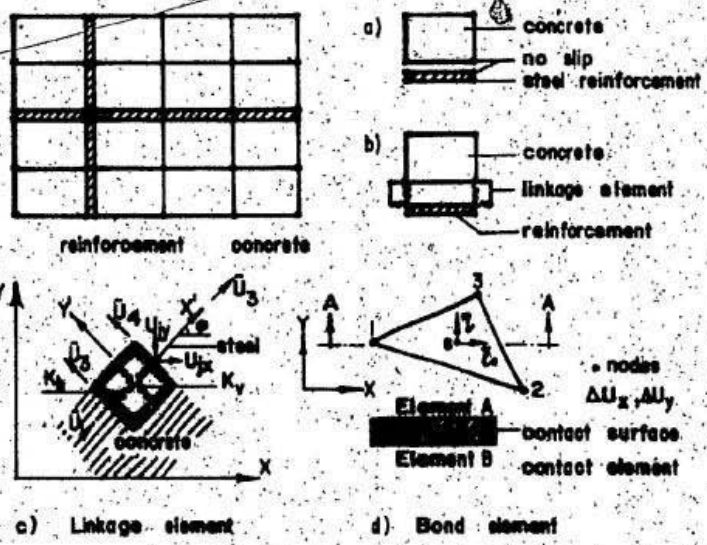

B. concrete and steel, one element

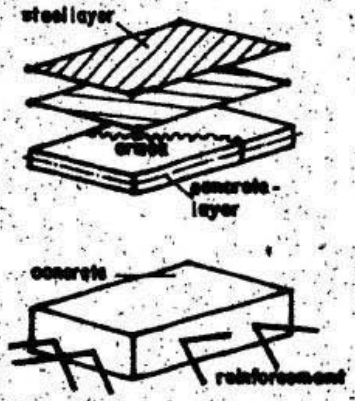

Fig. 2.5 Reinforced Concrete Represented by Finite Elements (Reproduced from Ref. 100)

The second model uses a single element for reinforced concrete. The constitutive relationship is found by adding up the stiffnesses of the concrete and reinforcement, Fig. 2.5e. The third possibility considers reinforced concrete as a homogenous material, wherein all components are included, Fig. 2.5f.

Ngo and Scordelis [68] were the first to introduce special elements modeling the interaction between the steel and concrete. In their study, a special linkage element was developed to represent bond-slip phenomena. This element, illustrated in Fig. 2.5c, links continuum elements representing steel reinforcing to those representing concrete at discrete points. With the aid of the linkage element, it was possible to construct an analytical model for the study of reinforced concrete beams. A number of beams with various predefined crack patterns were analyzed to evaluate concrete and steel stresses, bond stresses as well as deflections. The influence of decreasing stiffness due to various crack lengths was studied. Both steel and concrete were assumed to behave linearly.

Nilson [70] refined the work of Ref. 68 by introducing nonlinear material properties and a nonlinear bond-slip relationship into the model. He accounted for these nonlinearities by applying the load in small increments. Improved quadrilateral plane stress finite elements were used. Cracking was accounted for by stopping the solution when an element indicated a tensile failure. The new cracked structure was redefined, the revised information was then input into the computer, and the structure was reloaded incrementally. Nilson found bond stress patterns that are similar to those reported

in Ref. 68.

Ngo, Scordelis, and Franklin [69] formulated a more refined model of a reinforced concrete beam in which they introduced aggregate interlock linkages along diagonal tension cracks of various lengths; the linear behaviour of materials was retained. The influence of stirrups, and horizontal splitting along reinforcement near the support were considered. One-dimensional bar elements were used for the vertical stirrups.

Franklin [39] performed a nonlinear analysis in which cracking within the finite elements and redistribution of stresses was automatically accounted for, so that the response from initial loading to failure was obtained in one continuous computer analysis. Incremental loading with iterations within each increment, were used to account for cracking and nonlinear material properties. Unlike the preceeding studies, the crack is not predefined, and progressive cracking is assumed to occur over an entire element normal to a principal stress direction rather than along a single line. This permits the use of the same structural nodal point topology throughout the solution, eliminating the need for splitting the nodes after cracking and establishing a new topology, as required by Ref. 70 nonlinear approach.

Spokowski [89], Houde [45], and Mirza and Mufti [64] studied plane stress problems using a modeling system similar to that of Ref. 70. Experimental as well as finite element investigations were carried out in Ref. 89 on a beam-column joint, while an

empirical bond stress-slip formula was derived in Ref. 45 from tests on axially reinforced specimens which was incorporated into the finite element model.

Valliappan and Doolan [97] made two-dimensional stress studies that included the effects of tensile cracking and elastic-plastic behaviour in compression using an initial stress approach. The post-cracking stiffness of cracked finite elements was set equal to zero. The bond between concrete and steel elements was assumed to be rigid.

Yuzugullu and Schnobrich [103] studied the inelastic behaviour of shear wall-frame systems. They assumed that cracked concrete does not carry any tensile forces perpendicular to the cracks, but maintains some amount of shear stiffness because of the irregular surface of cracks. Uniaxial, perfectly plastic, behaviour was assumed for both the cracked concrete and reinforcing steel. A linkage element similar to that reported in Ref. 68 was used.

Suidan and Schnobrich [93] studied the behaviour of cracked beams applying a model similar to that shown in Fig. 2.5e. Perfect bond between the reinforcement and concrete was assumed and the stress-strain matrix of concrete was modified to allow for the presence of orthotropic reinforcement. Isoparametrit elements were used and the stress and strain vectors evaluated at the integration points of the elements in order to check cracking, yielding, and crushing of reinforced concrete at these points.

Schnobrich [82] also gave some numerical examples of analysing test structures, a two-way slab, conduit, a HP shell, and shear

panels using the finite element method. In these examples, the steel was idealized by nodally connected isolated elements for three-dimensional cases and as an orthotropic sheet for plane stress cases.

Isenberg and Adham [47] proposed a mathematical model for the constitutive relation for reinforced concrete as a composite material under combined stress, which may be used in finite element analysis. Until cracking occurs the properties of the model depend entirely on the concrete. After cracking a composite modulus is used which reflects the combined stiffness of steel and concrete and takes into account the extent to which the bond between the steel and concrete is broken. Some improvements - based on pertinent studies - were incorporated into this model by Adham, Bhaumic, and Isenberg [1]. This model was incorporated into the NONSAP code by Smith, Cook, and Anderson [87] and used to analyse a prestressed concrete pressure vessel.

Hossain [44] developed an incremental iterative method for determining the nonlinear response of reinforced concrete beams and frames subjected to cyclic loading. In this study, methods have been developed to model the nonlinear cyclic stress-strain properties of steel and concrete as well as the nonlinear cyclic bond-stress-slip relationship between them. Geometric nonlinearity due to the formation and propagation of cracks and the stress released by them were also considered.

The bond between concrete and steel may be taken - as shown in

Fig. 2.5 - as rigid or represented by link elements. In the latter case springs are often used. According to Ref. 100 this method is rather crude since it leads to incompatabilities between the nodal points. An alternative to springs has been introduced by Schäfer [81]. He proposed a special bond element, Fig. 2.5d, assuming that a relation between the shear stress and the frictional deformation is known, and using the principle of virtual work. Herrmann [42] modelled the interaction of contacting bodies by using refined bond springs. This model is capable of accounting for both slippage and separation of the mating surfaces. The capabilities of this model for representing reinforced concrete bond and soil structure interaction were illustrated by numerical examples.

Sarne [80] performed a time dependent, material nonlinear, three-dimensional finite element analysis of some reinforced and prestressed concrete structures. Concrete was modelled by twenty-node solid isoparametric elements, while the reinforcement layers were idealized as thin eight-node membrane shell elements. Similar idealization has been reported by Buyukozturk and Connor [24]; a nonlinear dynamic analysis, with impact considerations, of reinforced concrete was presented.

Buyukozturk [23] idealized the reinforcement using two geometrically identical finite elements at each physical location of the structure. The first, concrete element, is a "full" element. The second, rebar element, is basically an empty block element containing reinforcing bars running in prescribed directions simulating the actual reinforcement configuration. The strain compatability between

steel and concrete is maintained by using the same shape functions for both elements.

Axisymmetric idealization of reinforced and prestressed concrete structures has been reported by Argyris, Faust, Szimmat, Warnke, and William [4], and Bathe and Ramaswamy [11]. Membrane and cable elements were used in Ref. 4 in modelling reinforcement and prestressing cables respectively. Ring and truss elements were used in Ref. 11 in representing the prestressing cables.

2.4.3 Constitutive Relations for Concrete

Success in developing the finite element method for application to reinforced concrete structures is closely linked to the development of quantitative information on the load-deformation behaviour of concrete. Formulation of such information in a suitable form for use in the analytical technique is essential. Despite intensive and continued research, according to Refs. 11, 23, 24, and 82, no universally accepted constitutive law exists which fully describes the concrete behaviour in combined stress conditions.

Bresler and Pister [22] and McHenry and Karni [62] studied the strength only in biaxial compression-tension conditions. Kupfer, Hilsdorf, and Rusch [53], Robinson [79], Liu, Nilson, and Slate [56], and Darwin and Pecknold [32] investigated the biaxial stress states, while Bellamy [17], Hannant and Fredrik [41], Launay and Gashon [54], and Cedolin, Crutzen, and Poli [26] studied triaxial states of stress.

The failure criteria for plain concrete have been the object of

extensive research in recent years. Investigations reported in Refs. 22, 53, and 62 indicate that the intermediate principal stress has a considerable influence on the critical values in the compression-tension and in the biaxial compression states. The experimental results reported by Kupfer et al [53] were of great importance for other investigators, Refs. 5, 11, 56, and 63. A comparison between these results, the experimental results of Ref. 54, and the Mohr-Coloumb failure envelope were given by Argyris, Faust, and William [5], and are shown in Figs. 2.6, 2.7, and 2.8.

A failure envelope was proposed in Ref. 11, which can be used to represent a large number of different envelopes like the biaxial envelope of Liu et al [56], and the triaxial failure surface of Khan and Saugy [48] and Ref. 54. The failure surface given in Ref. 48 was used in Refs. 80 and 24. Argyris et al [4] presented two models for predicting failure of concrete type materials under triaxial conditions. A three-parameter extension of the Mohr-Coulomb criterion and a five-parameter elliptic paraboloid were incorporated into two incremental laws which describe the material in failure and post-failure regimes.

The work by Chen and Chen [27] is based on a plasticity theory which uses a combination of isotropic and kinematic hardening. In the model, the initial discontinuous surface is set at 30% ultimate strength. This represents the departure of stress-strain relations from linearity. The final failure surface represents rupture at which time the material loses all load-carrying capability. Incremental stress-strain relations are presented including those applic-

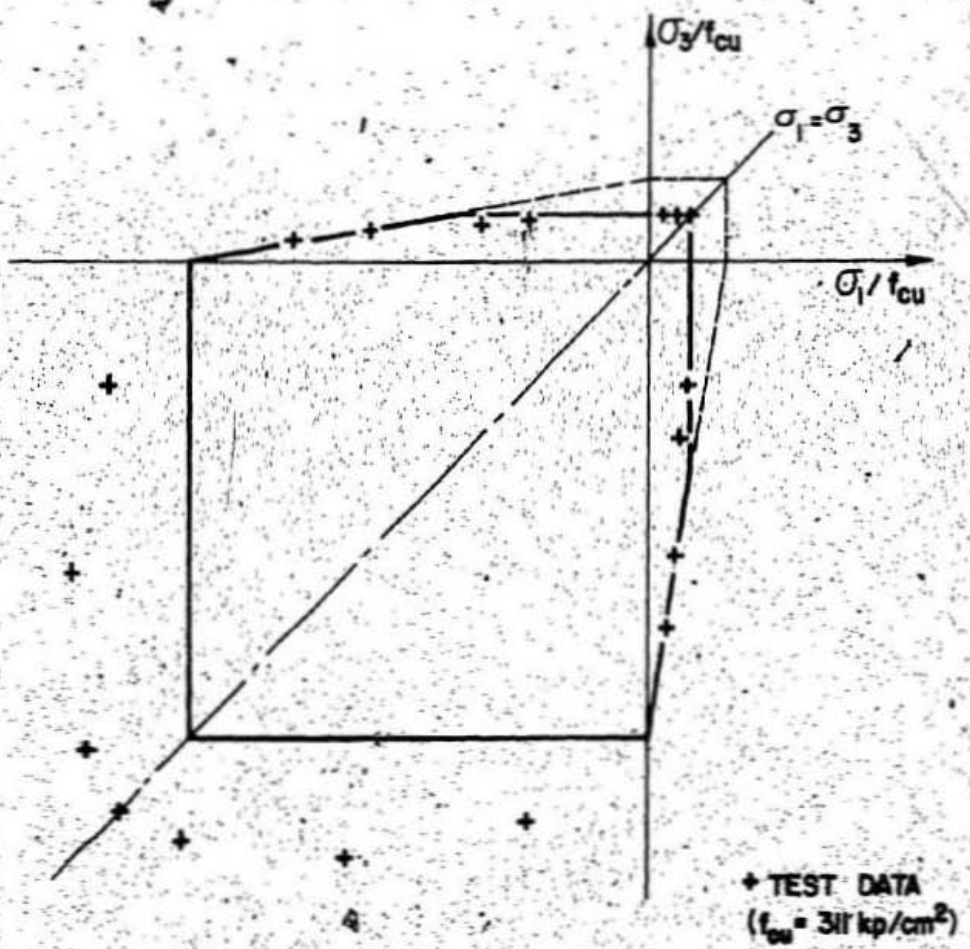

Fig. 2.6 Mohr-Coulomb Failure Envelope
Biaxial Test Data Kupfer et al [53]
(Reproduced from Ref. 5)

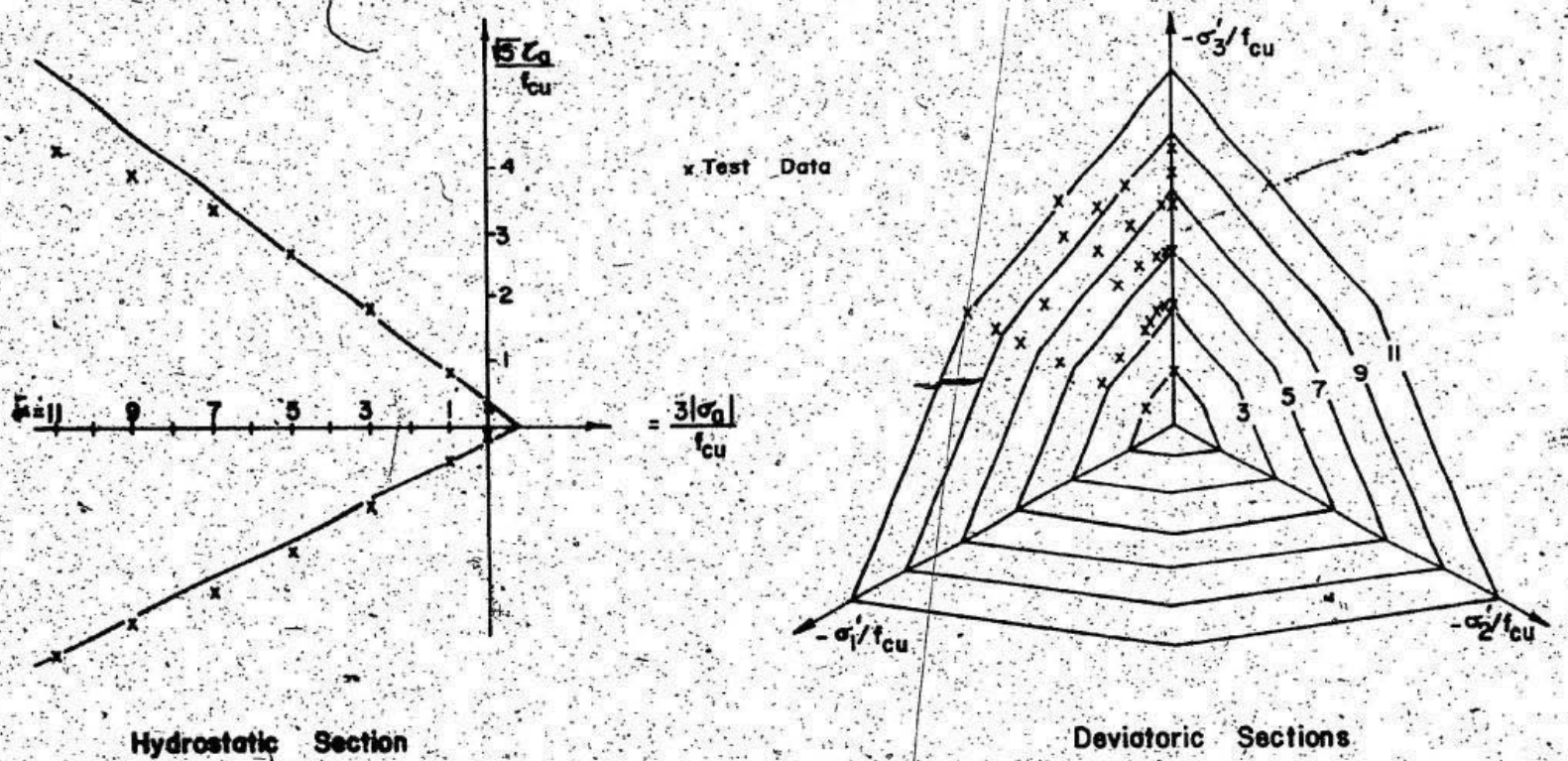

Fig. 2.7 Mohr-Coulomb Failure Envelope Triaxial Test Data Launay et al [54] (Reproduced from Ref. 5)

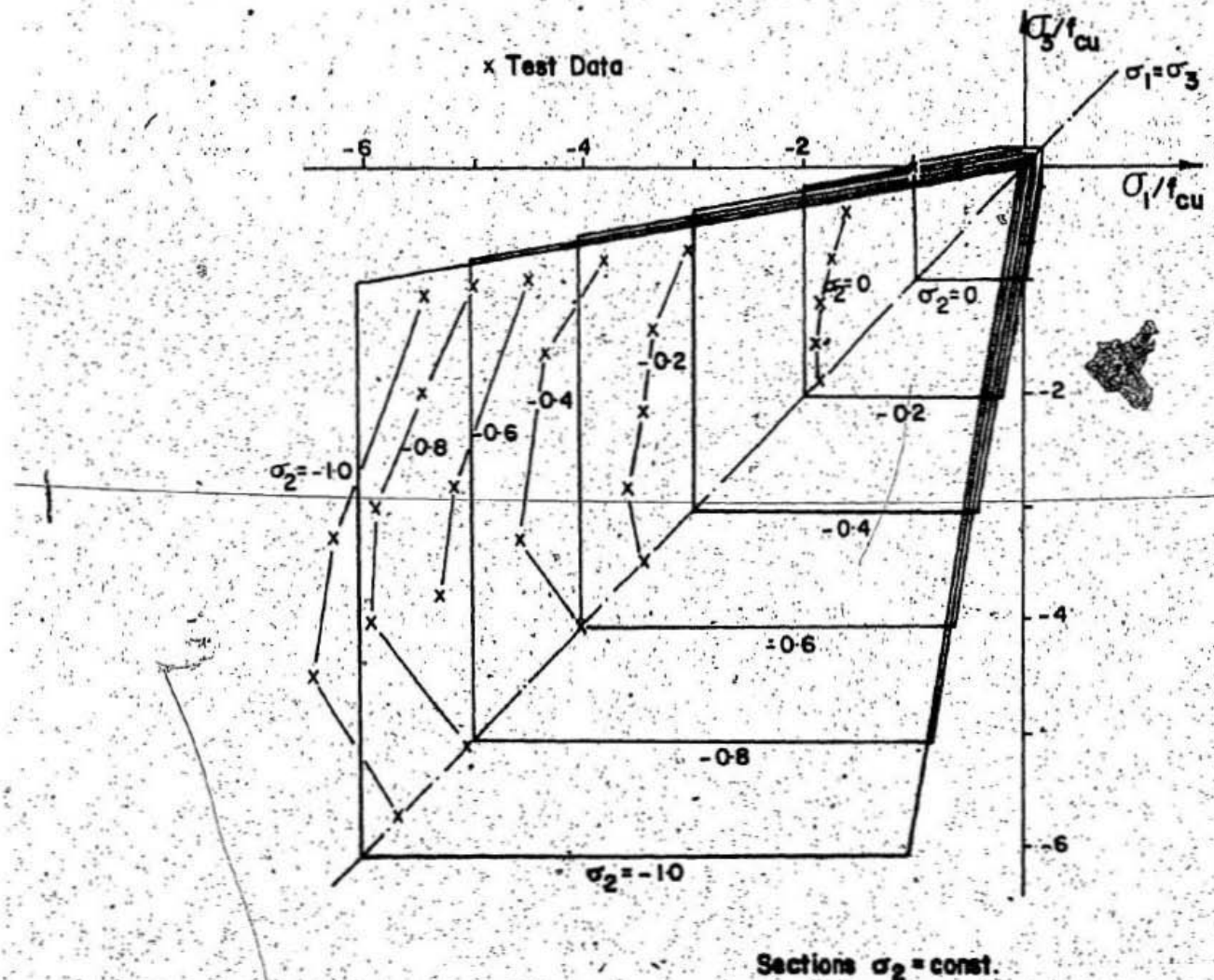

Fig. 2.8 Mohr-Coulomb Failure Envelope Triaxial Test Data Launay et al [54] (Reproduced from Ref. 5)

able to the three-dimensional case.

A constitutive model for plain concrete was proposed in Ref. 32 which was compared with experimental data of Refs. 53 and 56. This model gave good agreement with the experimental results. Cedolin et al [26] analysed some available experimental data and represented it in terms of hydrostatic and deviatoric components of stress and strain tensors. Assuming that failure depends on the stress state alone, they formulated an ultimate strength criterion as a relation between octahedral normal and shear stresses and the third stress invariant.

Ottosen [73] proposed a four-parameter failure criterion containing all the three stress invariants explicity. This criterion corresponds to a smooth convex failure surface with curved meridians, which open in the negative direction of the hydrostatic axis, and the trace in the deviatoric plane changes from nearly triangular to a more circular shape with increasing hydrostatic pressure.

In a recent paper, Kotsovos and Newman [49], described an experimental study to derive:

a) mathematical expressions for the variation of the bulk and shear moduli with stress, and

b) a correction function that takes into account volume changes that occur under deviatoric stress.

Bažant [15] distinguished between two types of constitutive relations:

1) Those where the relationship between stress and strain

increments is linear; and

2) Those where it is nonlinear.

The former type includes the total strain theory (deformation theory) as well as hypoelasticity and incremental plasticity. The latter includes a theory of plasticity without a yield surface which was first proposed by Valanis [96] and was called "endochronic theory". The best available representatives of incrementally linear plastic models are those of Argyris et al [5], and Ref. 27. A hypoelastic model is presented in Ref. 11 and a total-strain model in Ref. 26.

The term "endochronic" is used because the stress is considered to be a function of the strain history, defined with respect to a so-called "intrinsic time measure", which is an internal state variable of the material. The theory was extended and adapted to concrete by Bažant [14, 15, and 16]. Application of the theory to reinforced concrete structures has also been reported by Sorensen, Arnesen, and Bergan [88], and Ref. 20.

CHAPTER III

CONSTITUTIVE EQUATIONS OF PARISEAU'S MODEL

3.1 Introduction

In elastic-plastic analysis the material behaviour is described using three properties in addition to the elastic stress-strain relations. These properties are:

a) a yield condition, which specifies the state of multi-axial stress corresponding to start of plastic flow;

b) a flow rule relating plastic strain increments to the current stresses, and the stress increments subsequent to yielding;

c) a hardening rule, which specifies how the yield condition is modified during plastic flow.

The following discussion is directed towards the explicit determination of the above three properties and the elastic stress-strain relations of a nonlinear orthotropic model proposed by Pariseau [74]. The incorporation of the model into the NONSAP code is also presented.

3.2 Elastic Constitutive Equations

It is convenient to express elastic strains in terms of Hookean elasticity. Hooke's law for uniaxial deformation states that the deformation (strain) is proportional to the force (stress). In the more general case of three-dimensional bodies, six components of stress and strain will be present. As a natural extension of the Hooke's law, each of the six stress components may be expressed as a linear function of the six components of strain, and vice versa,

The strain-stress equations for orthotropic materials may be written in terms of the Young's moduli and Poisson's ratios as follows [33]:

$$\varepsilon_a = \frac{1}{E_a}\sigma_a - \frac{\nu_{ab}}{E_b}\sigma_b - \frac{\nu_{ac}}{E_c}\sigma_c ,$$

$$\varepsilon_b = -\frac{\nu_{ba}}{E_a}\sigma_a + \frac{1}{E_b}\sigma_b - \frac{\nu_{bc}}{E_c}\sigma_c ,$$

$$\varepsilon_c = -\frac{\nu_{ca}}{E_a}\sigma_a - \frac{\nu_{cb}}{E_b}\sigma_b + \frac{1}{E_c}\sigma_c ,$$

$$\gamma_{ab} = \frac{1}{G_{ab}}\tau_{ab} , \quad \gamma_{bc} = \frac{1}{G_{bc}}\tau_{bc} ,$$

and

$$\gamma_{ca} = \frac{1}{G_{ca}}\tau_{ca} \qquad (3.1a)$$

where a, b, and c are the material axes of orthotropy.

In matrix form, the elastic constitutive equations, (3.1a), are:

$$\begin{bmatrix} \varepsilon_a \\ \varepsilon_b \\ \varepsilon_c \\ \gamma_{ab} \\ \gamma_{bc} \\ \gamma_{ca} \end{bmatrix} = \begin{bmatrix} \frac{1}{E_a} & -\frac{\nu_{ab}}{E_b} & -\frac{\nu_{ac}}{E_c} & 0 & 0 & 0 \\ -\frac{\nu_{ba}}{E_a} & \frac{1}{E_b} & -\frac{\nu_{bc}}{E_c} & 0 & 0 & 0 \\ -\frac{\nu_{ca}}{E_a} & -\frac{\nu_{cb}}{E_b} & \frac{1}{E_c} & 0 & 0 & 0 \\ 0 & 0 & 0 & \frac{1}{G_{ab}} & 0 & 0 \\ 0 & 0 & 0 & 0 & \frac{1}{G_{bc}} & 0 \\ 0 & 0 & 0 & 0 & 0 & \frac{1}{G_{ca}} \end{bmatrix} \begin{bmatrix} \sigma_a \\ \sigma_b \\ \sigma_c \\ \tau_{ab} \\ \tau_{bc} \\ \tau_{ca} \end{bmatrix} \qquad (3.1b)$$

or

$$\{\varepsilon\} = [D]\{\sigma\} \qquad (3.1c)$$

where $\{\sigma\}$ and $\{\varepsilon\}$ are the stress and strain vectors, respectively. The parentheses, $\{\ \}$ and $[\ ]$, refer respectively to column vector and rectangular matrices; this notation will be used throughout.

There are twelve material parameters in Eqs. 3.1; however, only nine of these are independent because the following must be true:

$$\frac{E_a}{\nu_{ba}} = \frac{E_b}{\nu_{ab}}, \quad \frac{E_b}{\nu_{cb}} = \frac{E_c}{\nu_{bc}}, \quad \frac{E_c}{\nu_{ac}} = \frac{E_a}{\nu_{ca}}$$

For isotropy $E_a = E_b = E_c$, $\nu_{ab} = \nu_{ba} = \nu_{bc} = \nu_{cb} = \nu_{ca} = \nu_{ac} = \nu$ and, $G_{ab} = G_{bc} = G_{ca} = G = \frac{E}{2(1+\nu)}$.

Eqn. 3.1c may be inverted to obtain the values of the elements of the matrix $[C]$ in the following equation.

$$\{\sigma\} = [C]\{\varepsilon\} \qquad (3.2)$$

3.3 The Yield Criterion

3.3.1 General

The limit of elastic behaviour for uniaxial tension or compression is normally defined by the uniaxial tensile and compression yield stress respectively. For multiaxial states of stress, however, single values of stress cannot be used to determine the elastic limit. What is required is a functional relation among stresses at the onset of yield. This relation, a generalization of the yield point under uniaxial stress states, is called the yield function or

yield criterion. A discussion of different isptropic and Hill (for anisotropic metals) criteria is necessary to understand the Pariseau criterion proposed for anisotropic rocks and soils.

3.3.2 Isotropic Criteria

Isotropic criteria can be grouped into two categories; those that include the effect of the intermediate principal stress and those that do not. The latter can be obtained from:

$$|\tau_m|^n = A_2 \sigma_m + B_2 \qquad (3.3)$$

where

$$\tau_m = 1/2\ (\sigma_1 - \sigma_3)\ ,$$

$$\sigma_m = 1/2\ (\sigma_1 + \sigma_3)\ ,$$

A_2 and B_2 and $n(n \geq 1)$ are material constants, and, σ_1 and σ_3 are the major and minor principal stresses respectively.

Eqn. 3.3 can be used to describe many criteria in common use [74], the Tresca and Mohr-Coulomb criteria are typical examples. Fig. 3.1 is a table detailing several yield conditions obtained by particularisation of the constants in Eqn. 3.3. Fig. 3.2 is a graphical representation of Eqn. 3.3 for various values of n.

An invariant formulation of the yield condition can be used to include the effect of the intermediate principal stress. For the isotropic case, then

$$|J_2|^{n/2} = A_3 I_1 + B_3 \qquad (3.4)$$

YIELD CONDITION / *CONSTANT	TRESCA (constant)	COULOMB (linear)	TORRE (parabola)	GRIFFITH		MODIFIED GRIFFITH		GENERAL "n" TYPE	TENSION "CUTOFFS"
				$2\sigma_m \leq \tau_m$	$2\sigma_m \geq \tau_m$	$2\sigma_m \leq \tau_m$	$2\sigma_m \geq \tau_m$		
n =	1	1	2	1	2	1	1	n	$n \to \infty$
A_2 =	0	$\frac{C_o - T_o}{C_o + T_o}$	$\frac{1}{2}(C_o - T_o)$	1	$\frac{1}{2}C_o$ or $4T_o$	1	$\frac{C_o - 2T_o}{C_o}$	$\frac{(\frac{1}{2}C_o)^n - (\frac{1}{2}T_o)^n}{\frac{1}{2}C_o + \frac{1}{2}T_o}$	A_2
B_2 =	$\frac{1}{2}C_o$ or $\frac{1}{2}T_o$	$\frac{C_o T_o}{C_o + T_o}$	$\frac{1}{2}C_o T_o$	T_o	0	T_o	T_o	$\frac{T_o(\frac{1}{2}C_o)^n + C_o(\frac{1}{2}T_o)^n}{C_o + T_o}$	0
$\sin\phi$	0	A_2	$\frac{A_2}{2\lvert\tau_m\rvert}$	1	$\frac{A_2}{2\lvert\tau_m\rvert}$	1	A_2	$\frac{A_2}{n\lvert\tau_m\rvert^{n-1}}$	0
shape	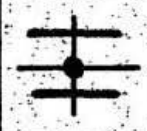								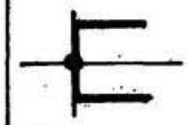

* Compression is positive. C_o = Uniaxial Compressive Strength, T_o = Absolute Value of the Uniaxial Tensile Strength

Note that the Griffith and Modified Griffith are branching formulas requiring two statements.

Fig. 3.1 A Tabulation of Details for Several Common Yield Conditions by Specialization of the Constants in Eqn. 3.3. (Reproduced from Ref. 74)

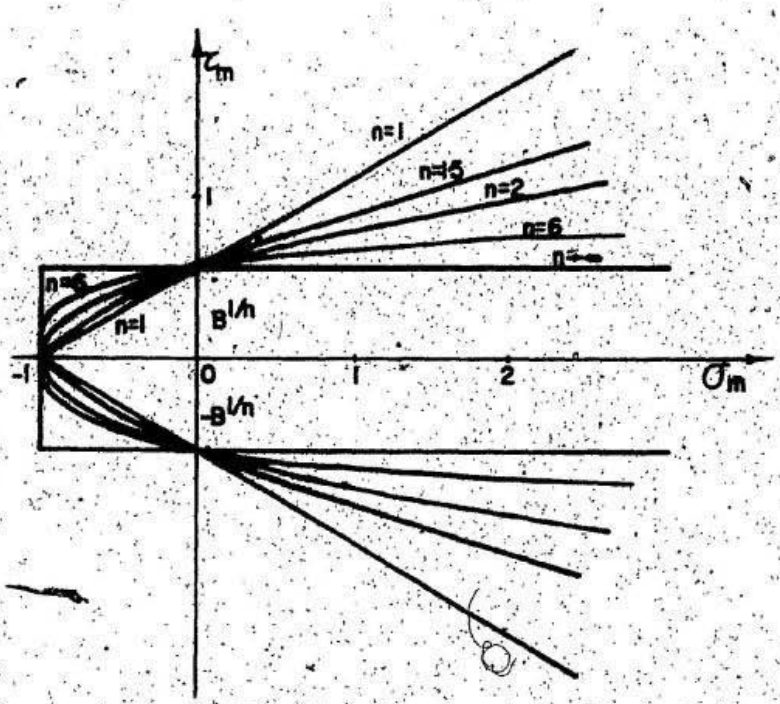

Fig. 3.2 Graphical Representation of General "n" Type Yield Condition for Selected Values of "n" (Reproduced from Ref. 74)

where A_3, B_3 and n ($n \geq 1$) are material properties, I_1 is the first stress invariant and J_2 is the second deviatoric stress invariant; the invariants are given by:

$$I_1 = \sigma_x + \sigma_y + \sigma_z$$

$$J_2 = 1/6 \quad (\sigma_y - \sigma_z)^2 + (\sigma_z - \sigma_x)^2 + (\sigma_x - \sigma_y)^2 + \tau_{yz}^2 + \tau_{zx}^2 + \tau_{xy}^2$$

The von Mises and the extended von Mises criteria are among those given by Eqn. 3.4.

3.3.3 Hill's Criterion

Hill [43] proposed a yield criterion for anisotropic metals assuming it to be quadratic in the stress components. With axes of references defined by a, b and c, the criterion is as follows:

$$2f(\sigma_{ij}) = F(\sigma_b - \sigma_c)^2 + G(\sigma_c - \sigma_a)^2 + H(\sigma_a - \sigma_b)^2 + 2L\tau_{bc}^2 + 2M\tau_{ca}^2 + 2N\tau_{ab}^2 = 1 \qquad (3.5)$$

where F, G, H, L, M and N are parameters characteristic of the current state of anisotropy.

This yield criterion has this form only when the principal axes of anisotropy are the axes of reference; otherwise the form changes in a way that can be found by transforming the stress components.

If T_a, T_b and T_c are the tensile yield stresses in the principal

direction of anisotropy, R, S and T are the yield stresses in shear with respect to the principal axes of anisotropy, then,

$$2F = \frac{1}{T_b^2} + \frac{1}{T_c^2} - \frac{1}{T_a^2} ,$$

$$2G = \frac{1}{T_c^2} + \frac{1}{T_a^2} - \frac{1}{T_b^2} ,$$

$$2H = \frac{1}{T_a^2} + \frac{1}{T_b^2} - \frac{1}{T_c^2} ,$$

$$2L = \frac{1}{R^2} , \quad 2M = \frac{1}{S^2} , \quad \text{and} \quad 2N = \frac{1}{T^2} \tag{3.6}$$

Hill's criterion (Eqn. 3.5) reduces to the Mises form (Eqn. 3.4) when the anisotropy tends towards zero.

3.3.4 Pariseau Criterion

Pariseau [74] presented a plasticity theory for anisotropic rocks and soils. The proposed theory is based on the work of Hill [43] in anisotropic metal plasticity and represents an extension of his work so as to include anisotropic rock and soil materials. The difference between the two criteria is the inclusion of the normal stresses as linear terms in the yield criterion of Pariseau. The yield criterion proposed by Pariseau for anisotropic materials having three mutually orhtogonal planes of symmetry is given by:

$$1 = \left| F(\sigma_b - \sigma_c)^2 + G(\sigma_c - \sigma_a)^2 + H(\sigma_a - \sigma_b)^2 + L\tau_{bc}^2 + M\tau_{bc}^2 + N\tau_{ab}^2 \right|^{1/2n} - (U\sigma_a + V\sigma_b + W\sigma_c) \tag{3.7}$$

where the nine coefficients of the stresses and n ($n \geq 1$) are material constants, and a, b and c are the material axes of anisotropy. The material constants of Eqn. 3.7 will change if another reference coordinate system is adopted. The material constants are defined in terms of unconfined tensile and compressive strength data in the anistropic reference axes (here a, b and c). Let n = 1 in Eqn. 3.7 and let the tensile stresses be positive. Then if C_a, C_b, C_c, T_a, T_b, T_c, R, S and T are the numerical values of the unconfined compressive, tensile and torsional strengths, referred to the principal axes of anisotropy, then,

$$2F = 1/4(\frac{1}{T_b} + \frac{1}{C_b})^2 + 1/4(\frac{1}{T_c} + \frac{1}{C_c})^2 - 1/4(\frac{1}{T_a} + \frac{1}{C_a})^2 ,$$

$$2G = 1/4(\frac{1}{T_c} + \frac{1}{C_c})^2 + 1/4(\frac{1}{T_a} + \frac{1}{C_a})^2 - 1/4(\frac{1}{T_b} + \frac{1}{C_b})^2 ,$$

$$2H = 1/4(\frac{1}{T_a} + \frac{1}{C_a})^2 + 1/4(\frac{1}{T_b} + \frac{1}{C_b})^2 - 1/4(\frac{1}{T_c} + \frac{1}{C_c})^2 ,$$

$$U = 1/2(\frac{1}{C_a} - \frac{1}{T_a}) ,$$

$$V = 1/2(\frac{1}{C_b} - \frac{1}{T_b}) ,$$

$$W = 1/2(\frac{1}{C_c} - \frac{1}{T_c}) ,$$

$$L = \frac{1}{R^2} , \quad M = \frac{1}{S^2} , \quad \text{and} \quad N = \frac{1}{T^2}$$

With $T_a = C_a$, $T_b = C_b$ and $T_c = C_c$ Eqn. 3.7 of Pariseau reduces to Eqn. 3.5 of Hill. Also, the Pariseau criterion reduces to Mises,

Eqn. 3.4, when the anisotropy is vanishingly small, i.e.,

$$F = G = H,\ L = M = N,\ U = V = W,\ L = 6F$$

Comparison of Eqn. 3.7 and Eqn. 3.4 shows that:

$$B_3 = (6F)^{-1/2\,n} \quad , \quad A_3 = U(6F)^{-1/2\,n}$$

3.4 Relations Between Stress and Strain-Increment

The initial and subsequent yield condition for kinematic or isotropic hardening can be written as:

$$f(d\varepsilon^P\ ,\ \sigma,\ K) = 0 \tag{3.9}$$

where $d\varepsilon^P$ is the increment of plastic strain, and K is a 'hardening' parameter. For isotropic hardening this yield condition reduces to [104]:

$$f(\sigma,\ K) = 0 \tag{3.10}$$

This yield condition can be visualized as a surface in n-dimension stress space. Fig. 3.3 for example, gives a yield surface in two-dimensional stress space. The basic constitutive relation defining the plastic strain was first suggested by von Mises, Ref. 104. Specifying a plastic potential function as g, if $d\varepsilon_n^P$ denotes the increment of plastic strain for any component, n, then

$$d\varepsilon_n^P = \lambda \frac{\partial g}{\partial \sigma_n} \tag{3.11}$$

where λ is a non-negative proportionality factor. The particular case of g = f is known as 'associated plasticity'. When this relation is not satisfied the plasticity is 'non-associated'. The

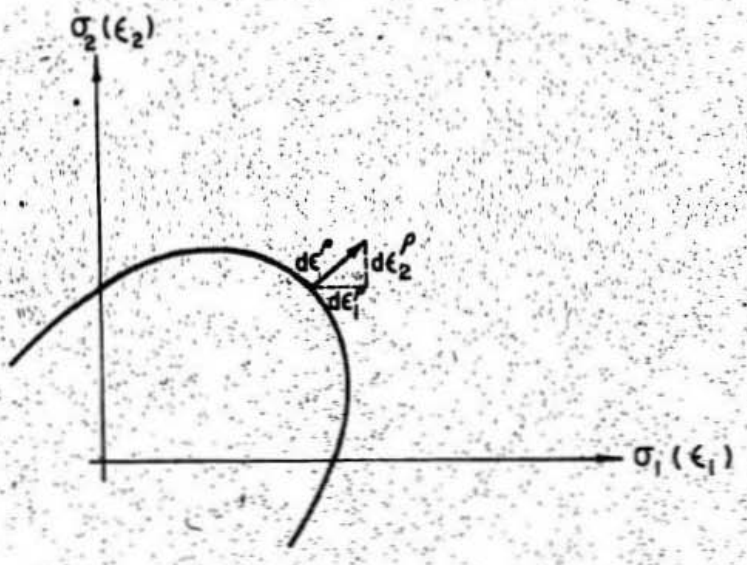

Fig. 3.3 Yield Surface and Normality Criterion in Two-Dimensional Stress Space

analysis here is restricted to associated plasticity, so,

$$d\varepsilon_n^p = \lambda \frac{\partial f}{\partial \sigma_n} \tag{3.12}$$

At the present time, this hypothesis (according to Ref. 104) is generally accepted. This is known as the 'normality' principle because the relation given by Eqn. 3.12 can be interpreted as requiring the normality of the plastic strain increment 'vector' to the yield surface in the space of n stress dimensions.

Applying the normality principle to Eqn. 3.7:

$$d\varepsilon_a = \lambda\{nJ^{1/2\,n-1}\,[G(\sigma_a-\sigma_c) + H(\sigma_a-\sigma_b)] - U\}\ ,$$

$$d\varepsilon_b = \lambda\{nJ^{1/2\,n-1}\,[H(\sigma_b-\sigma_a) + F(\sigma_b-\sigma_c)] - V\}\ ,$$

$$d\varepsilon_c = \lambda\{nJ^{1/2\,n-1}\,[F(\sigma_c-\sigma_b) + G(\sigma_c-\sigma_a)] - W\}\ ,$$

$$d\gamma_{bc} = \lambda\, nJ^{1/2\,n-1}\, L\,\tau_{bc}\ ,$$

$$d\gamma_{ca} = \lambda\, nJ^{1/2\,n-1}\, M\,\tau_{ca}\ ,$$

and

$$d\gamma_{ab} = \lambda\, nJ^{1/2\,n-1}\, N\,\tau_{ab} \tag{3.13}$$

where

$$J = |F(\sigma_b-\sigma_c)^2 + G(\sigma_c-\sigma_a)^2 + H(\sigma_a-\sigma_b)^2 + L\tau_{bc}^2 + M\tau_{ca}^2 + N\tau_{ab}^2|$$

The inclusion of the elastic strain rate components to Eqn. 3.13 provides the complete stress-strain relationship for elastic-plastic materials exhibiting three mutually orthogonal planes of

symmetry.

3.5 Total Stress-Strain Relations

Eqn. 3.12 in matrix form is given by:

$$\{d\varepsilon^P\} = \lambda \{q\} \tag{3.14}$$

where $\{q\}$ can be determined from Eqn. 3.13. For isotropic hardening, the parameter K is assumed to be associated with the plastic work done and this parameter, being a scalar quantity, will obviously change the yield surface by a simple expansion or contraction. Such models (isotropic hardening models) are found to be deficient in representing the true behaviour of some materials [104]. Therefore, kinematic hardening theories have been introduced in which dependence on the direction of plastic straining is noted and K is considered to be constant.

When plastic yield occurs, the stresses are on the yield surface given by Eqn. 3.9. Differentiating this gives:

$$df = \frac{\partial f}{\partial \varepsilon_1^P} d\varepsilon_1^P + \frac{\partial f}{\partial \varepsilon_2^P} d\varepsilon_2^P + \ldots\ldots + \frac{\partial f}{\partial \sigma_1} d\sigma_1 + \frac{\partial f}{\partial \sigma_2} d\sigma_2 \ldots = 0 \tag{3.15}$$

or, in matrix form:

$$\{p\}^T \cdot \{d\varepsilon^P\} = \{q\}^T \cdot \{d\sigma\} \tag{3.16}$$

The stress increments are calculated from the relation

$$\{d\sigma\} = [C^E] (\{d\varepsilon\} - \{d\varepsilon^P\}) \tag{3.17}$$

where $\{d\varepsilon\}$ are the total incremental strain quantities, and $[C^E]$ is the elastic stress strain relation, i.e., $[C^E] \equiv [C]$ in Eqn. 3.2.

Multiplying Eqh. 3.17 by $\{q\}^T$ and introducing it into Eqn. 3.16 gives:

$$\{p\}^T \{d\varepsilon^P\} = \{q\}^T [C^E](\{d\varepsilon\} - \{d\varepsilon^P\}) \tag{3.18}$$

Using Eqn. 3.14:

$$\lambda = \frac{\{q\}^T [C^E] \{d\varepsilon\}}{\{p\}^T \{q\} + \{q\}^T [C^E] \{q\}} \tag{3.19}$$

Substituting in Eqn. 3.17 from Eqn. 3.14 and Eqn. 3.19 for $\{d\varepsilon_p\}$ and λ, the elastic plastic material law becomes:

$$\{d\sigma\} = [C^{EP}] \{d\varepsilon\} \tag{3.20}$$

where $[C^{EP}]$ is the elastic-plastic material matrix, which is given by:

$$[C^{EP}] = [C^E] - \frac{[C^E] \{q\} ([C^E] \{q\})^T}{\{p\}^T \{q\} + \{q\}^T [C^E] \{q\}} \tag{3.21}$$

The condition of tangency associated with perfect plasticity, which is the case considered, is given by [31]:

$$\{\frac{\partial f}{\partial \varepsilon_n}\} = \{p\} = \{0\} \tag{3.22}$$

Eqn. 3.22 combined with Eqn. 3.21 can be used to determine the elastic-plastic material matrix.

3.6 Incorporation of Pariseau's Model into the NONSAP Code

3.6.1 General

The NONSAP code has been modified to accept a nonlinear material model not currently included in the material model library of the programme. The material model library for two-dimensional elements contains eight material models, namely: (1) linear isotropic; (2) linear orthotropic; (3) variable tangent moduli; (4) curve description model; (5) curve description model with tension cut-off; (6) elastic-plastic (von Mises); (7) elastic-plastic (Drucker-Prager); and (8) incompressible nonlinear elastic (Mooney-Rivlin). As the main purpose of this thesis is to analyze an underground nuclear containment vessel subjected to internal pressurization, a case which can be approximated well by axisymmetrix finite element analysis, the Pariseau model was incorporated as a two-dimensional model (model 9). No changes were required in the original of NONSAP; the material model subroutines were simply added and the appropriate calls to these subroutines incorporated.

The main subroutine corresponding to Pariseau's model is ELT2D9. Fig. 3.4, Ref. 13, shows that during execution, subroutine ELT2D9 must perform the following functions:

1) initialization of the working storage array, WA, during element information input phase;

2) calculation of element stresses and/or element tangent material law during the following solution phases:

a) formation of a new tangent stiffness matrix (element stresses and the tangent material matrix are calculated)

b) equilibrium iteration or incremental analysis without

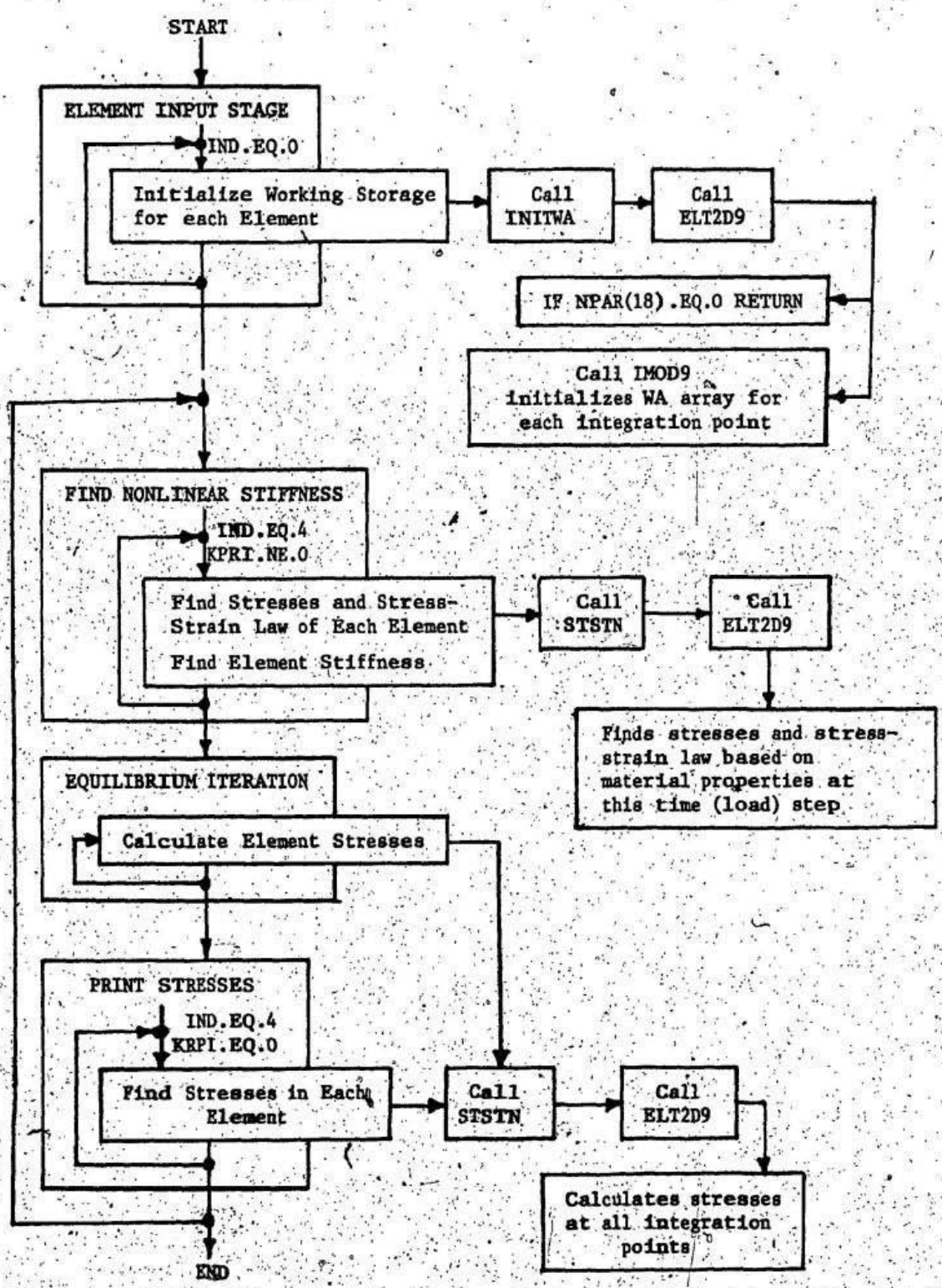

Fig. 3.4 Incorporation of a New Model Into the NONSAP Code (Reproduced from Ref. 13)

calculation of a new stiffness matrix (only stresses are calculated)

c) printing of stresses (only stresses are calculated).

The following discussion is directed towards describing how these functions were performed. It should be mentioned here that the elastic-plastic models already included in the material model library (von Mises and Drucker-Prager) were used as guidelines for writing the subroutines required for the Pariseau model.

3.6.2 Two-Dimensional Generalized Elasticity Matrix

For two-dimensional finite element analysis (axisymmetric, plane strain, and plane stress), all elastic stress-strain matrices can be derived from the general three-dimensional elastic stress-strain relationship, Eqn. 3.1b. The plane strain and axisymmetric stress-strain matrices are obtained simply by deleting, in the three-dimensional stress-strain matrix, the rows and columns that correspond to the zero-strain components. The stress-strain matrix for plane stress analysis is then obtained from the axisymmetric stress-strain matrix by using the condition that σ_c is zero. So, Eqn. 3.1b can now be reduced and re-arranged, for use with the NONSAP code, to obtain the relationship:

$$[C_i]^{-1} = \begin{bmatrix} \frac{1}{E_a} & -\frac{\nu ab}{E_b} & 0 & -\frac{\nu ac}{E_c} \\ & \frac{1}{E_b} & 0 & \frac{\nu bc}{E_c} \\ \text{Symmetric} & & \frac{1}{G_{ab}} & 0 \\ & & & \frac{1}{E_c} \end{bmatrix} \qquad (3.23)$$

where the subscript "ℓ" in $[C_\ell]^{-1}$ indicates that the elastic stress-strain matrix is given in the local system of material axes, because the material constants in this equation are defined, as mentioned before, in the principal material directions (a, b, c) of orthotropy. Consider the finite element in Fig. 3.5, for which the in-plane orthogonal material axes are 'a' and 'b'. The third orthogonal material direction is 'c' and is perpendicular to the plane defined by 'a' and 'b'. In order to evaluate the element stresses, the elastic stress-strain matrix in global coordinates x, y, z must be computed. First we calculate $[C_\ell]$ using Eqn. 3.23; then we evaluate the transformation matrix [Q] which calculates strains in the global system from strains in the (a, b, c) local system [10],

$$[Q] = \begin{bmatrix} \cos^2 & \sin^2 & \cos\ \sin & 0 \\ \sin^2 & \cos^2 & -\cos\ \sin & 0 \\ -2\cos\ \sin & -2\cos\ \sin & \cos^2 - \sin^2 & 0 \\ 0 & 0 & 0 & 1 \end{bmatrix} \qquad (3.24)$$

in which the angle, which must be defined for each element is measured from the global axis, y, to the material axis, a, the positive being clockwise. The global axis, y, was chosen because the NONSAP code specifies that two-dimensional elements must use the y-z plane, i.e., plane strain, plane stress, and axisymmetric elements can only be defined in the y-z plane.

The required stress-strain matrix in global coordinates is given by:

$$[C^E] = [Q]^T [C_\ell] [Q] \qquad (3.25)$$

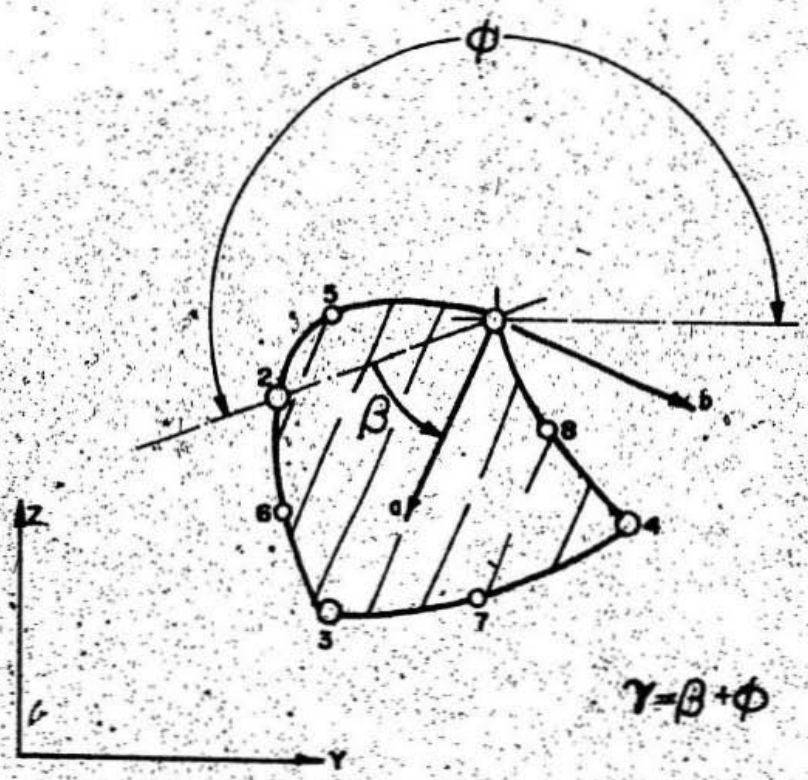

Fig. 3.5 Principal In-Plane Material Axes Orientation for the Pariseau Model

According to this discussion, seven material properties are required for determining the elastic stress strain matrix $[C^E]$. Seven other material properties are also required for the yield function of Eqn. 3.7 after deleting the terms corresponding to shear stresses in other planes than y-z or a-b. So, for this model fourteen material properties are required, namely: E_a, E_b, E_c, ν_{ab}, ν_{bc}, ν_{ca}, G_{ab}, T_a, T_b, T_c, C_a, C_b, C_c, and R.

3.6.3 Solution Algorithm for Elastic-Plastic Stress Calculation

It is necessary to discuss how stress increments are calculated due to given strain increments, since the elastic-plastic stress-strain law is defined in terms of current total stresses. It is required to calculate total stresses, $\{\sigma_{t+\Delta t}\}$, at time $t+\Delta t$, if total strains at time $t+\Delta t$, $\{\varepsilon_{t+\Delta t}\}$, total strains at time t, $\{\varepsilon_t\}$, and total stresses at time t, $\{\sigma_t\}$, are known. The strain increments $\{d\varepsilon\}$ can be obtained because they are the differences between $\{\varepsilon_{t+\Delta t}\}$ and $\{\varepsilon_t\}$. The stress increments can also be obtained now assuming that the material behaves elastically, and the following relation can be applied:

$$\{d\sigma\} = [C^E]\{d\varepsilon\} \tag{3.26}$$

where $[C^E]$ is the elastic stress-strain matrix determined from Eqn. 3.23.

The total stresses $\{\bar{\sigma}_{t+\Delta t}\}$ (assuming elastic behaviour) can be determined by adding the stress increment $\{d\sigma\}$ to the total stresses at time t, $\{\sigma_t\}$. With $\{\bar{\sigma}_{t+\Delta t}\}$ as the state of stress, the value of the yield function, f, can be determined using Eqn. 3.7. If f is

less than or equal to zero, the assumption of elastic behaviour holds, and $\{\sigma_{t+\Delta t}\}$ will be equal to $\{\bar{\sigma}_{t+\Delta t}\}$.

If f is greater than zero, the parts of incremental strains taken elastically have to be determined. So, a variable, α, is determined from the equation:

$$f(\sigma + \alpha d\sigma) = 0 \tag{3.27}$$

Since at stress levels, $\{\sigma + \alpha d\sigma\}$, the yield function f becomes equal to zero and yielding is initiated.

It is now clear that the value of α depends on the previous state of stress $\{\sigma_t\}$. If this state was already plastic, α should be equated with zero, otherwise it should be calculated using Eqn. 3.27. If the previous state of stress was elastic, and after the determination of α the vector, $\{\bar{\sigma}_{t+\Delta t}\}$, should be redefined as:

$$\{\bar{\sigma}_{t+\Delta t}\} = \{\sigma_t\} + \alpha \{d\sigma\} \tag{3.28}$$

Then, the elastic-plastic strain increments can be determined using the following equation:

$$\{d\varepsilon^p\} + (1-\alpha) \{d\varepsilon\} \tag{3.29}$$

Now for both cases, whether the previous state of stress $\{\sigma_t\}$ was elastic or plastic, to obtain the final stresses $\{\sigma_{t+\Delta t}\}$ that include the effect of the complete strain increments $\{d\varepsilon\}$, the stresses corresponding to $\{d\varepsilon^p\}$ must be added to $\{\bar{\sigma}_{t+\Delta t}\}$. As a result of this addition, the incremental stresses corresponding to $\{d\varepsilon^p\}$ will change the stress state from one below the failure

envelope to one above it. Implicit in the failure or yield criterion is the requirement that such a stress state cannot exist. Therefore, a correction has to be applied to reduce the computed stresses to values that are compatible with the envelope. At the same time the strains must be adjusted to satisfy the stress-strain relation.

One technique to do this correction is to subdivide the load increment into fractions such that elements which yield for the first time during this load increment end up on the failure envelope. Such a procedure, according to Ref. 61, is very time consuming. The common technique and the one employed here is to correct only the stresses so that they lie on the yield surface at the end of the load increment. This procedure is not entirely satisfactory because it produces errors in the strains and non-equilibrium in the stresses of adjacent elements. However, these difficulties can be overcome by analyzing each load increment more than once. Reanalyzing each load increment, a process known as iteration, generally reduces the errors in the strains and the non-equilibrium stress state.

According to this technique and since the material law is dependent on the current stresses, the elastic-plastic strain increment $\{d\varepsilon^p\}$ is divided into equal intervals, and $\{\bar{\sigma}_{t+\Delta t}\}$ is updated for each interval by the increments in stress corresponding to the interval increments in elastic-plastic strains. These increments in stress can be determined by using the relations discussed in Section 3.5. Then, the updated $\{\bar{\sigma}_{t+\Delta t}\}$ is corrected after each interval to stress values compatible with the yield envelope. In the calculations, the stress-strain matrix corres-

ponding to the latest available stress conditions is used.

According to the previous discussion, nine variables, namely, the previously calculated stresses and strains, and a parameter, β, identifying the previous state of stress (elastic $\beta = 1$ or plastic $\beta = 2$) need to be stored for each integration point in order to characterize history. These nine variables along with the numerical integration order of Gauss quadrature formulae determine the dimensions of the working storage array, WA.

3.7 Sample Solution Using the Pariseau's Model

After incorporation of the model into the NONSAP code, the programme was checked to solve two problems for which structural response computations from other investigations are available.

The thick walled cylinder in Fig. 3.6 subjected to internal pressure was analyzed using four 8-node axisymmetric elements. The purpose of this analysis was to study the case of vanishing anisotropy, and the reduction of the model to the von Mises model. The solution using Pariseau's model showed excellent agreement with the solution reported by Bathe et al [10], and Ref. 66 using the von Mises model. Fig. 3.7 shows the radial displacement response of the cylinder as a function of the applied load.

The second problem is the problem of a circular hole in a hydrostatic stress field. The problem was analyzed using Pariseau's criterion by Dahl [30]. The same finite element mesh reported by Dahl was used to study the progressive growth of plastic yield domain. The mesh contains 170 nodes and 288 plane strain triangular elements

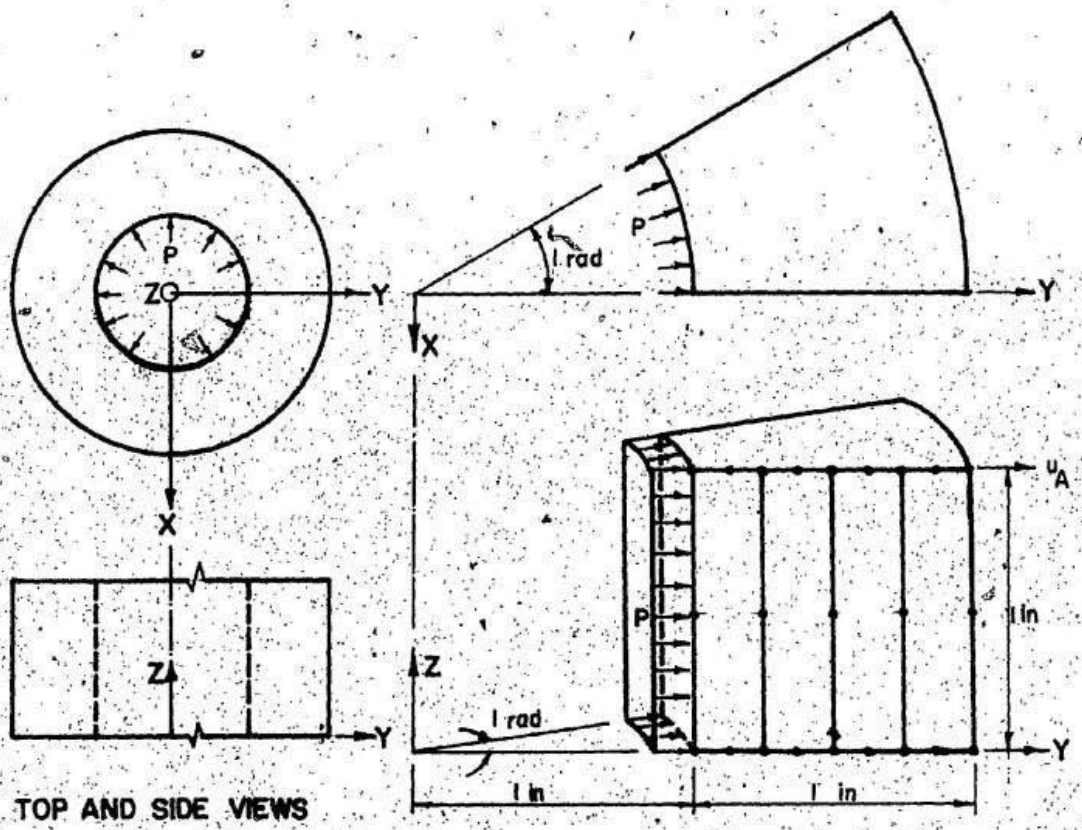

von Mises Yield Condition

$G = 10^5/3$ lb/in^2

$\nu = 0.3$

$\sigma_y = 17.32$ lb/in^2

Pariseau Yield Condition

$E_x = E_y = E_z = 86666.6$ lb/in^2

ν = constant = 0.3

$C_x = C_y = C_z = T_x = T_y = T_z = 17.32$ lb/in^2

$R = 8.66$ lb/in^2

Fig. 3.6 Finite Element Mesh of Thick-Walled Cylinder
(Reproduced from Ref. 10)

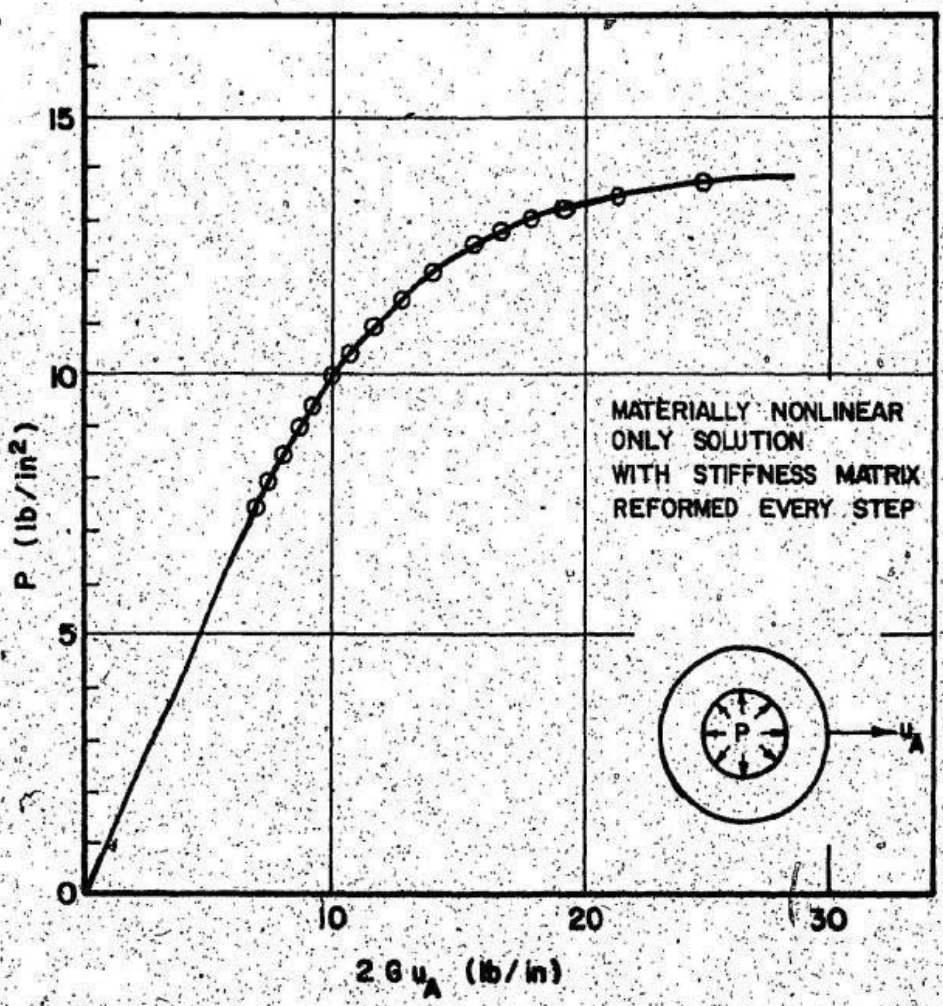

Fig. 3.7 Elastic-Plastic Displacement Response of Thick-Walled Cylinder (Reproduced from Ref. 10)

and is shown in Fig. 3.8. The material presented has low strength values in the Z-direction, i.e., in the direction that would tend to increase post yield deformation. As a result, the tendency for propagation of the yield domain along the 45° diagonal - as shown in Fig. 3.9 - is amplified by the material weakness in the Z-direction. The agreement between Dahl's solution and the NONSAP solution was excellent.

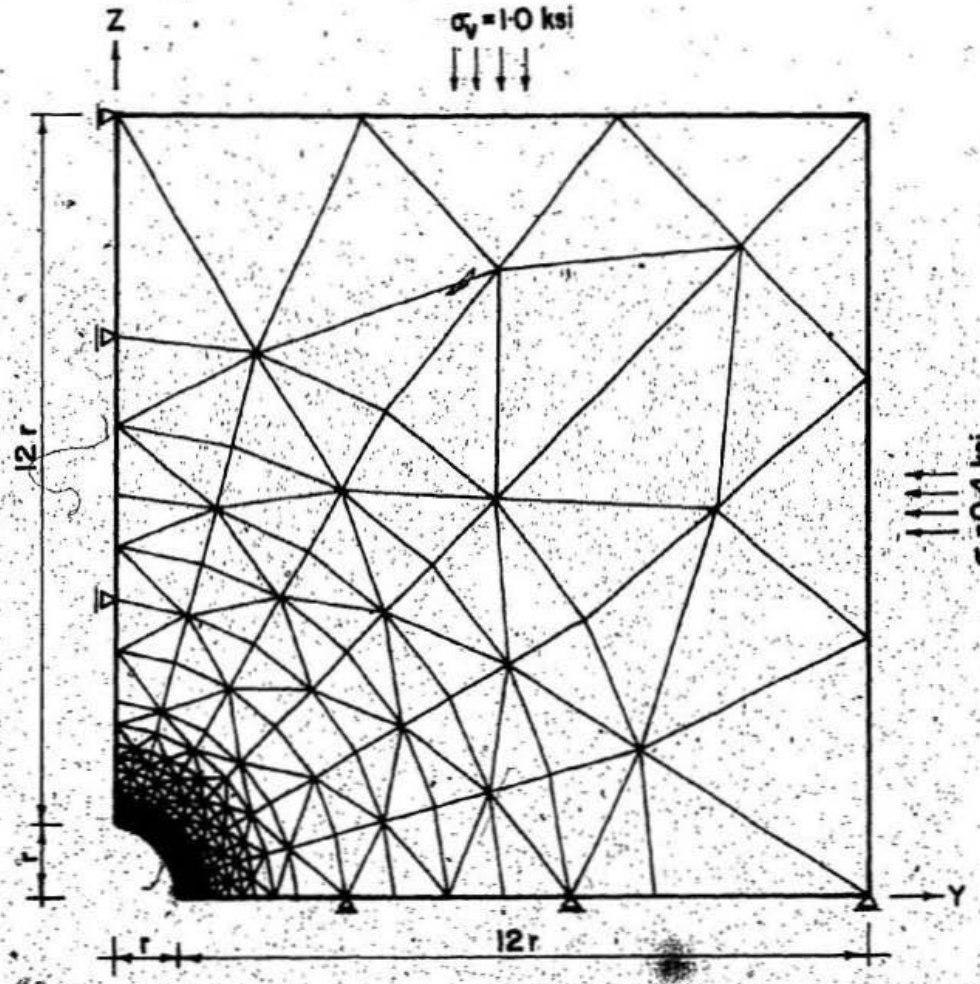

$E_x = E_y = E_z = 500$ ksi

$G_{yz} = 208$ ksi

$C_z = 372$ psi

$T_z = 211$ psi

v = constant = 0.2

$C_y = C_x = 558$ psi

$T_y = T_x = 316$ psi

R = 194 psi

Fig. 3.8 Finite Element Mesh for the Cylindrical Hole Problem (Reproduced from Ref. 30)

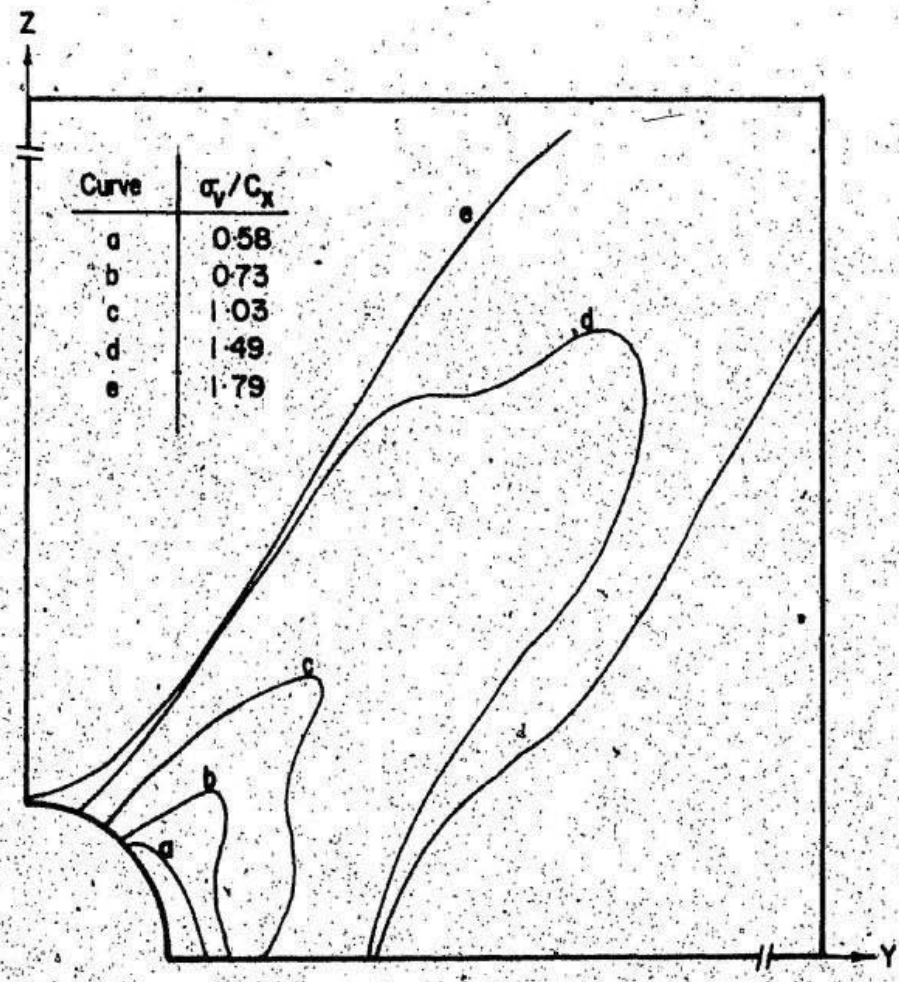

Fig. 3.9 Progressive Growth of Plastic Yield Domain for the Cylindrical Hole Problem (Reproduced from Ref. 30)

CHAPTER IV

ANALYSIS AND PARAMETERS DETERMINATION

4.1 General

This project is a continuation of previous investigations which have attempted to evaluate the behaviour of cut-and-cover type underground nuclear reactor containments subjected to different types of loading conditions. Previous investigations [36, 59, 76 and 77] indicated the effectiveness of the high horseshoe shape and the favourable effects of embedment to internal pressurization.

The structure considered is a reinforced concrete horseshoe-shaped containment, burried at 40m below ground surface. The height of the containment is 60m, the maximum radius 17m, and the base thickness 5m. These are typical containment dimensions for a 1100-MWe power plant. The containment structure, excavation and backfill for a typical case are shown in Fig. 4.1. In view of axial symmetry, only half the structure and the medium need to be considered.

4.2 Analytical Procedures

The purpose of this section is to present a brief discussion of the theory and implementation of the analysis procedures, related to the problem, that have been used in the general linear and nonlinear, static and dynamic finite element analysis programme NONSAP.

4.2.1 Principle of Virtual Displacements

Of the three finite element models; the displacement model, the mixed model, and the equilibrium model, the displacement model is

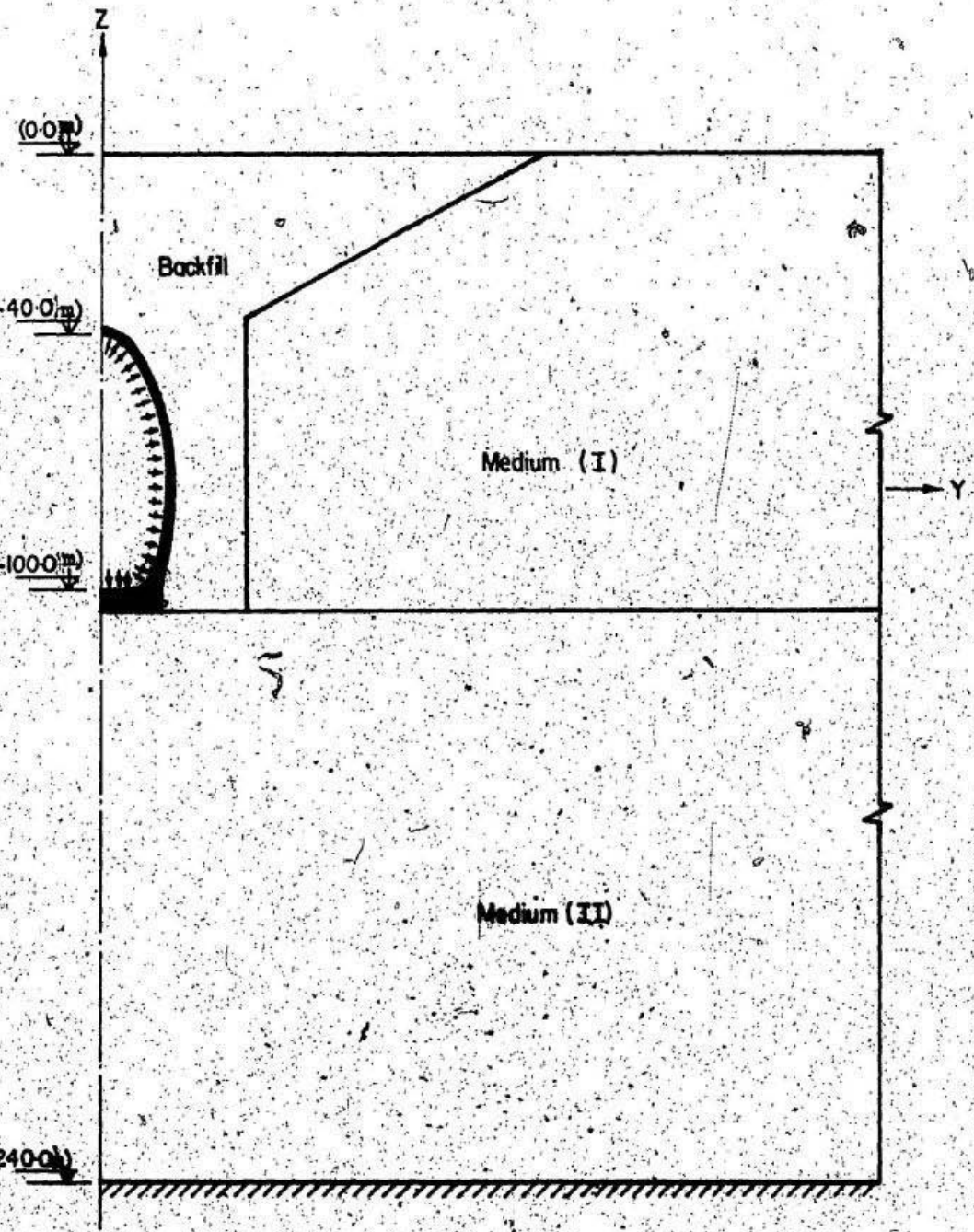

Fig. 4.1 Containment, Medium, and Backfill for a Typical Case

used more extensively than the other two, and is the one that is utilized for this investigation. It has a more efficient solution procedure than the other two models, and can easily be extended to nonlinear applications.

The finite element displacement method is based on the principle of virtual displacements. This principle states that the internal work done by the actual stresses as a result of arbitrary virtual displacements, $\{\delta U\}$, is equal to the external work done by body and surface forces.

$$\int\{\sigma\}^T \cdot \{\delta\varepsilon\} \cdot dV = \int\{b\}^T \cdot \{\delta U\} \cdot dV + \int\{P\}^T \cdot \{\delta U\} \cdot dS \qquad (4.1)$$

In the finite element displacement method the continuum is divided into small subregions (elements), and simple displacement functions are assumed for each element. These displacement functions are expressed in terms of unknown nodal displacements, $\{U_i\}$, for the element, and chosen such that continuity of displacements is preserved along boundaries of adjacent elements.

Since the displacement functions are element properties, the integrals in the principle of virtual displacements are replaced by summations over element domains. Internal work and external work are calculated for each element independently and the element stiffness matrix and consistent load vector are derived. These matrices and vectors are assembled into a system of linear algebraic equilibrium equations for the total structure in which the unknowns are the nodal displacements. Since the nodal displacements for all elements attached to one node are the same, the assemblage can be

done by superposition of all element matrices according to their nodal incidences.

4.2.2 Linear Finite Element Displacement Analysis

The linear finite element displacement analysis can be described in the following steps:

1) A displacement function for the element is assumed as a function of the nodal displacements $\{U_i\}$. These displacements are the unknowns of the problem in the finite element displacement method.

2) The relations between the element nodal displacements and the displacements at any point in the element are described by the chosen shape functions, $\{N_i\}^T$, for the element.

$$\{U\} = \{N_i\}^T\{U_i\} \tag{4.2a}$$

For example, if we assume u, v, and w are the displacements in the x, y, and z directions, respectively, and the element has r nodes, Eqn. 4.2a can take the form:

$$\{U\} = \begin{bmatrix} u(x,y,z) \\ v(x,y,z) \\ w(x,y,z) \end{bmatrix} = \begin{bmatrix} \sum_{i=1}^{r} N_i(x,y,z).u_i \\ \sum_{i=1}^{r} N_i(x,y,z).v_i \\ \sum_{i=1}^{r} N_i(x,y,z).w_i \end{bmatrix} = \begin{bmatrix} \{N_i\}^T . \{u_i\} \\ \{N_i\}^T . \{v_i\} \\ \{N_i\}^T . \{w_i\} \end{bmatrix} \tag{4.2b}$$

The shape functions $\{N_i\}^T$ are functions of the element nodal coordinates. They are chosen such that continuity of displacements is preserved between adjacent elements.

3) Differentiation of the assumed element displacements gives the state of strain throughout the element. The element strains are dependent on the element nodal displacements and the coordinate system.

$$\{\varepsilon_{(x,y,z)}\} = \frac{\partial}{\partial(x,y,z)}\{U\} = \frac{\partial}{\partial(x,y,z)}\{N_i\}^T \cdot \{U_i\}$$

$$= \frac{\partial\{N_i\}^T}{\partial(x,y,z)}\{U_i\}$$

$$= [B] \cdot \{U_i\} \qquad (4.3)$$

The matrix [B] is a geometric matrix derived from differentiation of the shape function matrix.

4) For a linear elastic material, the element stress-strain relations are expressed by the element rigidity matrix [C].

$$\{\sigma\} = [C](\{\varepsilon\} - \{\varepsilon_o\}) + \{\sigma_o\} \qquad (4.4)$$

where $\{\varepsilon_o\}$ and $\{\sigma_o\}$ are element initial strains and stresses, respectively.

5) The internal strain energy due to the virtual displacements is given by the product of the element strains and stresses.

$$\{\Delta\varepsilon\}^T\{\sigma\} = \{\Delta U_i\}^T[B]^T\{\sigma\} \qquad (4.5)$$

This internal work per unit volume is integrated over the element volume to obtain the element internal energy.

$$\int\{\Delta U_i\}^T \cdot \{B\}^T \cdot \{\sigma\} \cdot dV \qquad (4.6)$$

6) The external work is equal to the work done by the applied

nodal forces, $\{P_i\}$, and the distributed element body or surface loads, $\{b\}$. The distributed forces are expressed in terms of nodal forces by the shape functions $\{N_i\}^T$. $\{b\}$. The virtual nodal displacements are $\{\Delta U_i\}$, and the external work is equal to:

$$\{\Delta U_i\}^T \cdot \{P_i\} + \int \{\Delta U_i\}^T \cdot \{N_i\}^T \cdot \{b\} \cdot dV \qquad (4.7)$$

7) Based on the principle of virtual displacements, equating the external and internal virtual works results in the following equation:

$$\int \{\Delta U_i\}^T \cdot \{B\}^T \cdot \{\sigma\} \cdot dV = \{\Delta U_i\}^T \cdot \{P_i\} + \int \{\Delta U_i\}^T \cdot \{N_i\}^T \cdot \{b\} \cdot dV \qquad (4.8)$$

8) Since $\{\Delta U_i\}$ are arbitrary virtual displacements, the above equation can be reduced to:

$$\{P_i\} = \int [B]^T \cdot \{\sigma\} \cdot dV - \int \{N_i\}^T \cdot \{b\} \cdot dV \qquad (4.9)$$

Substituting the stress-strain relations and the strain-nodal displacements relations, the relationship between the element forces and displacements is obtained as follows:

$$\{P_i\} = \left(\int [B]^T \cdot [C] \cdot [B] \cdot dV\right) \{U\} - \int [B]^T \cdot [C] \cdot \{\varepsilon_o\} \cdot dV + \int [B]^T \cdot \{\sigma_o\} \cdot dV - \int \{N_i\}^T \cdot \{b\} \cdot dV \qquad (4.10)$$

By definition, the following can be established:

- Element stiffness matrix:

$$[K] = \int [B]^T \cdot [C] \cdot [B] \cdot dV \qquad (4.11)$$

- Equivalent nodal forces due to distributed (body) forces:

$$\{P_b\} = \int \{N_i\}^T \cdot \{b\} \cdot dV \qquad (4.12)$$

- Equivalent nodal forces due to initial strains:

$$\{P_\varepsilon\} = \int [B]^T \cdot [C] \cdot \{\varepsilon_o\} \cdot dV \qquad (4.13)$$

- Equivalent nodal forces due to initial stresses:

$$\{P_\sigma\} = -\int [B]^T \cdot \{\sigma_o\} \cdot dV \qquad (4.14)$$

Now, Eqn. 4.10 can be reduced to the form:

$$[K]\{U\} = \{P_i\} + \{P_b\} + \{P_\varepsilon\} + \{P_\sigma\} = \{F\} \qquad (4.15)$$

9) Since the equilibrium of internal and external nodal forces is satisfied for the whole structure, the element stiffness matrices are assembled into a total structure stiffness matrix, and the element load vectors are assembled into a structure load vector. If all element matrices and load vectors are in the same coordinate system, the assemblage is done by simple matrix addition.

10) The set of the structural equilibrium equations $[K] \cdot \{U\} = \{F\}$ is solved for the unknown nodal displacements.

11) The element strains can be obtained from the nodal displacements. For linear elastic material, the element stresses are obtained from the strain-stress relations:

$$\{\sigma\} = [C] \cdot [B] \cdot \{U_i\} - [C] \cdot \{\varepsilon_o\} + \{\sigma_o\} \qquad (4.16)$$

4.2.3 Equations of Motion for Dynamic Analysis

For dynamic analysis, the displacements are time-dependent and Eqn. 4.2b must take the form:

$$\{U\} = \begin{bmatrix} u(x,y,z,t) \\ v(x,y,z,t) \\ w(x,y,z,t) \end{bmatrix} = \begin{bmatrix} \sum_{i=1}^{r} N_i(x,y,z)\, u_i(t) \\ \sum_{i=1}^{r} N_i(x,y,z)\, v_i(t) \\ \sum_{i=1}^{r} N_i(x,y,z)\, w_i(t) \end{bmatrix} \qquad (4.17)$$

where u, v, and w are the time-dependent components of displacement in the three coordinate directions. The other important difference between static and dynamic analysis is that, the nodal body force vector must include the inertia and damping forces.

If {U} is the displacement field of an elastic body, the distributed inertia force acting throughout the body is given by $\rho\{\ddot{U}\}$, where ρ is the mass density of the material and $\{\ddot{U}\} = \frac{\partial^2}{\partial t^2}\{U\}$ is the column vector of distributed accelerations. According to the well-known D'Alembert principle, this inertia force is statically equivalent to the force $\{F^i\} = -\rho\{\ddot{U}\}$, that is, $\{F^i\}$ may be treated as a statically imposed body force.

Compared with the inertia force, the damping force is far more difficult to characterize in general. Usually the damping force is not linearly related to the rate of change of displacement in a body, but rather has a more complicated relationship. However, to simplify the analysis of a dynamically loaded structure, the conventional

procedure is to replace the actual damping force, which is usually unknown, by an approximate viscous damping force proportional to velocity. By this means we write the damping force acting on the body as $\{F^d\} = c\{\dot{U}\}$, where c is a known damping coefficient and $\{\dot{U}\} = \frac{\partial}{\partial t}\{U\}$. More details on damping forces will be discussed later.

Now, Eqn. 4.12 takes the form:

$$\{P_b\} = \int(\{N_1\}^T \{b\} - c\{N_1\}^T \{\dot{U}\} - \rho\{N_1\}^T \{\ddot{U}\}) \cdot dV \qquad (4.18)$$

The other terms of Eqs. 4.11, 4.13 and 4.14 remain the same, and Eqn. 4.15 will change to the form:

$$[K]^e \{U\} + [C]^e \{\dot{U}\} + [M]^e \{\ddot{U}\} = \{F(t)\}^e \qquad (4.19)$$

where

$$[C]^e = \int c\{N_1\}^T \cdot \{N_1\} \cdot dV \qquad (4.20)$$

and

$$[M]^e = \int \rho\{N_1\}^T \cdot \{N_1\} \cdot dV \qquad (4.21)$$

The interpolation functions, $\{N_1\}$, are the same as those used for the displacement model, and $[C]^e$ and $[M]^e$ are called the element damping and mass matrices, respectively. Further assembly gives the system equations of motion:

$$[K]\{U\} + [C]\{\dot{U}\} + [M]\{\ddot{U}\} = \{F(t)\} \qquad (4.22a)$$

Mathematically, this equation represents a system of linear

differential equations of second order. It should also be recalled that Eqn. 4.22a was derived from considerations of static at time t, i.e., Eqn. 4.22a may be written as:

$$\{F^{e}_{(t)}\} + \{F^{d}_{(t)}\} + \{F^{i}_{(t)}\} = \{F_{(t)}\} \qquad (4.22b)$$

where $\{F^{e}_{(t)}\}$, $\{F^{d}_{(t)}\}$ and $\{F^{i}_{(t)}\}$ are the elastic, damping, and inertia forces respectively, and all these forces are time dependent.

Therefore, in dynamic analysis, the static equilibrium at time t, which includes the effect of acceleration-dependent inertia forces and velocity-dependent damping forces, is considered. In static analysis the equations of motion in Eqn. 4.22 are considered neglecting inertia and damping effects.

4.2.4 Incremental Form of the Equations of Motion

Eqs. 4.22a and 4.22b are the basic equations of dynamic force equilibrium at the nodes of any discrete set of structural elements. An incremental form of these equations of motion may be used in the study of nonlinear behaviour arising from nonlinearities in material properties, large displacements, or both. Restricting attention to constant mass and damping matrices, Eqn. 4.22 may be written as:

$$[M](\{\ddot{U}_t\} + \{\Delta\ddot{U}_t\}) + [C](\{\dot{U}_t\} + \{\Delta\dot{U}_t\}) + [K_t](\{U_t\} + \{\Delta U_t\}) = \{F_{t+\Delta t}\} \qquad (4.23)$$

where $[K_t]$ = stiffness matrix at time t

$\{\Delta U_t\}$, $\{\Delta\dot{U}_t\}$ and $\{\Delta\ddot{U}_t\}$ = changes in nodal displacements, velocities, and accelerations during the next time increment.

The incremental form of these equations is then obtained as:

$$[M]\{\Delta\ddot{U}_t\} + [C]\{\Delta\dot{U}_t\} + [K_t]\{\Delta U_t\} = \{\bar{F}_{t+\Delta t}\} \tag{4.24}$$

where

$$\{\bar{F}_{t+\Delta t}\} = \{F_{t+\Delta t}\} - \{F_t\} + \{F_t^r\} \tag{4.25}$$

The residual nodal forces at the end of time t, $\{F_t^r\}$, arise from the approximations involved in Eqn. 4.24 and can be written as:

$$\{F_t^r\} = \{F_t\} - [M]\{\ddot{U}_t\} - [C]\{\dot{U}_t\} - \{F_t^e\} \tag{4.26}$$

The vector $\{F_t^e\}$ represents the internal resisting force at the nodes at time, t, and will be discussed further in Section 4.2.9.. Substitution of Eqn, 4.26 into Eqn, 4.25 yields:

$$\{\bar{F}_{t+\Delta t}\} = \{F_{t+\Delta t}\} - [M]\{\ddot{U}_t\} - [C]\{\dot{U}_t\} - \{F_t^e\} \tag{4.27}$$

In the step-by-step method of numerical integration, to be discussed in Section 4.2.11, the increments $\{\Delta\ddot{U}_t\}$ and $\{\Delta\dot{U}_t\}$ are expressed in terms of displacement increments $\{\Delta U_t\}$. Eqn. 4.24 can then be solved for $\{\Delta U_t\}$ and the increments of velocities and accelerations computed.

4.2.5 Finite Element Discretization

Generally, for the same number of degrees of freedom, better accuracy is achieved for larger elements with greater number of nodes. The disadvantage is that larger elements with straight boundaries cannot follow irregular geometric boundaries as smaller elements can. This difficulty was overcome with the introduction

of the isoparametric elements. In these elements, the same shape functions that describe the displacements are used to describe the boundaries as functions of the nodal coordinates. As a result, the element boundaries can be curved up to the degree of the displacement function on the same boundary. The isoparametric elements are capable of describing more closely complex curvatures in the structure geometry if more than two nodes exist on each boundary line of the element. With three nodes on a line, a quadratic geometric shape will be described accurately, and with four nodes a cubic shape.

The isoparametric elements are well described in the literature [12, 46 and 104]. The following is a brief summary of the isoparametric finite element principles.

The coordinates of a point inside the isoparametric element are defined by a normalized curvilinear coordinate system, s-r (for two dimensional analysis), which range in value from -1 to +1, Fig. 4.2.

The relationship between curvilinear and the Cartesian coordinates is:

$$X = N_1 X_1 + N_2 X_2 + \ldots = \{N\}^T \{X_n\}$$

$$Y = N_1 Y_1 + N_2 Y_2 + \ldots = \{N\}^T \{Y_n\} \qquad (4.28)$$

Functions that describe the element geometry are used to describe the element displacement as a function of the nodal displacements as follows:

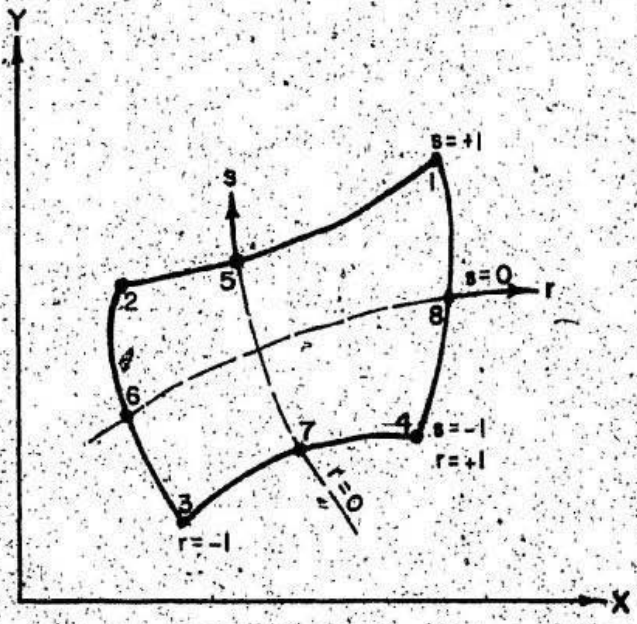

Fig. 4.2 Four to Eight Variable-Number-Nodes Two-Dimensional Element

$$u = N_1 u_1 + N_2 u_2 + \ldots . \qquad = \{N\}^T \{u\}$$

$$v = N_1 v_1 + N_2 v_2 + \ldots . \qquad = \{N\}^T \{v\} \qquad (4.29)$$

By inserting the coordinates r and s of a point into these equations the displacements u and v of that point can be calculated.

As with geometry, compatibility of displacements between two adjacent elements is ensured for all points on the boundary sides of the elements.

The [B] matrix, required for the evaluation of the element stiffness matrix and the load vector (see Section 4.2.2) is built up with the derivatives of the shape functions with respect to the Cartesian coordinates. Since the shape functions are functions of the curvilinear coordinates, a transformation of derivatives is required:

$$\begin{bmatrix} \frac{\partial N_i}{\partial r} \\ \\ \frac{\partial N_i}{\partial s} \end{bmatrix} = \begin{bmatrix} \frac{\partial x}{\partial r} & \frac{\partial y}{\partial r} \\ \\ \frac{\partial x}{\partial s} & \frac{\partial y}{\partial s} \end{bmatrix} \begin{bmatrix} \frac{\partial N_i}{\partial x} \\ \\ \frac{\partial N_i}{\partial y} \end{bmatrix} = [J] \begin{bmatrix} \frac{\partial N_i}{\partial x} \\ \\ \frac{\partial N_i}{\partial y} \end{bmatrix} \qquad (4.30)$$

where [J], the Jacobian matrix, can be determined from:

$$[J] = \begin{bmatrix} \frac{\partial N_1}{\partial r} & \frac{\partial N_2}{\partial r} & \ldots \\ \\ \frac{\partial N_1}{\partial s} & \frac{\partial N_2}{\partial s} & \ldots \end{bmatrix} \begin{bmatrix} X_1 & Y_1 \\ \\ X_2 & Y_2 \\ \vdots & \vdots \\ \vdots & \vdots \end{bmatrix} \qquad (4.31)$$

and the volume of the element, dx.dy.dz, in all integrations (see Section 4.2.2) is replaced by h.[J].dr.ds with integration limits of -1 and +1 and h equal to the thickness of the element.

Actual integration is done numerically using a number of Gauss integration points. This numerical integration by summation is incorporated without any computational difficulty in the computer programmes. Numerical integration procedures, as well as recommendations for choosing the order of numerical integration were discussed in detail by Bathe and Wilson [12]. Because the elements in this study were chosen to be undistorted, the integration order used is 2X2 for all elements.

4.2.6 Mass Matrix

Employing the same displacement field assumption used for element stiffness evaluation leads to a consistent mass matrix formulation. The advantage in using such a formulation is the existence of upper bounds when used in conjunction with a displacement compatible finite element. The primary disadvantage lies in the greater computational effort involved compared to the physical lumped mass procedure [33]. Lumping mass at the nodes for simple elements is straightforward but may present some difficulties in the case of more complex elements for which special procedures may have to be devised. Details of different procedures for mass lumping was discussed by Zienkiewicz [104]. The NONSAP code has the option of using consistent or lumped mass matrices. In this study the lumped mass matrix formulation was used to save computing time.

4.2.7 Stiffness Matrix

The evaluation of the incremental tangent stiffness in the elastic-plastic analysis follows standard procedures. The state of loading is determined at the end of each increment; and, whenever plastic loading is predicted, the elastic-plastic stress-strain transformation matrix is evaluated according to flow theory laws of plasticity. The evaluation of the elastic-plastic stress-strain matrix for the Pariseau model has been discussed in detail in Chapter III. This matrix is used in the virtual work equations and the stiffness matrix is obtained using the methodology of finite element displacement formulation.

4.2.8 Damping Matrix

One of the means available for considering the variation of damping in different elements is to incorporate damping using a Rayleigh damping matrix of the form:

$$[C] = \alpha[M] + \beta[K_o] \qquad (4.32)$$

where α and β are the mass proportional and stiffness proportional damping factors respectively; the matrix $[C]$ is assumed to remain constant; and $[K_o]$, the initial elastic stiffness matrix, is used in Eqn. 4.32. This assumption is made because the damping mechanism in any structure is really quite complex.

It is worth noting that mass proportional damping causes negligible damping in higher modes whereas stiffness proportional damping has the tendency to suppress them. This property might be used to advantage in problems in which undesirable higher modes need to be

eliminated. The Wilson-θ step-by-step algorithm introduces artificial viscosity to achieve this effect, but the use of $\beta[K_o]$ damping may provide better means of suppressing the unwanted modes.

The values of α and β can be determined from two given damping ratios that correspond to two unequal natural frequencies of vibration, and using the equation (Ref. 12):

$$\alpha + \beta \omega_i^2 = 2\omega_i \zeta_i \qquad (4.33)$$

In this study, 10% critical damping was assumed in the first two modes.

4.2.9 Internal Resisting Forces

The application of any incremental solution method has the tendency to cause the solution to diverge from the true solution. To improve convergence, an "iteration" procedure is used in the NONSAP code. The procedure, which is discussed in detail in Ref. 10, consists of simply adding the "out-of-balance" or residual nodal forces to the subsequent increment of nodal loads. These residual forces $\{F_t^r\}$ are given by Eqn. 4.26. In order to evaluate this expression, the internal resisting forces $\{F_t^e\}$ need to be determined. The summation of the incremental force changes $\{\Delta F_t^e\}$ is a poor method of obtaining $\{F_t^e\}$. This is due to the fact that the stiffness matrix, $[K_t]$, is assumed constant within each increment and the approximation involved leads to an accumulation of errors in evaluating the internal resisting forces. These forces can be easily found in terms of the total stress field, $\{\sigma\}$, by the use of the principle of virtual work.

$$\{\delta U\}^T \cdot \{F_t^e\} = \Sigma \int_V \{\delta\varepsilon\}^T \cdot \{\sigma\} \cdot dV \qquad (4.34)$$

The summation indicates that the vector $\{F_t^e\}$ for the entire structure is obtained by a direct assembly of the element force vectors.

4.2.10 Solution of Equilibrium Equations in Dynamic Analysis

The normal mode superposition procedure for the solution of the equations of motion is applicable only for linear dynamic analysis. Even in the case of linear problems, however, it may be more advantageous to use the so-called step-by-step or direct integration methods when analysing large systems subjected to short duration loads where a large number of modes are excited. This is generally the method chosen for blast or impact problems. It is also the only feasible approach for problems in which nonlinear behaviour due to material properties and/or large displacements needs to be considered. Several direct integration operators are known and discussed in Ref. 12. NONSAP has the option of using the Newmark method or the Wilson-θ method. In this study the Wilson-θ method is used.

4.2.11 Wilson-θ Method

The linear acceleration method of step-by-step procedures was modified by Wilson [102] to generate an unconditionally stable algorithm. This modification assumed a linear variation of acceleration to exist over a time interval $\tau = 2\Delta t$, at the end of which a solution is obtained using the standard procedure of linear acceleration method. Then the solution at the end of the interval, Δt, is obtained by the use of the kinematic relations originating from the assumption of linear acceleration variation. This method

was shown to be unconditionally stable for linear systems but possessed considerable amount of inherent damping, more than sufficient to suppress the spurious oscillations of discretized systems. A further extension of this method was made by Farhoomand [37] to obtain an optimal value for τ. Linear acceleration was taken over an interval $\tau = \theta\Delta t$, and it was shown that θ must be greater than 1.37 for unconditional stability. Reduction of θ from the previous value of 2 has the effect of reducing the amount of damping introduced into the system. The full derivation of the θ-method is presented in Ref. 37. Table 4.1, Ref. 12 gives a summary of the procedures.

4.3 Pressure-Time History

The determination of the pressure and temperature transiets inside a containment after the maximum credible accident (MCA) is an important aspect of nuclear power plant safety design. The MCA is usually the double-ended rupture of a primary loop piping, known as the loss-of-coolant accident (LOCA). According to the federal regulations of the U.S.A. published by the Nuclear Regulatory Commission,

> "..The reactor containment structure, including access openings, penetrations and the containment heat removal system shall be designed so that the containment structure and its internal compartments can accomodate, without exceeding the design leakage rate and, with sufficient margin, the calculated pressure and temperature conditions resulting from any loss of coolant accident." [91]

The calculations of the pressure-time history, following a LOCA, have been performed by Carbajo and Munno [25], and Augustin,

TABLE 4.1 Step-by-Step Solution Using Wilson θ Integration Method (Reproduced from Ref. 12)

A. Initial Calculations:

1. Form stiffness matrix K, mass matrix M, and damping matrix C.
2. Initialize U_o, $\dot{U}_o$, and $\ddot{U}_o$.
3. Select time step Δt and calculate integration constants, $\theta = 1.4$ (usually):

$$a_0 = \frac{6}{(\theta\,\Delta t)^2}\ ;\quad a_1 = \frac{3}{\theta\,\Delta t}\ ;\quad a_2 = 2a_1\ ;\quad a_3 = \frac{\theta\,\Delta t}{2}\ ;$$

$$a_4 = \frac{a_0}{\theta}\ ;\quad a_5 = \frac{-a_2}{\theta}\ ;\quad a_6 = 1 - \frac{3}{\theta}\ ;\quad a_7 = \frac{\Delta t}{2}\ ;\quad a_8 = \frac{\Delta t^2}{6}\ .$$

4. Form effective stiffness matrix $\hat{K}$: $\hat{K} = K + a_0 M + a_1 C$.
5. Triangularize $\hat{K}$: $\hat{K} = LDL^T$.

B. For Each Time Step:

1. Calculate effective loads at time $t+\Delta t$:

$$\hat{R}_{t+\theta\Delta t} = R_t + \theta(R_{t+\Delta t} - R_t) + M(a_0 U_t + a_2 \dot{U}_t + 2\ddot{U}_t) + C(a_1 U_t + 2\dot{U}_t + a_3 \ddot{U}_t)$$

2. Solve for displacements at time $t+\theta\Delta t$:

$$LDL^T U_{t+\theta\Delta t} = \hat{R}_{t+\theta\Delta t}$$

3. Calculate displacements, velocities, and accelerations at time $t+\Delta t$:

$$\ddot{U}_{t+\Delta t} = a_4(U_{t+\theta\Delta t} - U_t) + a_5 \dot{U}_t + a_6 \ddot{U}_t$$

$$\dot{U}_{t+\Delta t} = \dot{U}_t + a_7(\ddot{U}_{t+\Delta t} + \ddot{U}_t)$$

$$U_{t+\Delta t} = U_t + \Delta t \dot{U}_t + a_8(\ddot{U}_{t+\Delta t} + 2\ddot{U}_t)$$

Kafka, Bauer, Schueller, Zech and Wittmann [6]. An estimated curve for underground containment has been given by Watson et al [99]. Fig. 4.3 presents the results of different investigators which show acceptable agreement.

These curves show that the maximum pressure occurs after approximately 10 seconds. Fig. 4.4a, Ref. 21 shows the relation between dynamic load factor (DLF) and the time for a dynamic constant force with finite rise time, while Fig. 4.4b shows the relation between the DLF and the ratio (t_r/T), where t_r is the rise time of F(t), and T is the natural period of a single spring mass. For the containment system, it is expected that the natural period is small and the ratio (t_r/T) will be greater than 6 at least. From these curves, it is concluded that the maximum DLF will almost reduce to 1 and not much difference is expected between dynamic and static analyses.

4.4 Model Dimensions and Boundary Conditions

The idealization of a semi-infinite medium with a finite domain for the use in finite element analysis has been the object of several investigations. For static analysis (according to Ref. 30) the assumption of infinity can be approached by specifying the outer boundaries as fixed, and at distances equal to 12 radii from the hole centre in the case of circular hole. In this study, for static analysis, the side boundaries were located at 200m from the Z-axis, which is almost 12 times the maximum radius. The bottom boundaries were located nearer, due to the considerable thickness of the containment base and the assumption that the containment should rest on a considerable stiff strata. These boundaries were located

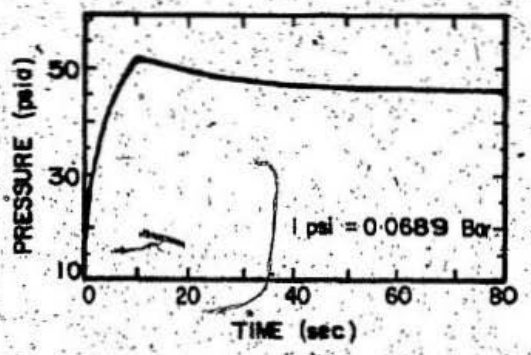

(a)

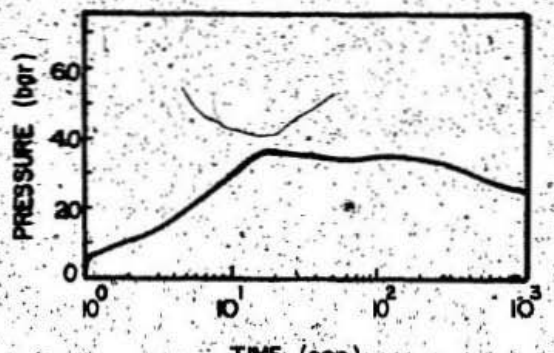

(b)

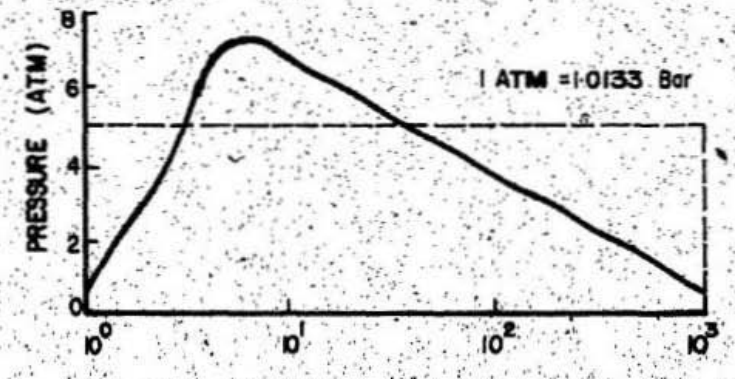

(c)

Fig. 4.3 Pressure-Time History for the Containment Following a LOCA (a - Reproduced from Ref. 24; b - Reproduced from Ref. 5; and c - Reproduced from Ref. 99)

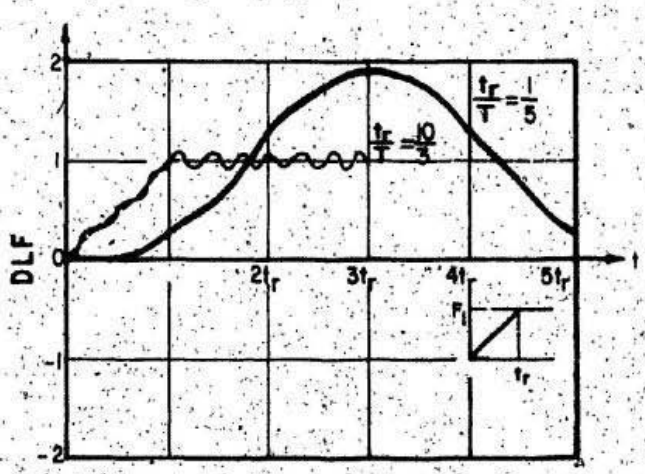

Fig. 4.4a Typical Response of One Degree Elastic System to Constant Force With Finite Rise Time (Reproduced from Ref. 20)

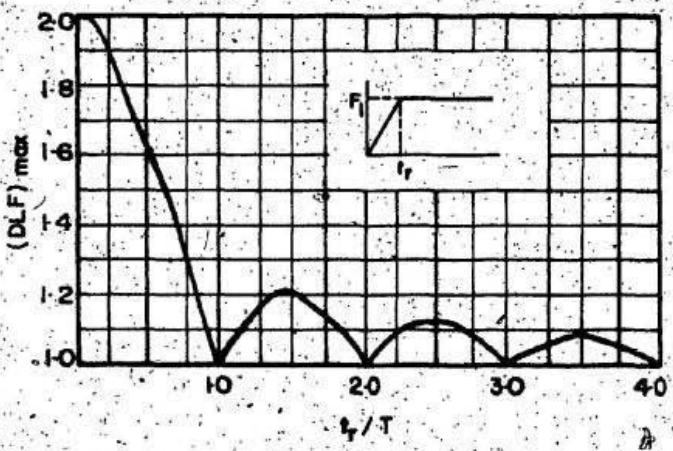

Fig. 4.4b Maximum Response of One Degree Elastic System Subjected to Constant Force With Finite Rise Time (Reproduced from Ref. 20)

140m below the base of the containment.

For dynamic analysis, the problem is more complicated due to the action of the waves reflecting from the boundaries. Lysmer and Kuhlemeyer [57], [52] developed a viscous boundary which would be exact for the one-dimensional condition of body waves normal to the boundary, and a Rayleigh boundary which would absorb the first Rayleigh mode. Their results showed reasonable accuracy for a half-space under vertical excitation, but could not reproduce well the situation of a shallow layer. Wass and Lysmer [98], [58] developed a transmitting boundary which reproduces the far field in a way consistent with the finite element expansion used to model the core region. The model is based on the exact solution of the general two-dimensional wave propagation problem in a layered stratum.

In this study, the viscous boundary approach, in which a valid finite model will be shown to consist of a finite portion of the medium with dashpots attached to the boundaries, has been adopted. Calculations of the constant of the dashpots for different cases were reported in Ref. 52. In NONSAP additional concentrated dampers can be specified at selected degrees of freedom of certain nodal points. So, incorporation of viscous boundaries does not require any modification of the programme. Only the constants of the dashpots are required. The use of these viscous boundaries allows the reduction of the overall dimensions of the model.

4.5 Finite Element Meshes

The finite element mesh for static analysis is shown in Fig. 4.5.

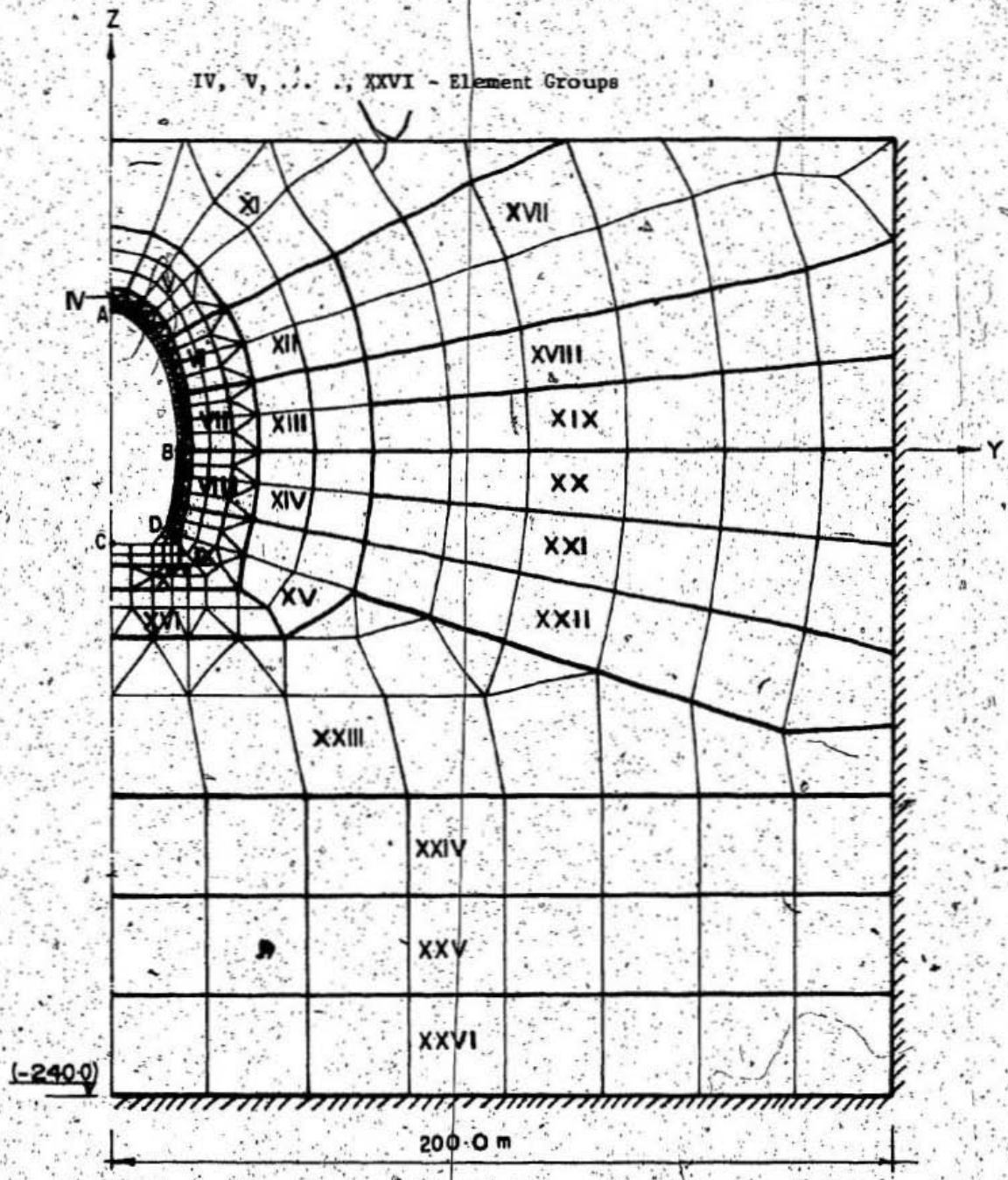

Fig. 4.5 Finite Element Mesh and Element Groups for Static Analysis

It is made up of 370 elements and 478 nodal points. The elements are organized into 26 element groups. The mesh for dynamic analysis (Fig. 4.6) comprised 418 nodal points and 316 elements organized into 23 element groups. Nodal dampers were specified at 13 nodal points to represent the semi-infinite medium as shown. The containment in both cases comprised 84 six-node elements and 4 four-node elements organized in three element groups as shown in Fig. 4.7.

In these meshes, incompatible elements (e.g., joining of the 3-node edge of an element with the 2-node edge of another) were avoided. According to Ref. 29, this incompatibility may cause 10% increase in stresses at certain points and the same ratio decrease in stresses at others.

The aspect ratio (the ratio of an element's smallest dimension to its largest dimension) of the elements was chosen to be near to unity. According to Ref. 46, long, narrow elements should be avoided because they lead to a solution with directional bias that may not be corrected.

Some investigators recommend certain limitations for element size in dynamic analysis because the dimension of the element in the direction of wave propagation has a major influence on the frequency of motions that can be transmitted. Lysmer and Kuhlemeyer [57] proposed the empirical rule that the required element size for effective transmission of any motion should not be more than one-quarter, or preferably one-eighth of the wave length of the motion. However, according to Ref. 84, the element size effect does not show

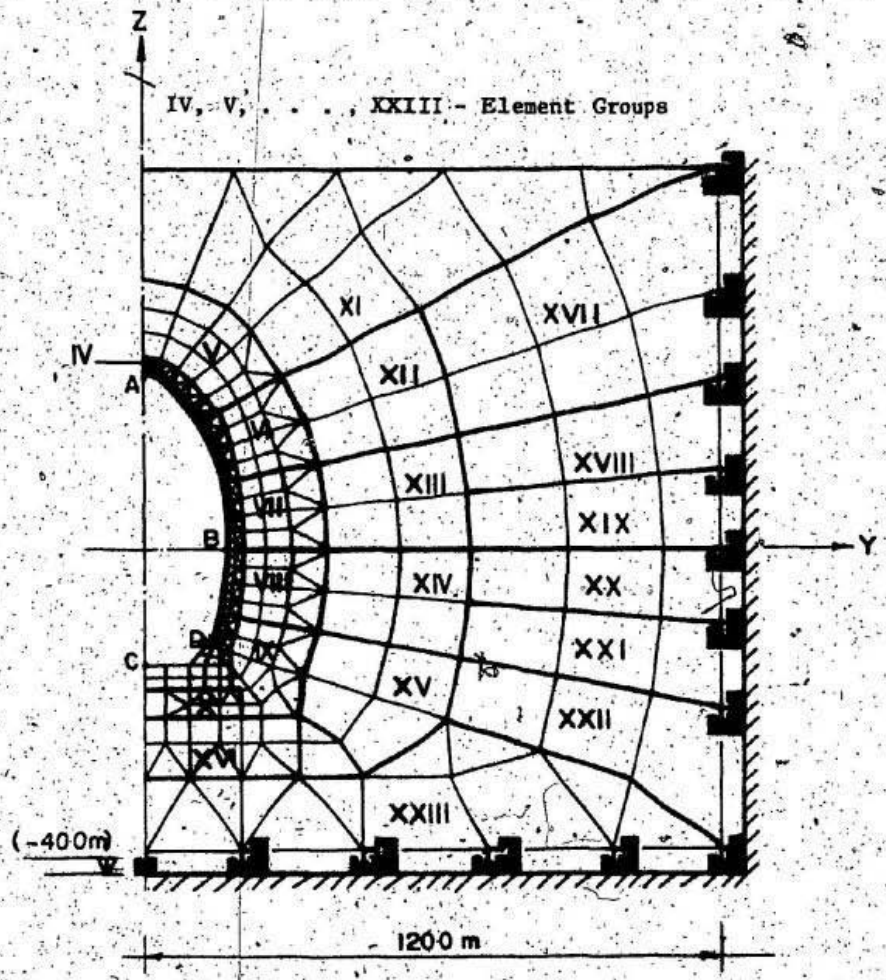

Fig. 4.6 Finite Element Mesh and Element Groups For Dynamic Analysis

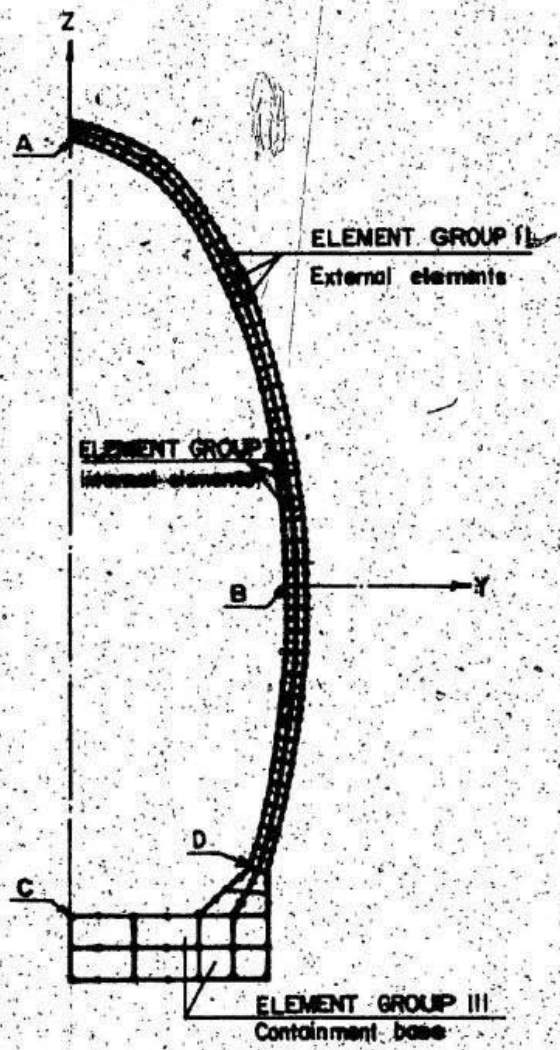

Fig. 4.7 The Finite Elements and Element Groups of the Containment

up in finite element analysis using Rayleigh damping which is the case considered in this study.

4.6 Reinforced Concrete Idealization

The reinforcement and concrete of the containment were idealized by using a single stress-strain relationship and the Pariseau yield condition. The principal directions of orthotropy were defined by the directions of steel reinforcement. Consider the element shown in Fig. 4.8; the direction of the main steel A_{s1} defines the axis, a, of the material. Similar relations to those proposed by Ref. 1, were considered for calculating the composite moduli of reinforced concrete which are given by:

$$E_i = E^c A_i^c + E^s A_i^s \tag{4.35}$$

where E_i = effective composite moduli in the i-direction,

E^c = initial value of modulus of elasticity of concrete ($40{,}000\ MN/m^2$ in this study),

E^s = modulus of elasticity of steel ($200{,}000\ MN/m^2$ in this study),

A_i^s = effective steel ratio in direction i, and

$A_i^c = 1 - A_i^s$ = effective concrete ratio in direction i.

The composite shear modulus is given by a similar relation [1]:

$$G = G^s A_i^s + G^c A_i^c \tag{4.36}$$

in which $G^s = \frac{E^s}{2(1+\nu^s)}$, $G^c = \frac{E^c}{2(1+\nu^c)}$, and ν^c and ν^s are the Poisson's ratios of steel and concrete respectively.

The composite Poisson's ratio of reinforced concrete was taken as constant values in this study. For determining the compressive,

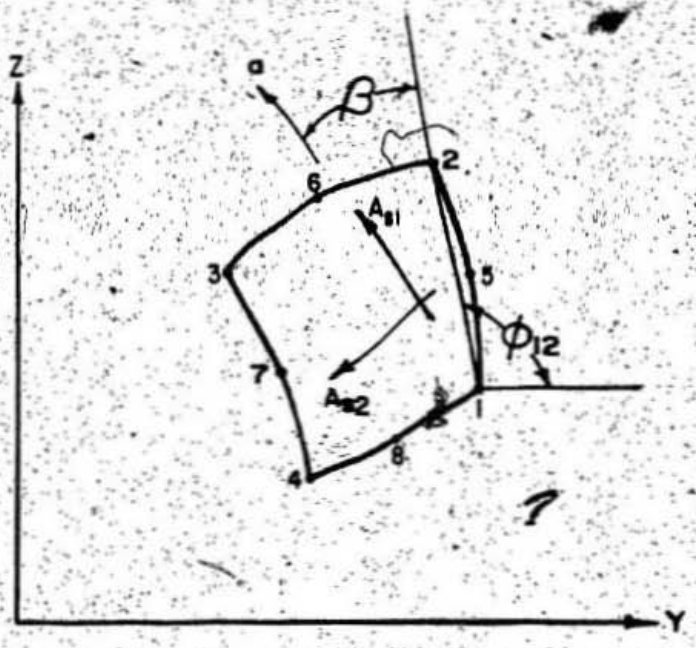

Fig. 4.8 Principal In-Plane Material Axes Orientation for the Reinforced Concrete Model

tensile, and shear strength of reinforced concrete in the principal directions of orthotropy, the same relations were used and the different moduli were replaced by the compressive, tensile and shear strength of both concrete and steel.

4.7 Numerical Illustrations

There are some parameters, other than the discussed before, which affect the solution. The time interval in dynamic analysis, as well as the load increment in static elastoplastic analysis, have great effect on the solution of the problem. Another parameter is the distance of the viscous boundaries from the containment. In this section numerical illustrations are performed to determine acceptable values of these parameters.

The containment considered is of 1.5m thickness. Radial and circumferential reinforcement of the containment are similar to those in Fig. 2.3. The distance between the reinforcing bars (#18 bars) in both directions is taken as 0.25m. Medium sand ($E = 150\ MN/m^2$, $\nu = .15$, $C = .01\ MN/m^2$, and $\phi = 35^o$) is the backfill material of thickness 18.5m, governed by Drucker-Prager yield condition. Sand stone (medium I), underlaid by stiff isotropic granite (medium II), represents the surrounding medium with the Drucker-Prager yield condition for sand stone ($E = 300\ MN/m^2$, $\nu = 0.25$, $\phi = 37.2^o$, and $C = 8\ MN/m^2$) and the Pariseau condition for isotropic granite ($E_{(a,b,c)} = 41{,}200\ MN/m^2$, $\nu = 0.12$, $C_{(a,b,c)} = 161.3\ MN/m^2$, $T_{(a,b,c)} = 5.6\ MN/m^2$, and $R = 50\ MN/m^2$). The load function considered in dynamic analysis is a gradually increasing pressure from zero to 10 bars in 10 seconds.

Five cases are considered to determine the parameters mentioned before:

Case (A): static analysis with load increment equal to 0.5 bar, and the stiffness matrix reformed after each increment.

Case (B): static analysis with load increment equal to 0.25 bar and the stiffness matrix reformed after each increment.

Case (C): dynamic analysis with time step equal to 0.1 second - stiffness matrix reformed after every five steps, side viscous boundaries at a distance 120m from the z-axis, and bottom viscous boundaries 40m below the containment base.

Case (D): dynamic analysis with time step equal to 0.1 second - stiffness matrix reformed after every five steps, side viscous boundaries at a distance 200m from the x-axis, and bottom viscous boundaries 140m below the containment base.

Case (E): dynamic analysis with the time step equal to 0.05 second - stiffness matrix reformed after every five steps, and viscous boundaries similar to that of case (C).

The values of the time step in both the case (C) and (E) are less than a tenth of the natural period of the third mode of the system.

Table 4.2 shows the results for the static and dynamic analyses for an internal pressure of 7 bars of different cases which show an excellent agreement. Fig. 4.9 shows plotting of the response of different points of the containment for case (A), while Fig. 4.10 gives the stress-displacement relationship for case (C) of point D (refer to Figs. 4.5, 4.6 and 4.7) which is the point of maximum stress concentration.

TABLE 4.2 Comparison Between The Response For Different Cases At Internal Pressure 7 Bar

	Case (A)	Case (B)	Case (C)	Case (D)	Case (E)
Displacement (m) X 10^4					
A - vertical	1.0424	1.04067	0.982643	1.03957	0.981797
B - horizontal	2.52482	2.52488	2.52529	2.52523	2.5253
B - vertical	0.372387	0.370532	0.312307	0.369806	0.311335
C - vertical	-0.474915	-0.474921	-0.537827	-0.478262	0.536645
Stresses at D(MN/m^2)					
Max stress	5.15094	5.41142	5.60692	5.60531	5.56906
Min stress	-0.454197	-0.560343	-0.670687	-0.669537	-0.609505
Circumferential stress	4.7171	5.58326	5.90189	5.89817	5.8272

* For points A, B, C and D refer to Figs. 4.5, 4.6 and 4.7

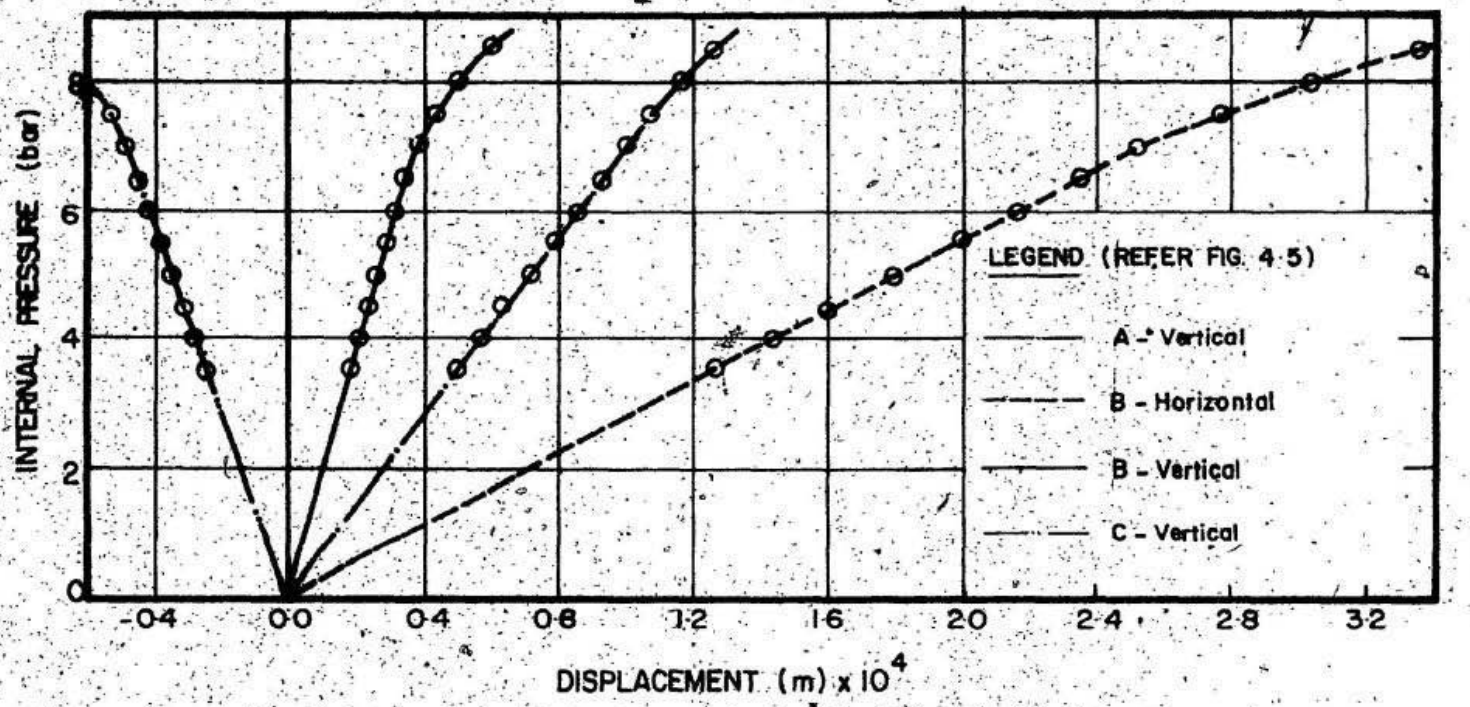

Fig. 4.9 Static Response for Case (A)

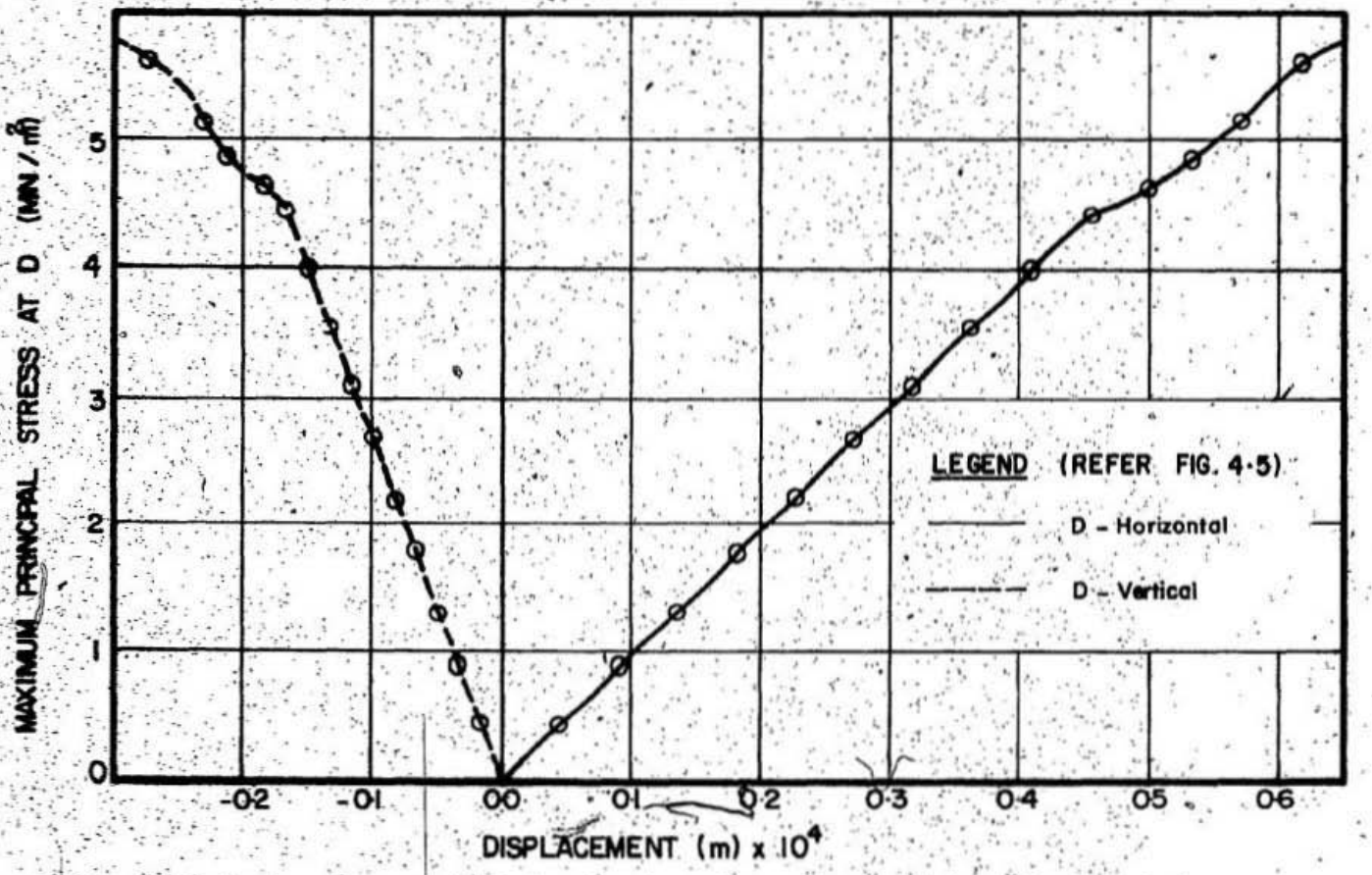

Fig. 4.10 Dynamic Stress-Displacement Relationship at Point D For Case (C).

The loading is gradual and as discussed in Section 4.3 the inertial effects are found to be negligible. From these numerical illustrations, a load increment equal to 0.5 bar for static analysis, a time step equal to 0.1 sec for dynamic analysis, and viscous boundaries similar to that of case (C) seem to be adequate to give an acceptable solution.

CHAPTER V

PARAMETRIC STUDIES

5.1 General

Parametric studies are described to investigate the structural integrity of a 'cut-and-cover' type underground reactor containment. The five different parameters are, stiffness of the backfill, its thickness, reinforcement of the containment, its thickness, and the effect of the medium in which the containment is buried.

5.2 Cases of Analysis

Sixteen different cases of static analysis are analyzed. The properties of concrete and steel reinforcement are kept constant during this study (see Section 4.6). The shape of the containment, its overall dimensions and base thickness, its burial depth and the finite element meshes, have already been considered in the previous chapter. The bottom medium, medium II (see Fig. 4.1), was assumed to be sand stone for all the analysis cases. The configuration of the containment reinforcement, used in this study, is similar to that shown in Fig. 2.3. The loading condition is a linearly increasing internal pressure. The properties of the materials used as backfill and surrounding medium in this study, are given in Table 5.1. The thickness of the containment, backfill, type of reinforcing bars, and the distance between them for different cases of analysis are shown in Table 5.2, while Table 5.3 gives the material used in each element group.

Table 5.1 Properties of the Materials Used as Backfill and Surrounding Medium in Parametric Studies

	E (MN/m^2)	ν	ϕ (degree)	C (MN/m^2)
Sandy Loam (SL)	40.	0.1	38.3°	0.034
Stabilized SL 2% Cement (SL 2%)	1280.	0.11	46.4°	0.24
Stabilized SL 6% Cement (SL 6%)	6500.	0.12	46.1°	1.03
Stabilized SL 10% Cement (SL 10%)	11200.	0.14	44.4°	2.19
Clay (C)	2.2	0.48	1°	0.011
Silty Clay (SC)	40.	0.15	25°	0.09
Sand Stone (SS)	300.	0.25	37.2°	8.

* Drucker-Prager yield condition is used to represent these materials.

Table 5.2 Thickness of Containment and Backfill, and Reinforcement for Different Cases Used in Parametric Studies

Case	Thickness of containment (m)	Thickness of backfill (m)	Reinforcement	
			Bars	Distance between bars (m)
1	1.5	18.5	#18	0.25
2	1.5	18.5	#18	0.25
3	1.5	18.5	#18	0.25
4	1.5	18.5	#18	0.25
5	1.5	12.5	#18	0.25
6	1.5	7.5	#18	0.25
7	1.5	2.5	#18	0.25
8	1.5	18.5	#18	0.35
9	1.5	18.5	#14	0.35
10	1.5	18.5	-	-
11	1.5	18.5	#18	0.25
12	1.25	18.5	#18	0.25
13	2.00	18.5	#18	0.25
14	2.5	7.5	#18	0.25
15	1.5	7.5	#18	0.25
16	1.5	7.5	#18	0.25

Table 5.3 Materials Used in Each Element Group for Different Cases Used in Parametric Studies

Case	Element Groups					
	IV, V, & XI	VI, VII, & VIII	IX	XV	XII-XIV, & XVII-XXII	X, XVI, & XXIII-XXVI
1	SL	SL	SL/SS	SL/SS	SL	SS
2	SL2%	SL2%	SL2%/SS	SL/SS	SL	SS
3	SL6%	SL6%	SL6%/SS	SL/SS	SL	SS
4	SL10%	SL10%	SL10%/SS	SL/SS	SL	SS
5	SL2%	SL/SL2%	SL2%/SL/SS	SL/SS	SL	SS
6	SL2%	SL/SL2%	SL2%/SL/SS	SL/SS	SL	SS
7	SL2%	SL	SL/SS	SL/SS	SL	SS
8	SL2%	SL2%	SL2%/SS	SL/SS	SL	SS
9	SL2%	SL2%	SL2%/SS	SL/SS	SL	SS
10	SL2%	SL2%	SL2%/SS	SL/SS	SL	SS
11	SL2%	SL2%	SL2%/SS	SL/SS	SL	SS
12	SL2%	SL2%	SL2%/SS	SL/SS	SL	SS
13	SL2%	SL2%	SL2%/SS	SL/SS	SL	SS
14	SL2%	C/SL2%	SL2%/C/SS	C/SS	C	SS
15	SL2%	SS/SL2%	SL2%/SS	SS	SS	SS
16	SL2%	SC/SL2%	SL2%/SC/SS	SC/SS	SC	SS

* Refer to Fig. 4.5 for element groups.

* Refer to Table 5.1 for material properties.

5.3 Equilibrium Iteration

The success of the equilibrium iteration procedure, discussed in Ref. 10, depends on the material model, load increment, and reformation of the tangent stiffness matrix. For both static and dynamic analyses, the loading conditions are input into NONSAP as load-time curves. In other words, all forcing functions are input as tables of F(t) versus t, and the solution time step, Δt, for static problems, is used as an equivalent 'load step' or 'loading increment'. Also, an interval of time steps, N_1, for formation of a new tangent stiffness matrix, and a second interval of time steps, N_2, in which equilibrium iteration is to be performed should also be specified. In the analysis of systems with path-dependent material properties, and sufficiently small load steps, N_1 and N_2, success of equilibrium iteration can be expected. Some library material models of the NONSAP (curve description model and the variable tangent moduli model) have not been considered for equilibrium iteration, since solutions using these models, according to Ref. 10, would probably always require small load increments.

The determination of optimum values for load steps, N_1 and N_2, required for the success of equilibrium iteration by trial can consume considerable computer time especially for large structural systems. Comparisons between solutions of different problems, with and without equilibrium iteration, were reported in Ref. 10. These comparisons show, for certain problems, an acceptable percentage of error between the two solutions.

In these parametric studies, a load increment equivalent to 0.5.

bar internal pressure, and stiffness matrix reformation, as well as equilibrium iteration after each step, are specified. It is found that equilibrium iteration fails after certain steps for some cases, and for others, the number of iterations required for equilibrium, is considerably great and time consuming. For example, in case 10, where equilibrium iteration does not fail, an average of five iterations are required for equilibrium with as many as eleven iterations for certain steps. So, decreasing the load increment to a value less than the one indicated, 0.5 bar, was avoided to save computing time. However, two cases, case 2 where equilibrium iteration fails, and case 10 where it does not, were resolved without equilibrium iteration and the comparisons between the two solutions, with and without equilibrium iteration, are presented in Figs. 5.1 and 5.2. The 'kinks' in the curves of case 2, Fig. 5.1, are due to the plastic yield of a large number of elements around the midspan of the containment wall and adjacent backfill elements at this load increment. This is mainly due to the increase of circumferential stresses in these elements, which cause the displacement values at point A and B, to double and decrease, respectively, hence causing failure of equilibrium iteration. The solution path for case 10, Fig. 5.2, is represented by smooth curves which for both solutions, with and without equilibrium iteration, have the same configuration. The differences in the response, during the elastic stage, between the two solutions are very small and the errors increase as load increases in the plastic range. This is also applicable to Fig. 5.1.

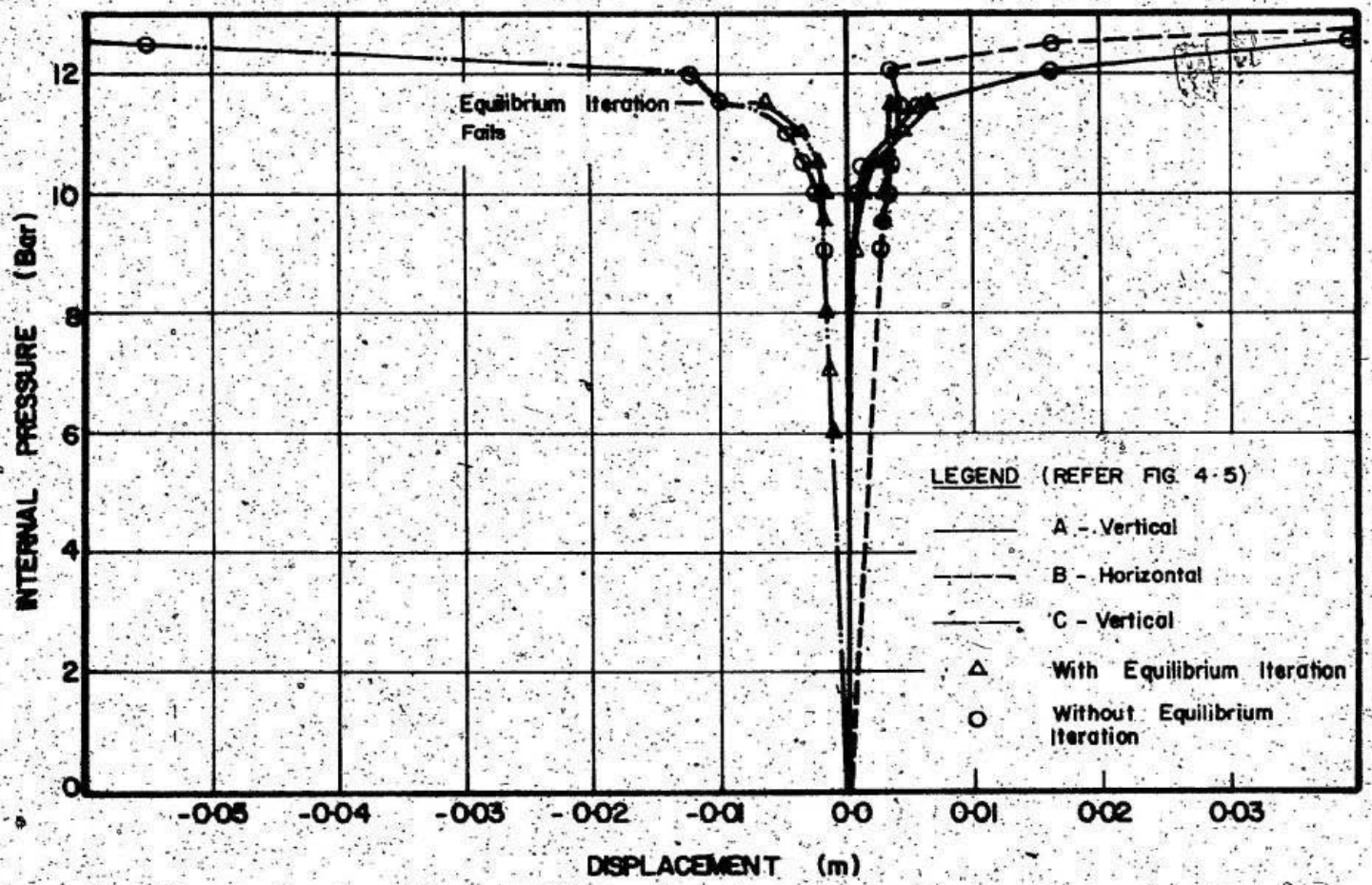

Fig. 5.1 Solutions for Case 2 With and Without Equilibrium Iteration

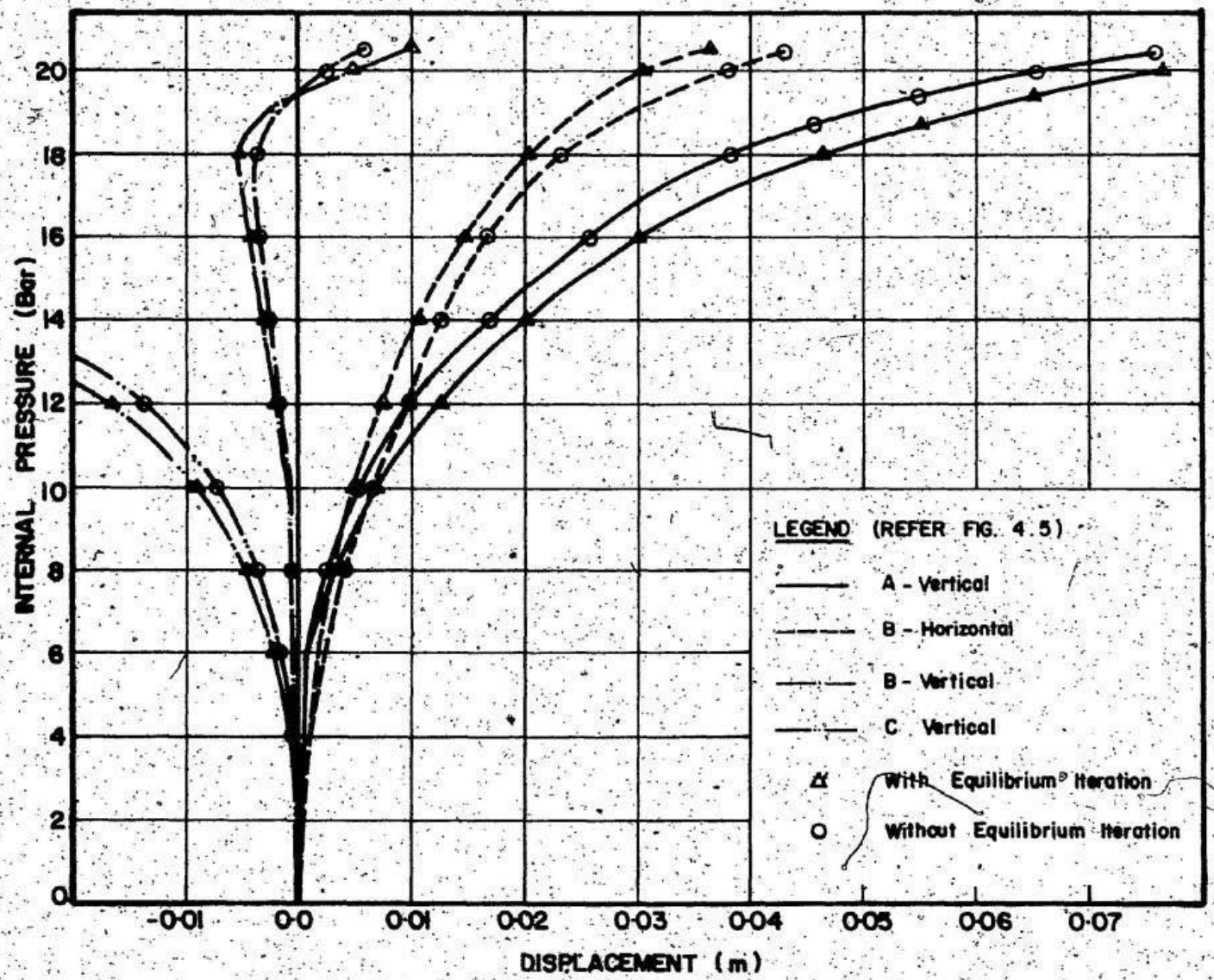

Fig. 5.2 Solutions for Case 10 With and Without Equilibrium Iteration

5.4 Stiffness of Backfill

The effect of the backfill material on the response of the containment is studied by comparing the behaviour of the original and stabilized sandy loam fill with different cement ratios, 2%, 6%, and 10%. The backfill material properties (see Table 5.1) are chosen according to the experimental triaxial shear results reported by Balmer [7], on stabilized soil. Cases 1, 2, 3 and 4 (see Tables 5.2 and 5.3) represent this investigation. The containment considered is of 1.5m thickness with backfill material thickness of 18.5m. The distance between the reinforcing bars (#18 bars) is taken as 0.25m. Sandy loam (medium I) represents the surrounding medium. The comparative values of i) vertical displacement at point A (maximum positive), ii) vertical displacement at point C (maximum negative), iii) vertical and horizontal displacements at B (maximum horizontal displacement), and iv) stress-displacement relationship at point D (maximum principal stress), are presented in Figs. 5.3 to 5.5. The results show that plastic yield starts, at point D at internal pressures 5, 6.5, 9 and 10.5 for cases 1, 2, 3 and 5 respectively, but displacement curves become non-linear at pressures 6.5, 9, 14.5, and 19 when plastic yield starts at some of the midspan elements of the containment wall. The effect of the backfill stiffness is apparent on the vertical and horizontal displacement at A and B, respectively. The results also indicate that the increasing of backfill stiffness by increasing the cement content of the stabilized sandy loam, reduces the displacements and stresses of the containment. For example, at internal pressure 6 bars, using 2% cement, reduces the vertical displacement at A by almost 50% and

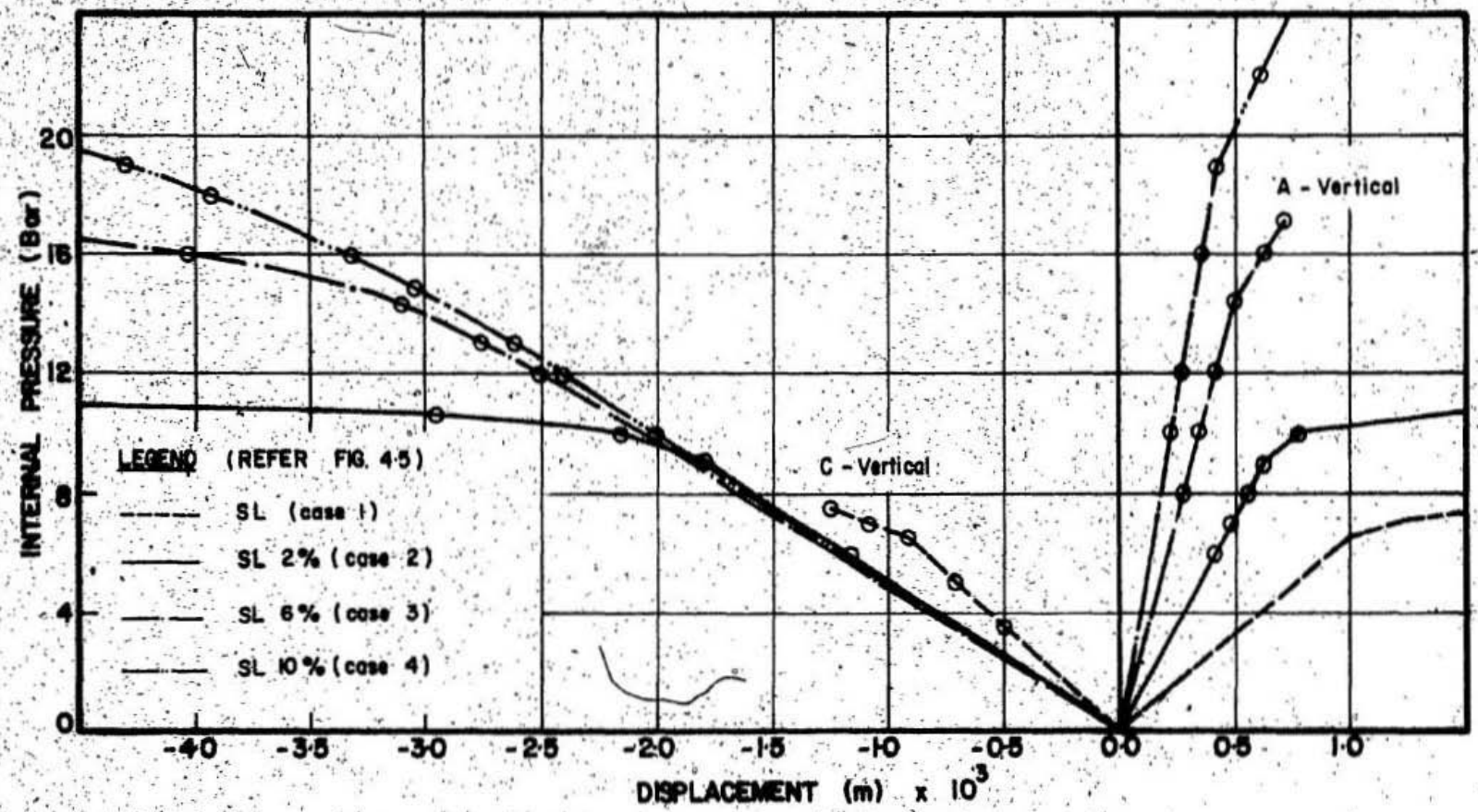

Fig. 5.3 Maximum Positive and Negative Vertical Displacement for Different Backfill Stiffnesses

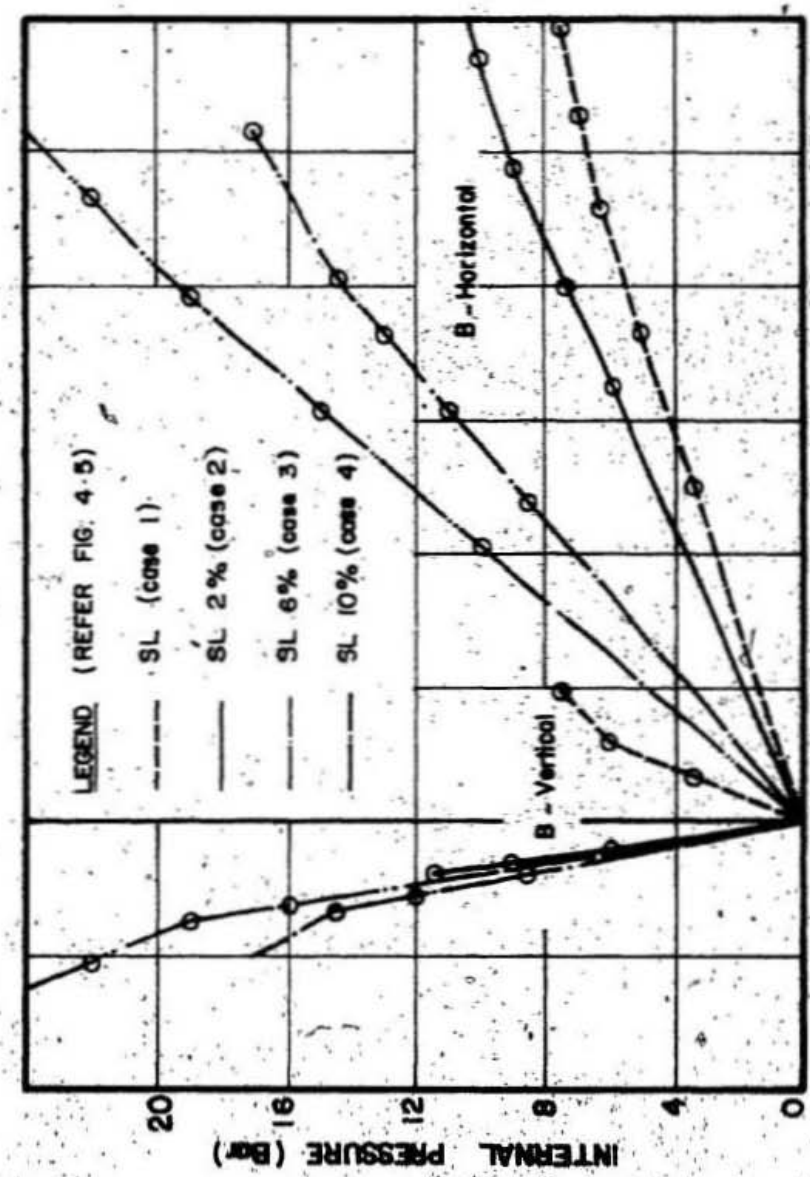

Fig. 5.4 Displacements at the Point of Maximum Horizontal Displacement for Different Backfill Stiffnesses

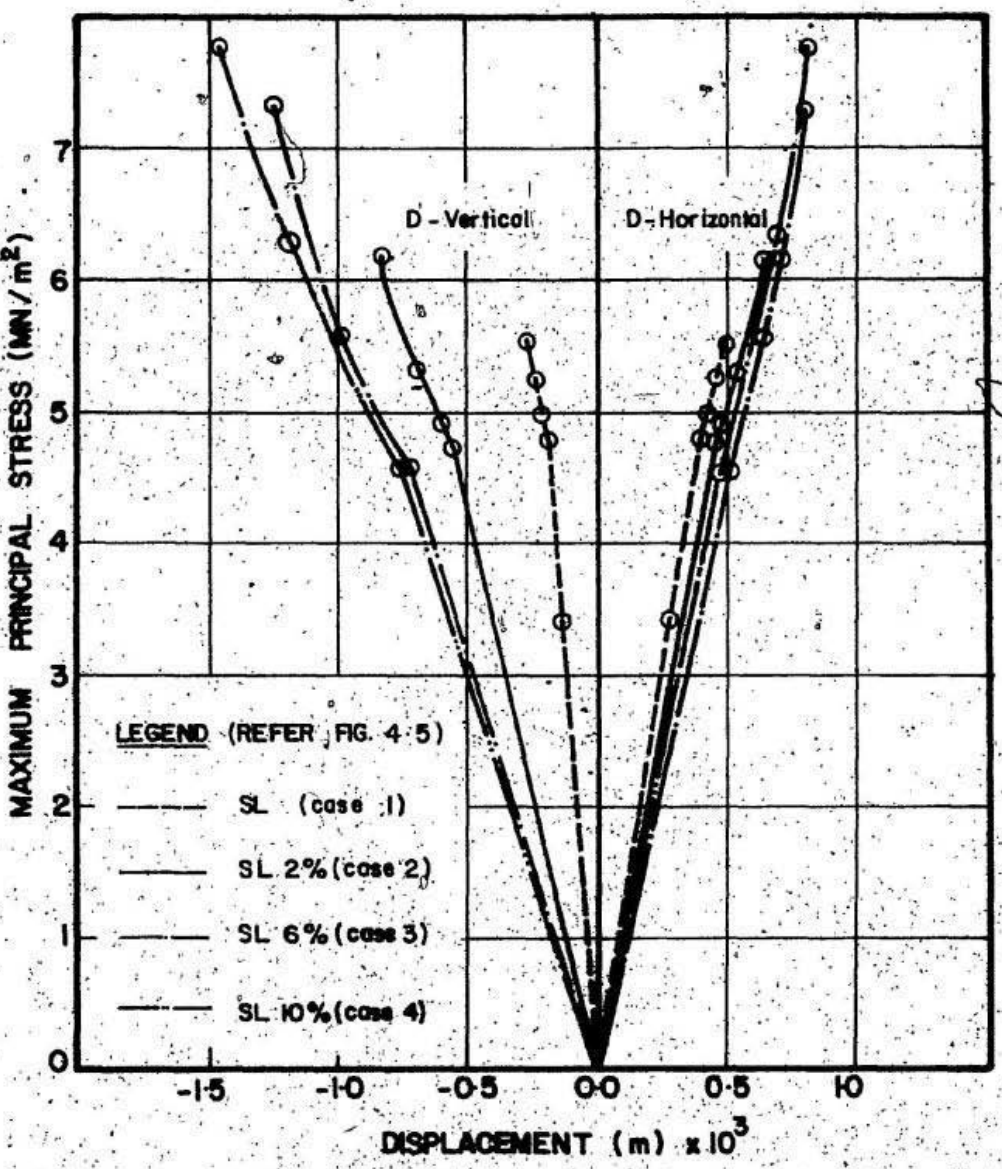

Fig. 5.5 Maximum Principal Stress-Displacement Relationships for Different Backfill Stiffnesses

the horizontal displacement at B by 25%, while using 6% cement reduces both by 50% more. It should also be mentioned here, that according to Ref. 35, the use of stiff materials as backfill increases the stresses in the containment when subjected to earthquake excitation.

5.5 Thickness of Backfill

There are certain factors which affect the determination of the thickness of backfill, such as the type of medium in which the containment is buried, the surrounding installations, and some construction considerations. The effect of the thickness of a 2% stabilized sandy loam backfill on the response of the containment was studied by comparing the behaviour of 18.5, 12.5, 7.5 and 2.5m backfills (cases 2, 5, 6 and 7 respectively). The containment and surrounding medium are similar to those described in the previous section. Comparisons of maximum positive and negative vertical displacements, stress-displacement relationships at point of maximum horizontal displacement are presented in Figs. 5.6, 5.7 and 5.8.

The results show that the use of a thicker backfill increases the maximum positive vertical displacements and decreases the maximum negative values. The differences between the maximum horizontal displacements are amplified in the plastic range. Plastic flow starts at the point of maximum principal stress, D, for cases 2, 5, 6 and 7 at internal pressures 6.5, 6.5, 6 and 6 bars, respectively. Obvious differences are observed, in the four cases considered, between the vertical displacements at points B and D.

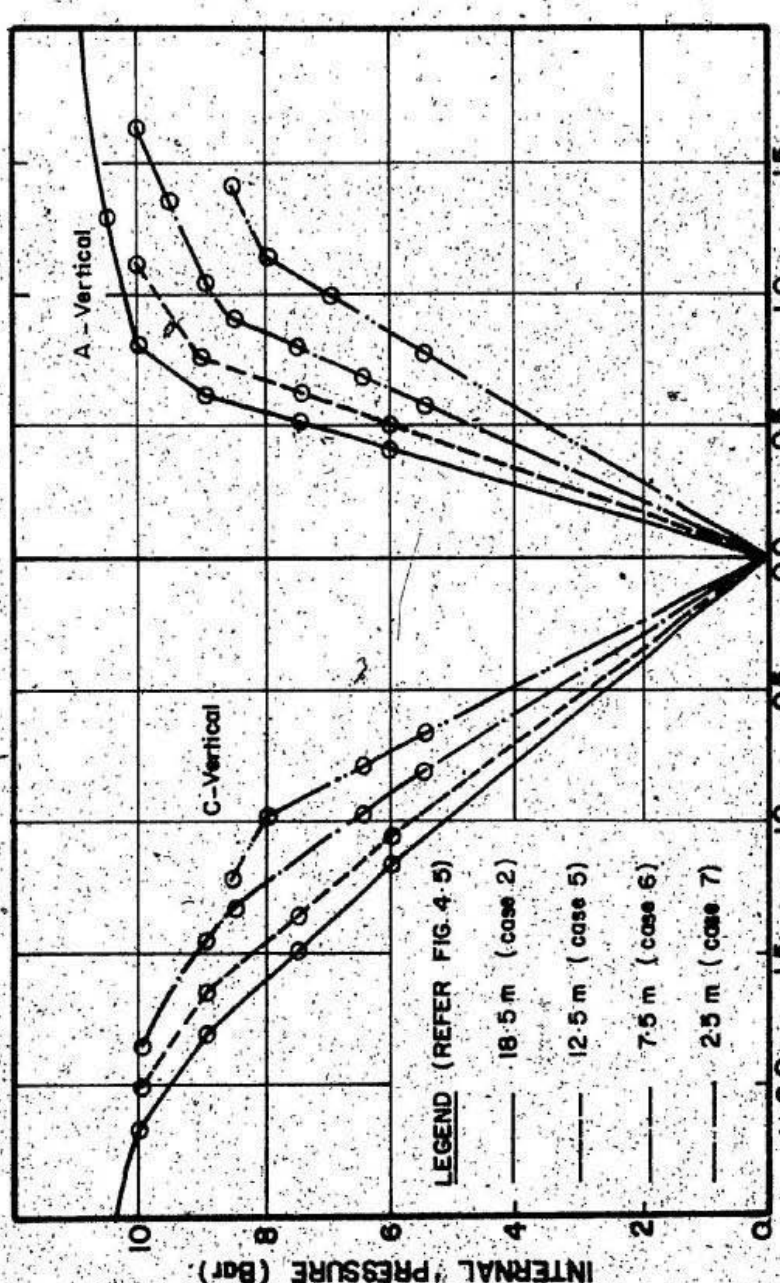

Fig. 5.6 Maximum Positive and Negative Vertical Displacements for Different Backfill Thicknesses

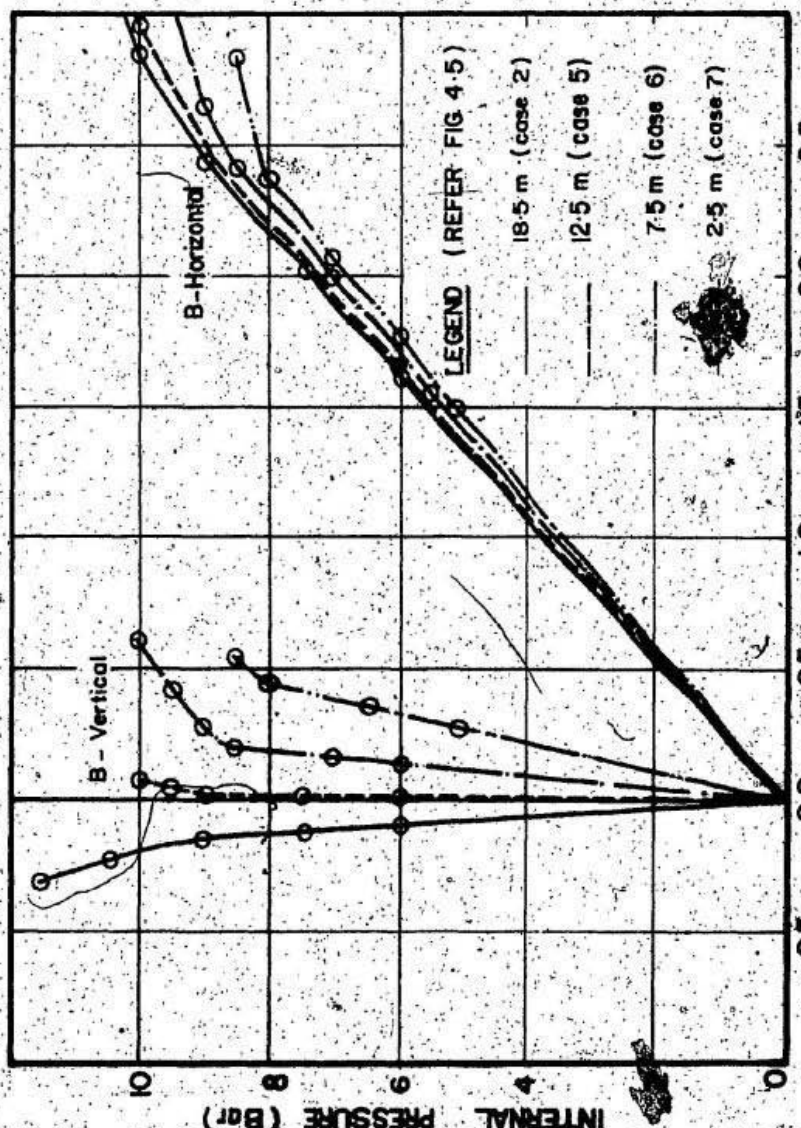

Fig. 5.7 Displacements at the Point of Maximum Horizontal Displacement for Different Backfill Thicknesses

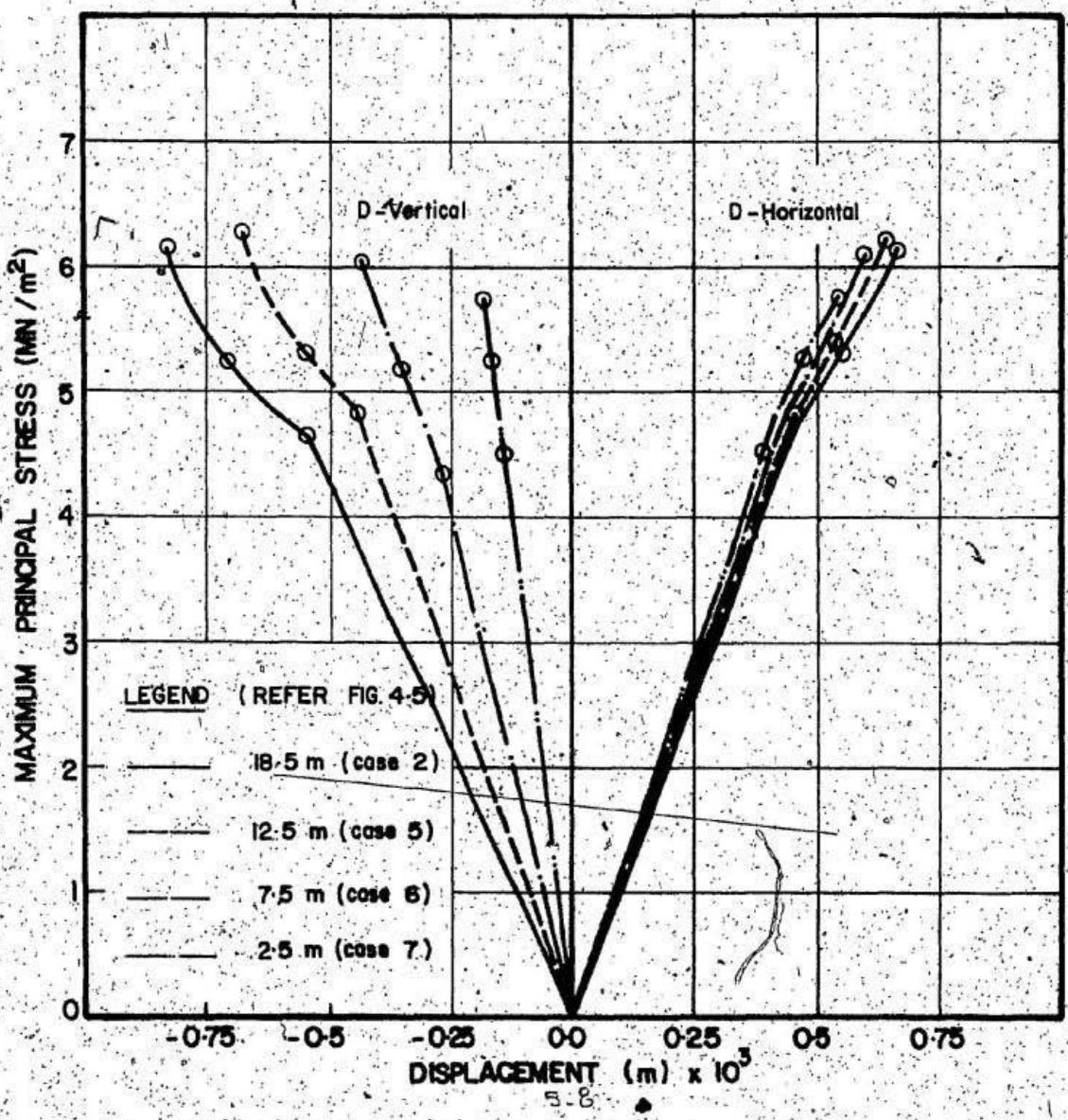

Fig. 5.8 Maximum Principal Stress-Displacement Relationships for Different Backfill Thicknesses

5.6 Stiffness of Containment Structure

The response of any structure is dependent on its stiffness. The two main factors affecting the stiffness of any concrete structure are the dimensions of its sections and the percentage of reinforcing steel. In order to study the effect of these parameters, the containment is assumed to be buried in a sandy loam medium (medium I), underlaid by sand stone (medium II). The backfill is assumed to be 2% stabilized sandy loam of thickness 18.5m (see Figs. 4.5, 4.7 and Table 5.1).

5.6.1 Percentage of Reinforcing Steel

According to Ref. 19, the types of bars used frequently as main reinforcement in reactor containment structures are #18 and #14. The four cases considered in this section are 2, 8, 9 and 10 (see Tables 5.2 and 5.3). The configurations of radial and circumferential reinforcement, shown in Fig. 2.3, are taken as guidelines. For case 2, #18 bars are used with a constant spacing (0.25m) between the reinforcing bars in both directions. The same bars are used with different spacing (0.35) for case 8, and #14 bars with 0.35m for case 9. The containment is assumed to have no reinforcement for case 10.

The results, presented in Figs. 5.9, 5.10 and 5.11, indicate that the small differences between the displacements in the four cases, which appear in the elastic range, start to double in the plastic range. Plastic flow commences at the point of maximum principal stress, D, when the internal pressures are 6.5, 6.5, 6 and 4 bars, for cases 2, 8, 9 and 10, respectively, and at the elements around the midspan of the wall, due to the increase of

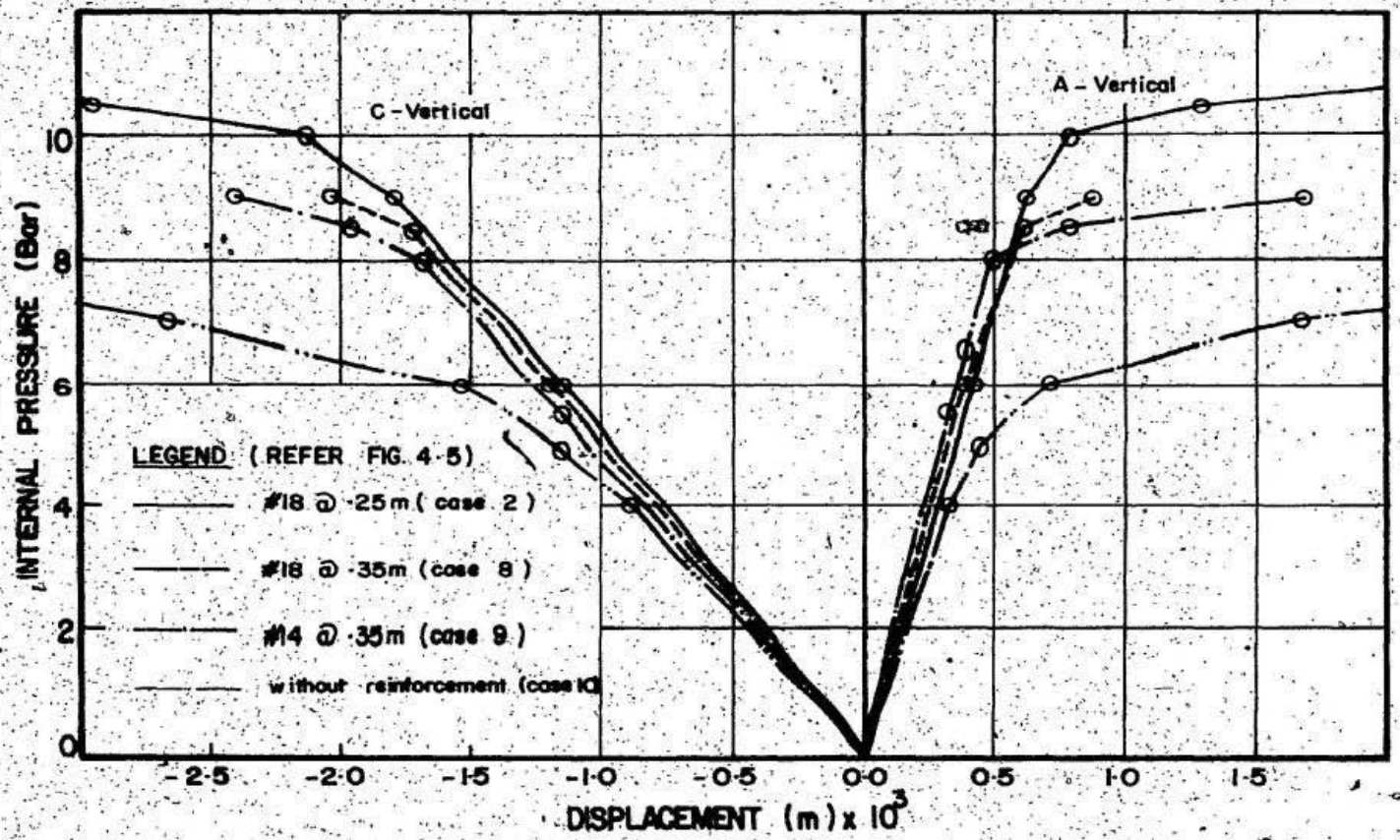

Fig. 5.9 Maximum Positive and Negative Vertical Displacements for Different Cases of Containment Reinforcement

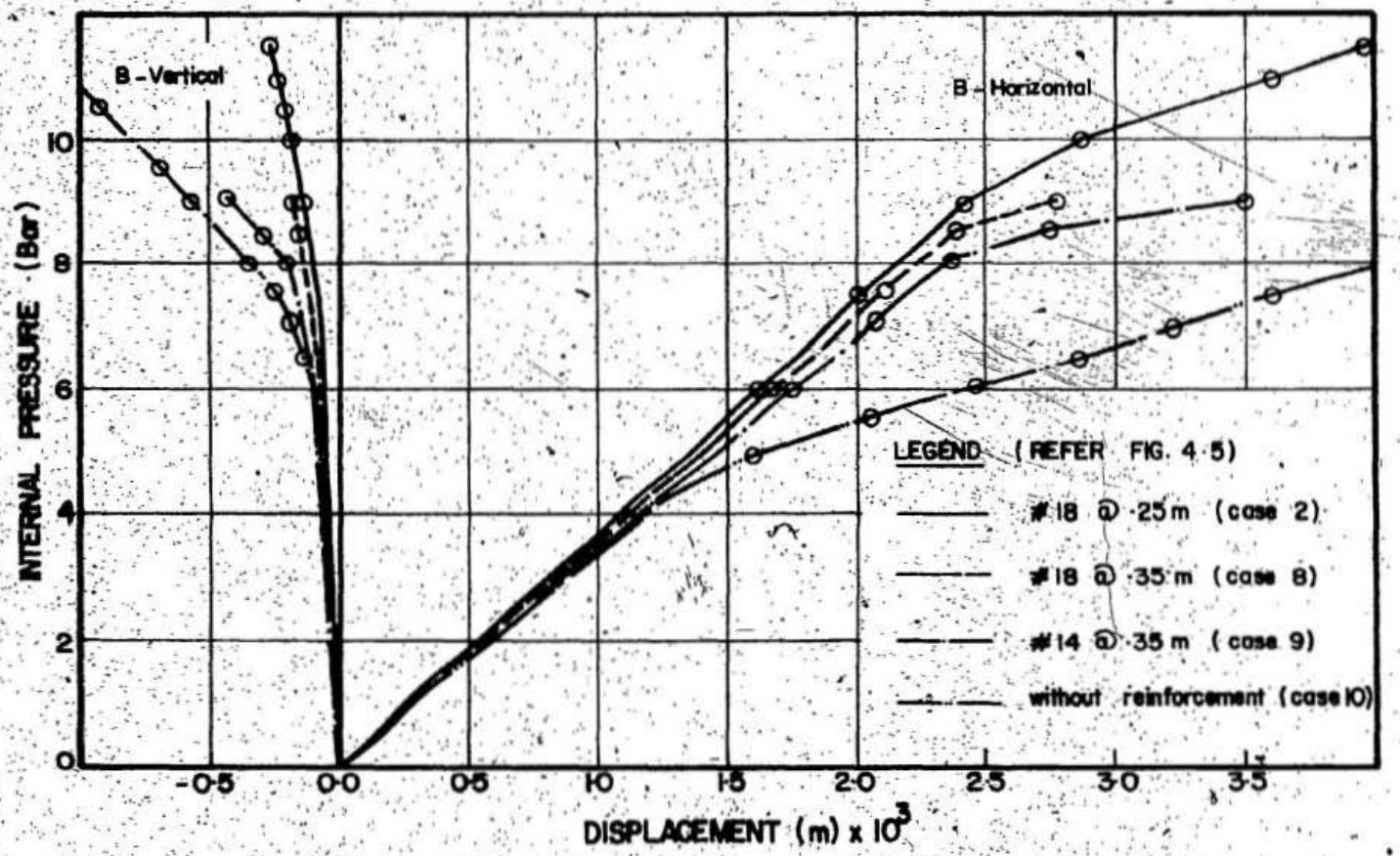

Fig. 5.10 Displacements at the Point of Maximum Horizontal Displacement for Different Cases of Containment Reinforcement

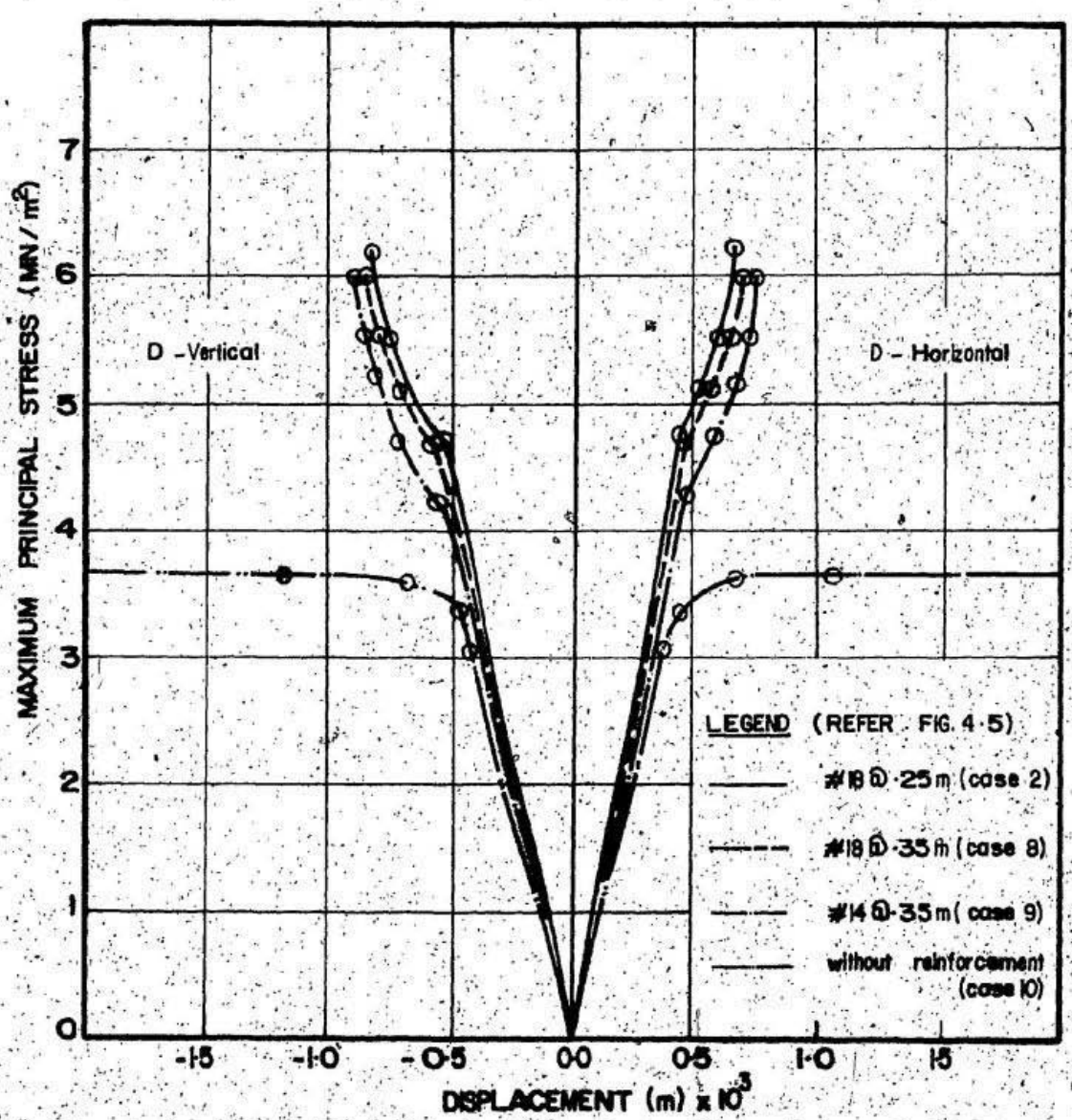

Fig. 5.11 Maximum Principal Stress-Displacement Relationships for Different Cases of Containment Reinforcement

circumferential stresses, when the pressures reach 9, 8.5, 8 and 5 bars.

5.6.2 Thickness of the Containment

Four different cases of containment thickness have been considered in this section. The wall thicknesses in cases 11, 2, 12 and 13 are 1.25, 1.5, 2 and 2.5m, respectively and the base thickness was kept constant at 5m. The results presented in Figs. 5.12, 5.13 and 5.14, show that the containment thickness has greater effect on the response than the other parameters discussed before. Apparent differences between the displacements of the four cases can be observed in the maximum vertical positive and negative values, and in the maximum horizontal displacements. For example, at an internal pressure of 6 bars, the maximum vertical displacement for a containment thickness, 2m, is 50% more than that for the 2.5m thickness and the value for a 1.25m thickness is 50% more than that for 2m thickness. Plastic flow starts at point D when internal pressures reach 5, 6.5, 9 and 11 bars for the cases 11, 2, 12 and 13 respectively, and at elements around the wall midspan for pressures of 8.5, 9, 11.5 and 13 bars. It should be mentioned there that for case 13, the point of maximum principal stress is shifted almost 1.5m below point D.

5.7 Surrounding Medium

This section considers the effect of the surrounding medium (medium I) on the response of the containment. The containment considered is of 1.5m thickness and the spacing between reinforcing bars (#18 bars) in both directions is 0.25m. Stabilized sand with

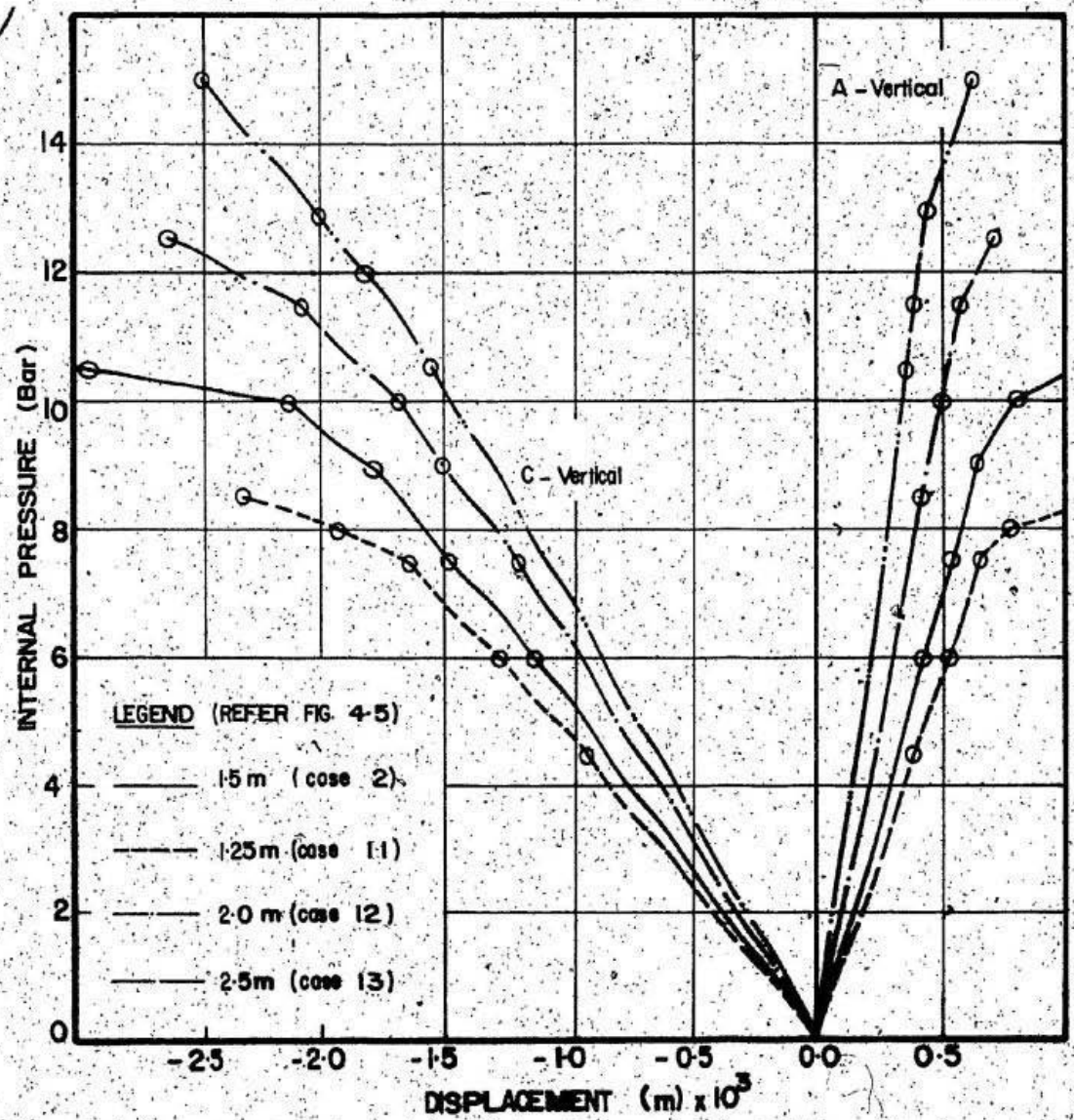

Fig. 5.12 Maximum Positive and Negative Vertical Displacements for Different Containment Thicknesses

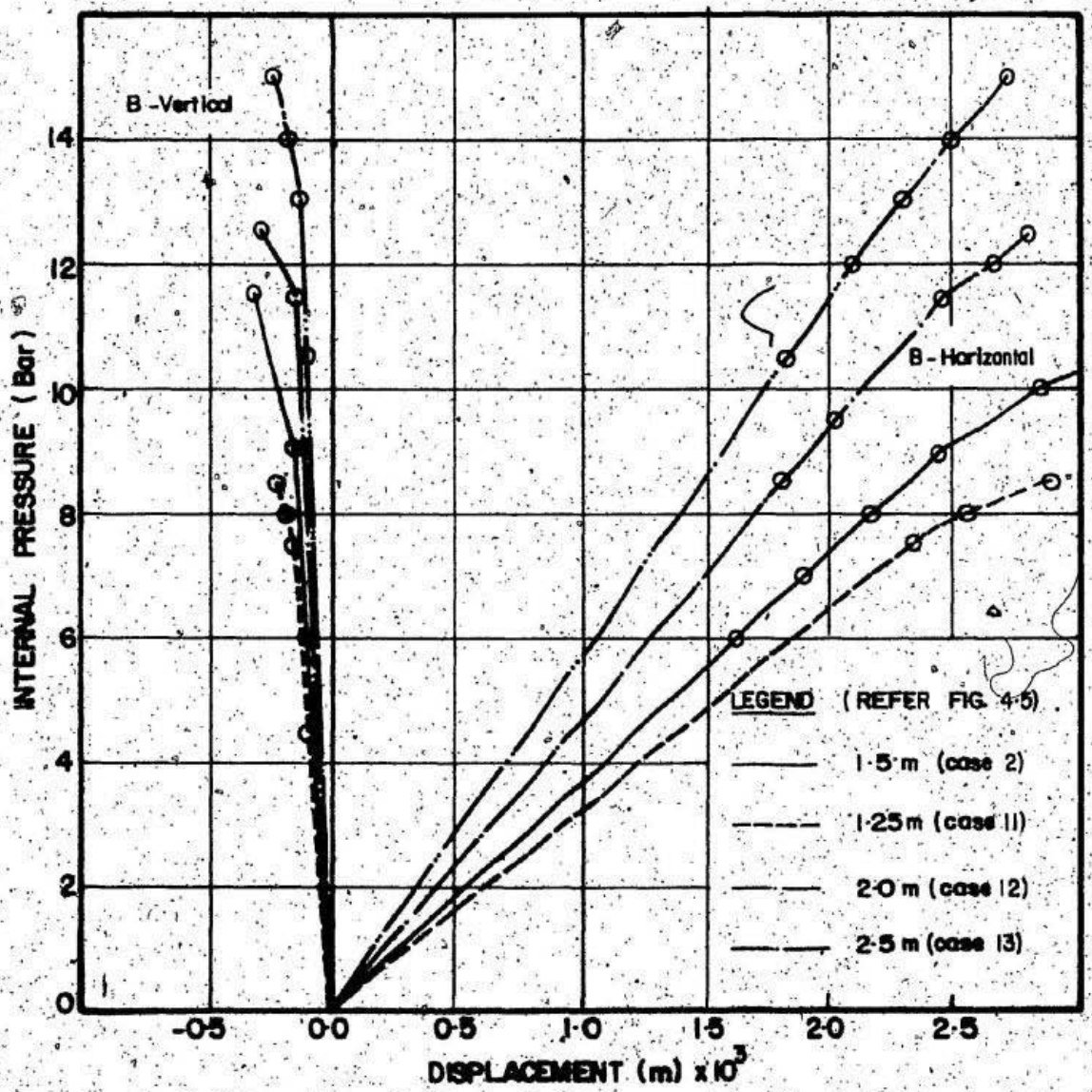

Fig. 5.13 Displacements at the Point of Maximum Horizontal Displacements for Different Containment Thicknesses

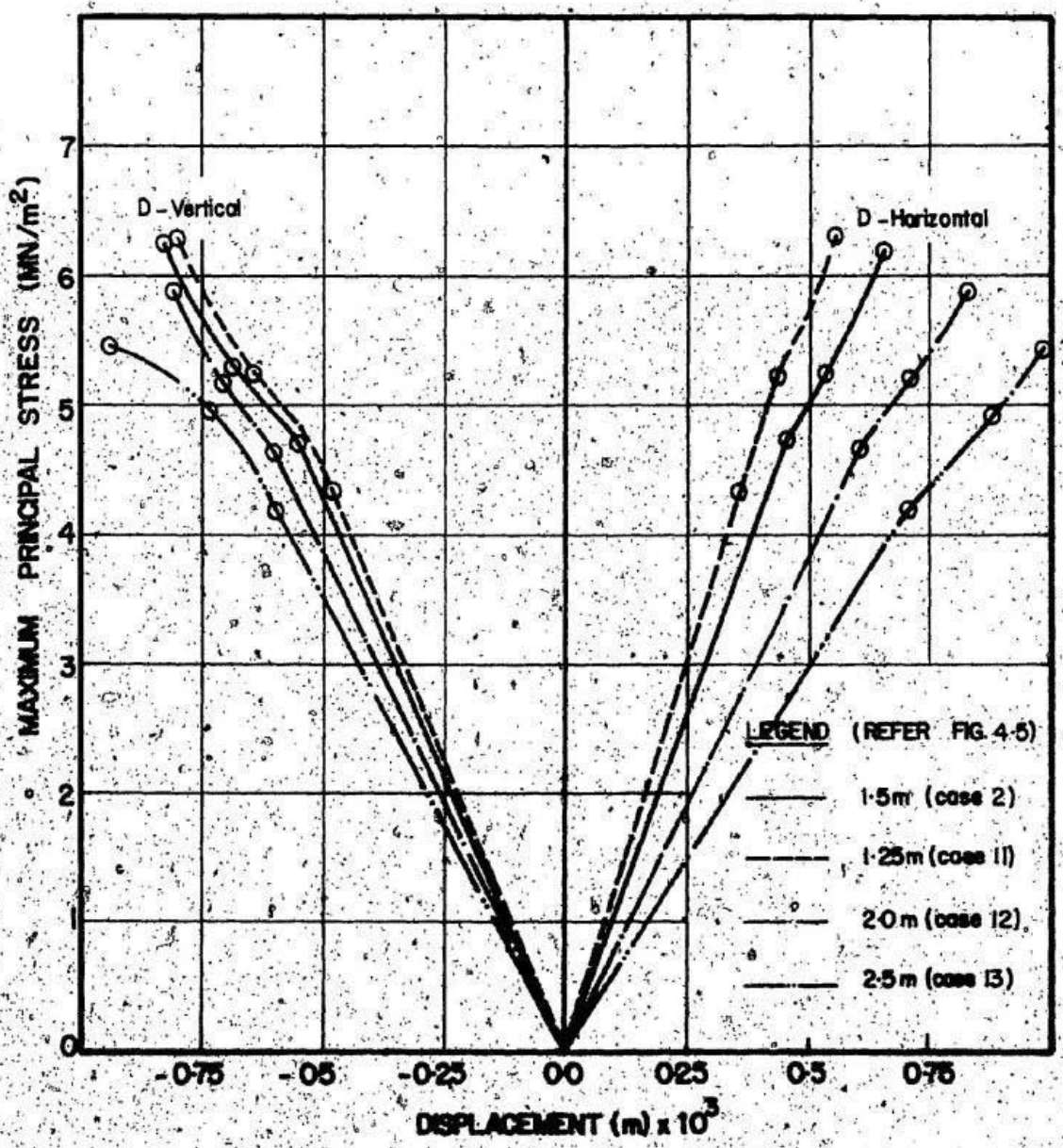

Fig. 5.14 Maximum Principal Stress-Displacement Relationships for Different Containment Thicknesses

2% cement is the backfill material of thickness 7.5m. The containment is resting on a sand stone medium (medium II). The four cases 6, 14, 15 and 16 which describe this study consider sandy loam, clay, sand stone, and silty clay media respectively. The properties of these materials and their distribution on the element groups have already been presented in Tables 5.1, 5.2 and 5.3. Comparisons of the results for different surrounding media are presented in Figs. 5.15, 5.16 and 5.17.

The results show that the surrounding medium affects the maximum positive and negative vertical displacements, as well as the vertical displacements at D. The maximum horizontal displacement at B is almost identical in the four cases, as it seems to be only affected by the stiffness of the backfill and containment. Plastic flow starts at point D for the case of sand stone at 6.5 bars internal pressure, while for other cases it commences at 6 bars. The effect of the surrounding medium on the response of the structure is relatively small compared to the effect of the containment thickness or backfill stiffness.

5.8 Dynamic Analysis for a Typical LOCA

The pressure time-history following MCA has already been discussed in Section 4.3. The pressure time curve used in this analysis is a linear increase from zero to 6 bars in 10 seconds, followed by a decrease to zero in 1000 seconds, which is similar to that estimated in Ref. 99 and shown in Fig. 4.3. A reduced finite element mesh with viscous boundaries, Fig. 4.6, is used and the containment, backfill, and surrounding medium of case 6, are

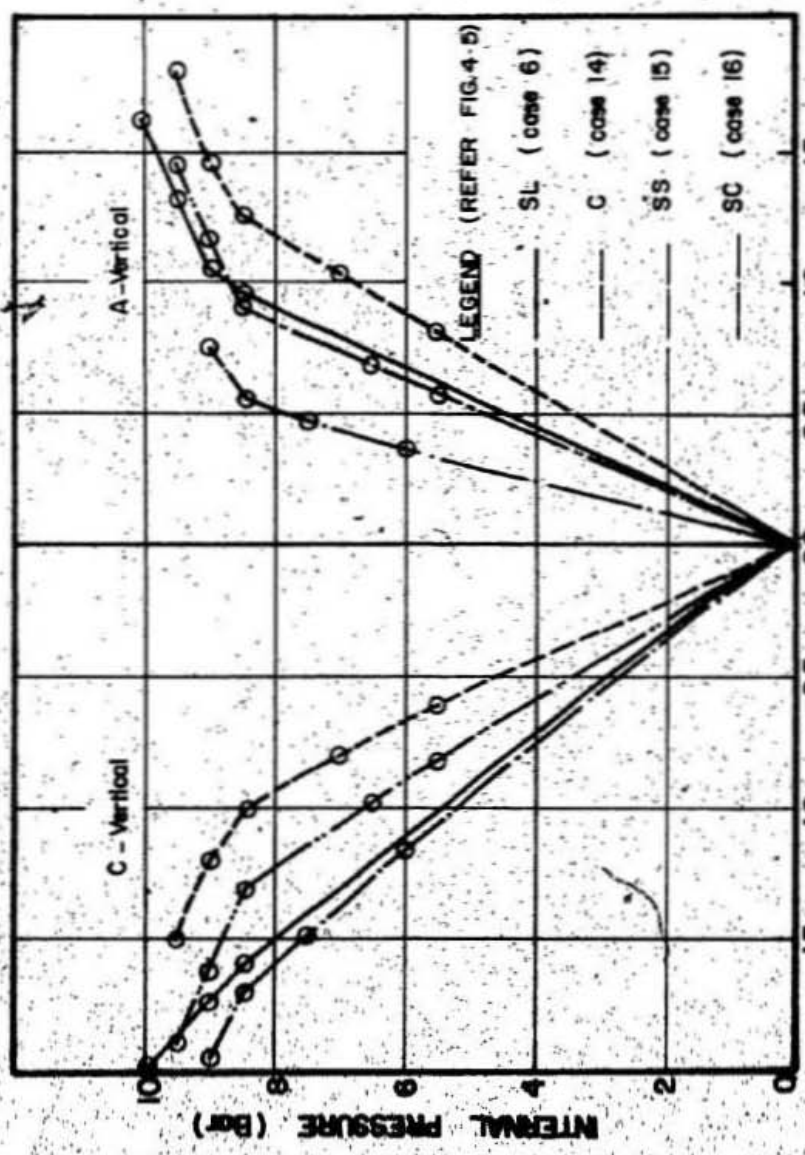

Fig. 5.15 Maximum Positive and Negative Vertical Displacements for Different Media

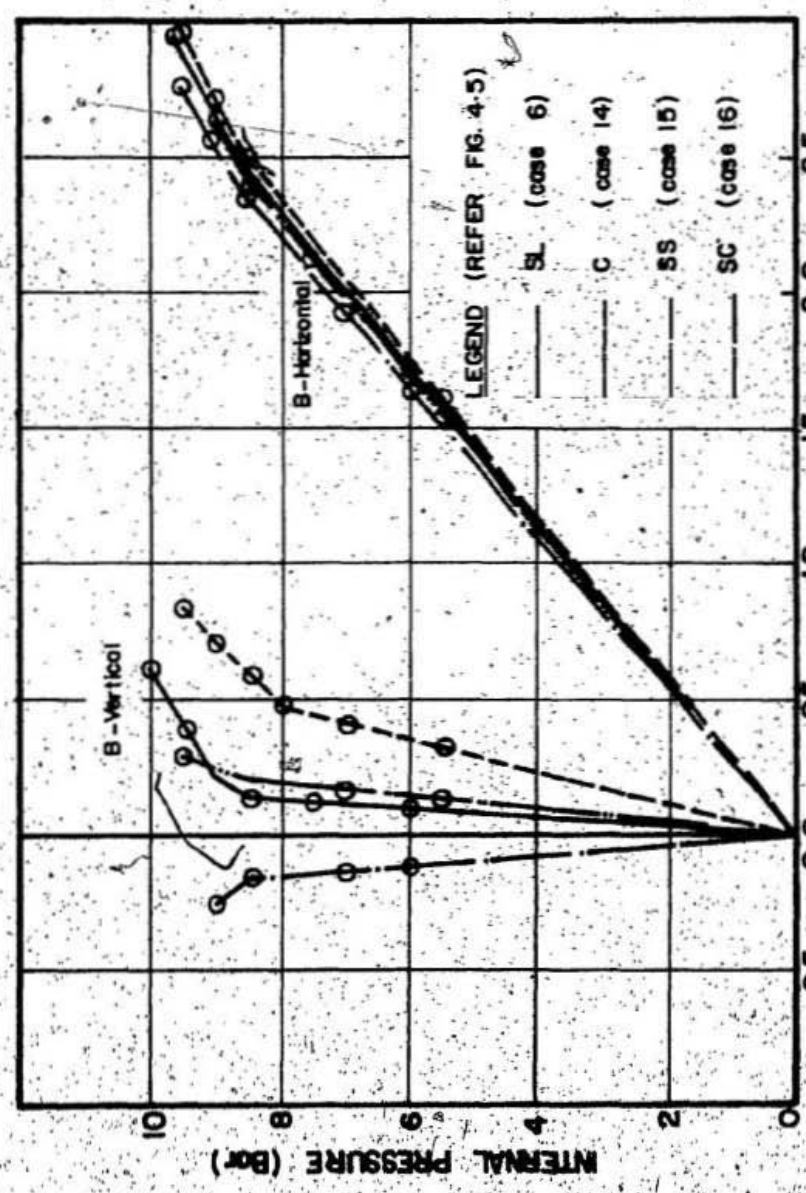

Fig. 5.16 Displacements at the Point of Maximum Horizontal Displacement for Different Media

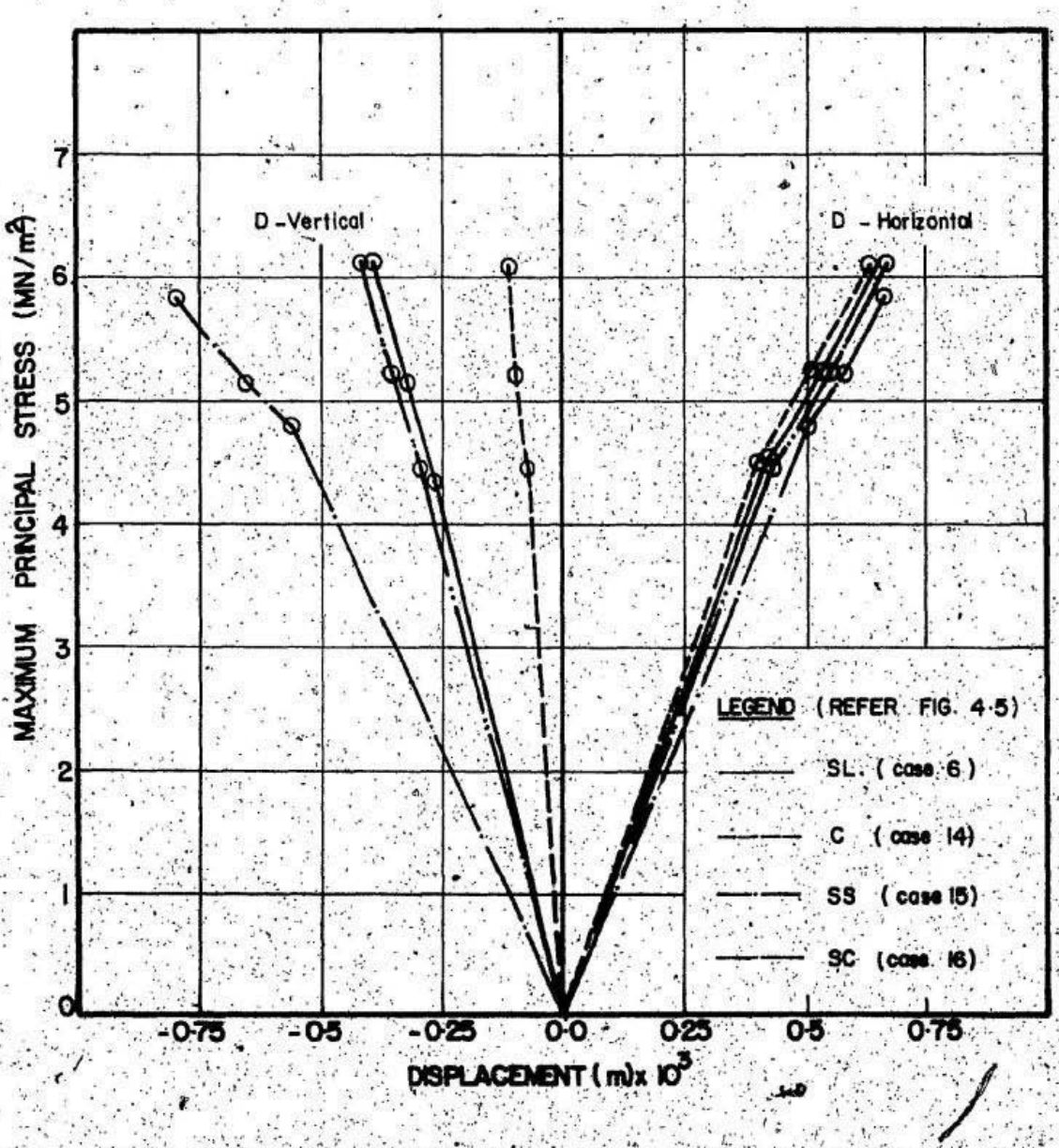

Fig. 5.17 Maximum Principal Stress-Displacement Relationships for Different Media

considered. A dynamic analysis is carried out with the time step equal to 0.1 second, reforming the stiffness matrix after every five steps. The analysis is stopped after 20 seconds to save computing time.

The results, presented in Figs. 5.18 and 5.19, show that the displacements increase linearly until 10 seconds. The following two seconds appear to be a disturbance period, after which a steady decrease is observed. The maximum principal stress increases linearly until 9 seconds when plastic flow starts, then increases with very small rates until 10.5 seconds, and finally decreases. The maximum circumferential stress-time curve is similar to the displacement curves.

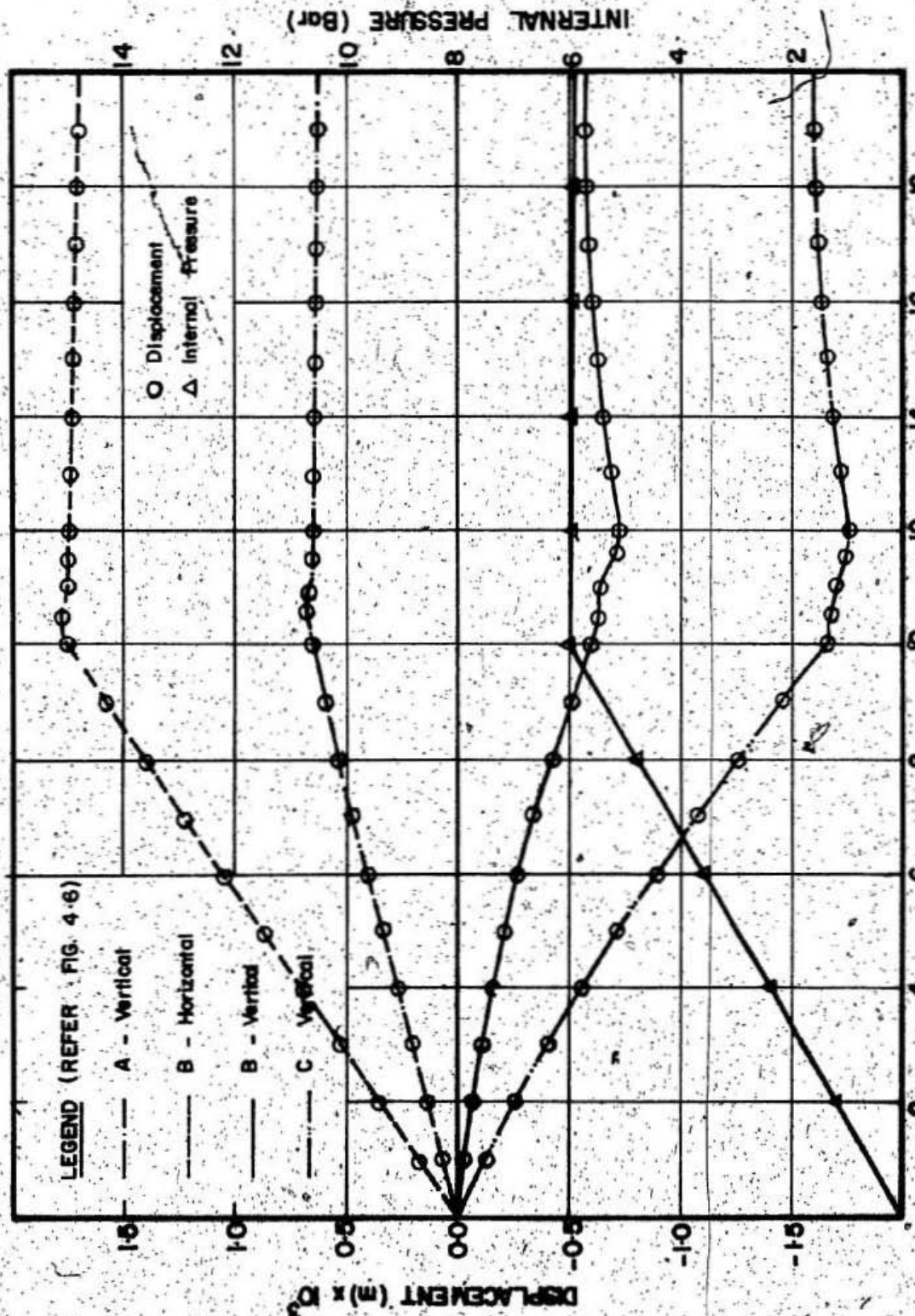

Fig. 5.18 Dynamic Response for a Typical LOCA Analysis

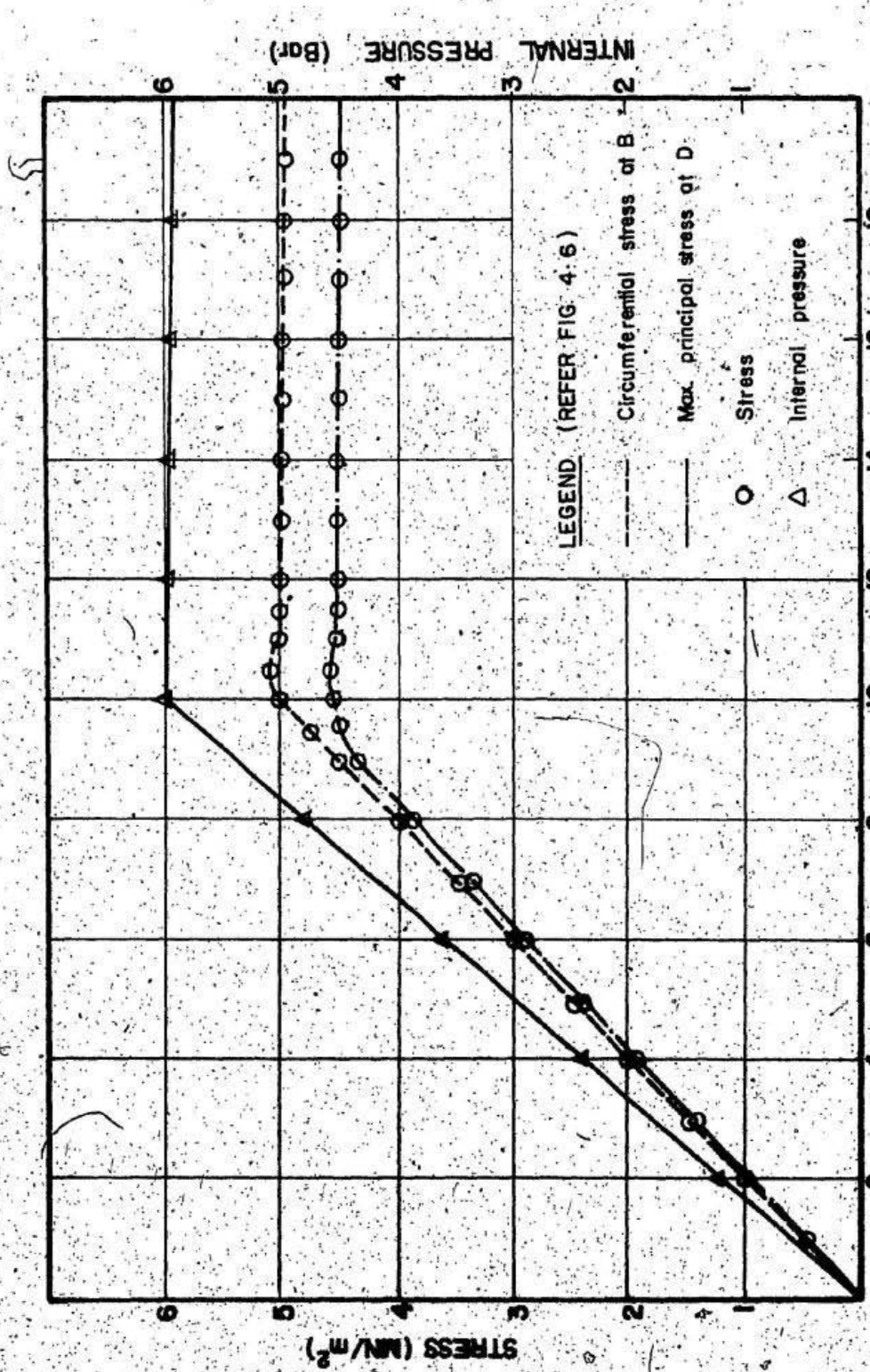

Fig. 5.19 Dynamic Stress-Time Histories for a Typical LOCA Analysis

CHAPTER VI

SUMMARY AND CONCLUSION

6.1 Summary

a. General: The purpose of the investigation is to evaluate the response of a 'cut-and-cover' type underground reinforced concrete nuclear containment, to internal pressurization following an accident, such as a Loss-of-Coolant-Accident (LOCA), and to study the effect of certain parameters on this response.

b. Nonlinear Anisotropic Model: A nonlinear anisotropic model, proposed by Pariseau [74] for anisotropic rocks and soils, has been adapted and incorporated into a general linear and nonlinear, static and dynamic finite element analysis programme, NONSAP, to account for the orthotropic behaviour of reinforced concrete. This model reduces to the von Mises form, when the anisotropy is vanishingly small. After incorporation of the model into the NONSAP, the programme was checked to solve two problems for which structural response computations, from other investigations, are available. The first problem is an isotropic thick-walled cylinder subjected to internal pressure. The second problem is that of a circular hole in a hydrostatic stress field, where the material presented has low strength values in one direction. Excellent agreement is obtained with solutions reported by other investigators.

c. Finite Element Idealization: Idealization of the containment and the surrounding medium for finite element analysis are discussed, and two finite element meshes, for static and dynamic analyses, presented. For dynamic analysis, the viscous boundary approach

proposed by Kuhlemeyer [52], is adopted. A typical case of a containment buried in sand stone and underlaid by stiff granite, with medium sand as backfill material, is analyzed to study the effect of load increment in the static analysis, and the time interval and the distance of the viscous boundaries from the containment in dynamic analysis. A linearly increasing load function is considered for both static and dynamic analyses. A load increment equivalent to 0.5 bar pressure for static analysis, and a time step equal to 0.1 second, with side viscous boundaries at a distance 120m from the containment centre line, and a bottom boundary 40m below the containment base for dynamic analysis, appear to be adequate. Differences in response between dynamic and static analysis, are very small, as the ratio of the pressure rise time, to the natural period of the containment system is greater than 6.

d. Equilibrium Iteration: Stability of the equilibrium iteration procedure, required for the reduction of the divergence of the incremental solution from the true solution, is investigated numerically through two typical cases, one where equilibrium iteration fails, and another where it does not. Each case is solved twice, with and without equilibrium iteration, and comparison between the two solutions, for each case, presented. Equilibrium iteration fails when plastic flow starts at a large number of elements in one load step. However, when it does not fail, it consumes a considerable amount of computing time.

e. Parametric Studies: Parametric studies are carried out for the stiffness and thickness of backfill, reinforcement and thickness of containment and different types of surrounding medium.

Four cases are considered in studying each parameter:

- a) backfill stiffness, the original and stabilized sandy loam fill with different cement ratios, 2%, 6% and 10%,

- b) backfill thicknesses, 2.5, 7.5, 12.5 and 18.5m to study their effect on the response of the containment,

- c) reinforcement: i) #18 bars with constant spacing 0.25m between reinforcement bars in both directions, ii) the same bars with different spacing (0.35m), iii) #14 bars with 0.35m spacing, and iv) a containment without any reinforcement,

- d) wall thickness, 1.25, 1.5, 2.0 and 2.5m,

- e) sandy loam, clay, sand stone, and silty clay, for the effect of the surrounding medium.

The comparative values of i) maximum positive vertical displacement, ii) maximum negative vertical displacement, iii) maximum positive horizontal displacement and iv) stress-displacement relationship at the point of maximum principal stress, are studied for each parameter. Generally, differences are better observed between maximum positive vertical displacements because the containment is assumed to be resting on stiff strata in all cases, which reduces the differences between the maximum negative displacements; the use of double circumferential reinforcement around the point of maximum horizontal displacement reduces the differences between these displacements. Stiffness of the backfill and thickness of the containment have a greater effect than other parameters on the response of the containment. Plastic flow in all cases commences earlier at point of maximum principal stress, but considerable increases in

displacements can be observed when plastic flow starts at elements around the midspan of containment wall, due to the increase in circumferential stresses.

f. Dynamic Analysis For A Typcial LOCA: A case of 'cut-and-cover' containment has been analyzed, considering a typical pressure-time curve following a LOCA. Linear increases in displacements and stresses are observed until the rise time of the curve (10 seconds), then followed by a disturbance period of 2 seconds, after which a steady state response is achieved.

6.2 Conclusions

a. General: The results of the investigation confirmed the effect of the different parameters discussed on the response of the containment. Increasing the stiffness of the backfill material has considerable effect on reducing the response of the containment when subjected to internal pressure, but other types of loading, such as earthquakes, may limit the increase of this stiffness. The main factors which can contribute to the stiffness of the containment are the percentage of steel reinforcement and its thickness. The effect of the former is obvious after plastic flow, while the effect of the latter can be observed in both elastic and plastic stages. The effect of the thickness of backfill, and type of medium on the response of the containment is less compared to other parameters. It is also clear that the parameters are inter-dependent. Plastic flow, in all cases considered, commences first near the wall-base connection which represent the area of maximum stress-concentration, but considerable increases in all displacements are observed when

plastic flow starts at the midspan of the containment wall due to the increase in circumferential stresses. The configuration of containment reinforcement in all the cases considered is similar to the reinforcement of actual containments; redistribution of reinforcement will produce a better distribution of stresses, and initiation of plastic flow in different areas at the same internal pressure.

Dynamic analysis is required when studying the actual response to a typical pressure-time function following a LOCA, for the displacements and stresses continue increasing up to a certain period, even after the pressure rise time has elapsed, and pressure decrease starts. On the other hand ultimate values obtained from static analysis gives an indication of the capacity of the containment as the dynamic magnification factor is close to one.

b. Suggestions For Further Research:

1. The Pariseau model incorporated into the NONSAP in this study, is an isotropic hardening model. Extending this model to account for kinematic hardening theories, which take into account the dependence on the direction of plastic straining, would be a valuable extension of the research presented herein.

2. The Pariseau yield criterion is an anisotropic generalization of the von Mises criterion; generalization of Mohr-Coulomb yield criterion and comparison of results obtained from the two criteria (Pariseau and generalized Mohr-Coulomb), would be of great interest.

3. Extension of the model to account for different rein-

forced concrete complexities (bond, bond slip, dowel action, cracks, etc.).

4. Extensive studies are required to avoid failure of the equilibrium iteration procedure and to reduce the computing time, especially for large systems.

5. Study of different possible configurations of reinforcing steel.

6. Increased complexity of structural detail in the reactor structure (variable thickness, connections with other structures, etc.).

APPENDIX A

LISTING OF THE SUBROUTINES INCORPORATED INTO THE NONSAP CODE

```
      SUBROUTINE ELT209
C
C.....................................................
C.                                                   .
C.   S U B R O U T I N E                             .
C.         TO PERFORM THE FOLLOWING FUNCTIONS :      .
C.              1-INITIALIZING WORKING STORAGE FOR EACH ELEMENT
C.                (IND.EQ.0)                         .
C.              2-CALCULATING STRESS-STRAIN LAW OF EACH ELEMENT
C.                (IND.EQ.4.AND.KPRI.NE.0)           .
C.              3-CALCULATING AND PRINTING(IF REQUIRED)OF STRESSES
C.                IN EACH ELEMENT (IND.EQ.4.AND.KPRI.EQ.0)
C.                                                   .
C.                                                   .
C.   M O D E L  =  9                                 .
C.                                                   .
C.   A N I S O T R O P I C . E L A S T O P L A S T I C  M O D E L
C.   ( P A R I S , E A U )                           .
C.                                                   .
C.....................................................
C
      IMPLICIT REAL*8(A-H,O-Z)
      COMMON /EL     / IND,ICOUNT,NPAR(20),NUMEG,NEGL,NEGNL,IMASS,IDAMP,
     1                 ISTAT,NDOF,KLIN,IEIG,IMASSN,IDAMPN
      COMMON /DIMEL  / N101,N102,N103,N104,N105,N106,N107,N108,N109,N110,
     1                 N111,N112,N113,N114,N120,N121,N122,N123,N124,N125
      COMMON /MATMOD/ STRESS(4),STRAIN(4),D(4,4),IPT,NEL
      COMMON A(1)
      DIMENSION IA(1)
C
      EQUIVALENCE (NPAR(10),NINT),(NPAR(3),INDNL)
      EQUIVALENCE (A,IA)
C
C
C     FOR ADDRESSES N101,N102,N103,... SEE SUBROUTINE TODMFE
C
C
      IDUM=9
      IDU=10
      NCON=14
      IF (INDNL.NE.4) IDU=9
      IF (INDNL.NE.4) IDUM=8
      NPT=NINT*NINT
      MATP=IA(2*N107+NEL-2)
      NN=N109 +.(MATP-1) * NCON
      IF (IND.NE.0) GO TO 100
C
C
C     I N I T I A L I Z E  W A  W O R K I N G  A R R A Y
C
C
      NN=N110 + (NEL -1)*NPT*IDU
```

```
      CALL IMOD9 (A(NN),A(NN),A(NM),NPT,IDM,IDUM)
C
C
      RETURN
C
C
C     F I N D   S T R E S S - S T R A I N   L A W   A N D   S T R E S S
C
C
  100 NS=N110 + ( (NEL-1)*NPT + (IPT-1) ) * IDM
      CALL ANIS (A(NM),A(NS),A(NS+4),A(NS+IDUM))
C
C
      RETURN
C
C
      END
```

```
      SUBROUTINE IMOD9 (WA,IWA,PROP,NPT,IDW,IDUM)
C
C.....................................................................
C.
C.    S U B R O U T I N E
C.          TO INITIALIZE WORKING STORAGE FOR EACH ELEMENT
C.
C.....................................................................
C
      IMPLICIT REAL*8(A-H,O-Z)
      DIMENSION WA(IDW,1),IWA(IDW,1),PROP(1)
C
C
      DO 25 J=1,NPT
C
C
C     SET INITIAL STRESSES AND STRAINS EQUAL TO ZERO
C
C
      DO 15 I=1,IDUM
      WA(I,J)=0.0
   15 CONTINUE
C
C
C     SET INITIAL STRESS STATE TO -ELASTIC-
C
C
      IWA(IDUM+1,J)=1
   25 CONTINUE
C
C
      RETURN
C
C
      END
```

```
      SUBROUTINE ANIS (PROP,SIG,EPS,IPEL)
C
C.....................................................................
C.                                                                    .
C.   S U B R O U T I N E                                             .
C.         TO PERFORM THE FOLLOWING FUNCTIONS :                       .
C.              1-CALCULATING STRESS-STRAIN LAW FOR EACH ELEMENT      .
C.              2-CALCULATING AND PRINTING(IF REQUIRED)OF STRESSES    .
C.                   IN EACH ELEMENT                                  .
C.                                                                    .
C.                                                                    .
C.                                                                    .
C.   IST       NUMBER OF STRESS COMPONENTS                            .
C.   ISR       NUMBER OF STRAIN COMPONENTS                            .
C.   SIG       STRESSES AT THE END OF THE PREVIOUS UPDATE             .
C.   EPS       STRAINS  AT THE END OF THE PREVIOUS UPDATE             .
C.   RATIO     PART OF STRAIN INCREMENT TAKEN ELASTICALLY             .
C.   DELEPS    INCREMENT IN STRAINS                                   .
C.   DELSIG    INCREMENT IN STRESSES, ASSUMUNG ELASTIC BEHAVIOR       .
C.                                                                    .
C.                                                                    .
C.   IPEL      = 1, MATERIAL ELASTIC,                                 .
C.             = 2, MATERIAL PLASTIC                                  .
C.                                                                    .
C.....................................................................
C
C
      IMPLICIT REAL*8(A-H,O-Z)
      COMMON /EL     / IND,ICOUNT,NPAR(20),NUMEG,NEGL,NEGNL,IMASS,IDAMP,
     1                 ISTAT,NDOF,KLIN,IEIG,IMASSN,IDAMPN
      COMMON /VAR    / NG,KPRI,MODEX,KSTEP,ITE,ITEMAX,IREF,IEQREF,INOCMD
      COMMON /DISDER/ DISD(5)
      COMMON /MATMOD/ STRESS(4),STRAIN(4),C(4,4),IPT,NEL
      COMMON /ORT2/ CE(4,4),CEN(4,4)
      COMMON /PAR12/ H,F,G,U,V,W,L,M,N,IST,ISR,STRAIN(4)
      COMMON /TRANS/ T(4,4)
      REAL*8 L,M,N
C
      DIMENSION PROP(1),SIG(1),EPS(1)
      DIMENSION TAU(4),DELSIG(4),DELEPS(4),DEPS(4),STATE(2)
      DIMENSION GRAD(4),D(4,4)
C
      EQUIVALENCE (NPAR(3),INDNL),(NPAR(5),ITYP2D),(DELEPS,DEPS)
C
      DATA NGLAST/1000/, STATE/1HE,1HP/
C
C
C
      IF (IPT.NE.1) GO TO 110
C
      IST=4
      IF (ITYP2D.EQ.2) IST=3
```

```
      ISR=3
      IF (ITYP2D.EQ.0) ISR=4
C
C
C     CALCULATE THE CONSTANTS FOR PARISEAU MATERIAL
C
C
      A = 0.5*(1./PROP(8) + 1./PROP(11) )
      B = 0.5*(1./PROP(9) + 1./PROP(12) )
      Q = 0.5*(1./PROP(10) + 1./PROP(13))
      H = 0.5*(A*A + B*B - Q*Q)
      F = 0.5*(B*B + Q*Q - A*A)
      G = 0.5*(Q*Q + A*A - B*B)
      U = 0.5*(1./PROP(8) - 1./PROP(11))
      V = 0.5*(1./PROP(9) - 1./PROP(12))
      W = 0.5*(1./PROP(10) - 1./PROP(13))
      L = 1./(PROP(14)*PROP(14))
C
C
C     FORM THE STRAIN-STRESS LAW. SYSTEM (A.B.C)
C
C
      DUM = PROP(1)* PROP(2)* PROP(3)* PROP(7)
      IF (DUM.GT.1.0E-08) GO TO 25
      WRITE (6,2010)
      STOP
   25 CE(1,1) =1.0/PROP(1)
      CE(2,2) =1.0/PROP(2)
      CE(3,3) =1.0/PROP(7)
      CE(4,4) =1.0/PROP(3)
      CE(1,2) =-PROP(4)* CE(2,2)
      CE(1,4) =-PROP(5)* CE(4,4)
      CE(2,4) =-PROP(6)* CE(4,4)
      CE(1,3) = 0.0
      CE(2,3) = 0.0
      CE(3,4) = 0.0
      DO 30 I=1,4
      DO 30 J=I,4
   30 CE(J,I) = CE(I,J)
C
C
C     FORM THE STRESS-STRAIN LAW. SYSTEM (A.B.C)
C
C
      CALL POSINV (CE,4,4)
C
      DO 35 I=1,4
      DO 35 J=1,4
   35 CEN(I,J)=CE(I,J)
C
C
```

```
C     FOR PLANE STRESS - CONDENSE STRESS-STRAIN MATRIX-
C
C
      IF(ITYP2D.NE.2) GO TO 45
      DO 40 I=1,3
      A=CEM(I,4)/CEM(4,4)
      DO 40 J=I,3
      CEM(I,J)=CEM(I,J)-CEM(4,J)*A
   40 CEM(J,I)=CEM(I,J)
C
   45 CONTINUE
C
C
C     ROTATE STRAIN TO MATERIAL COORDINATES
C
C
  110 CONTINUE
C
C
      DO 60 I=1,4
      STRAIN(I)=0.
      DO 60 J=1,4
   60 STRAIN(I)=STRAIN(I)+T(I,J)*STRAIN(J)
C
C
C        1. CALCULATE INCREMENTAL STRAINS
C
C
      DELEPS(4) =0.
      DO 120 I=1,ISR
  120 DELEPS(I)=STRAIN(I)-EPS(I)
C
C
C        2. CALCULATE THE STRESS INCREMENT,
C           ASSUMING ELASTIC BEHAVIOR
C
C
      DO 121 I=1,4
  121 DELSIG(I)=0.0
      DO 122 I=1,IST
      DO 122 J=1,ISR
  122 DELSIG(I)=DELSIG(I)+CEM(I,J)*DELEPS(J)
C
C
C        3. CALCULATE TOTAL STRESSES,
C           ASSUMING ELASTIC BEHAVIOUR
C
C
  150 TAU(4) = 0.
      DO 160 I=1,IST
  160 TAU(I) = SIG(I)+ DELSIG(I)
```

```
C
C
C         4. CHECK WHETHER 'TAU' STATE OF STRESS FALLS
C            OUTSIDE THE LOADING SURFACE
C
C
      CALL YIEL2(FT,TAU)
C
      IF (FT) 170,170,300
C
C
C     STATE OF STRESS WHITIN LOADING SURFACE - ELASTIC BEHAVIOR
C
C
  170 IPEL=1
      IF (ITYP2D.EQ.2) STRAIN(4)=EPS(4)-(CE(4,1)*DELEPS(1)+CE(4
     *                          ,2)*DELEPS(2) + CE(4,3)*DELEPS(3))/CE(4,4)
      GO TO 400
C
C
C     STATE OF STRESS OUTSIDE LOADING SURFACE - PLASTIC BEHAVIOR
C
C
  300 IF (IPEL.EQ.1) GO TO 320
C
C
C     .......WAS PLASTIC
C
C
      IPEL=2
      RATIO = 0.
      STRAIN(4)=EPS(4)
      DO 315 I=1,IST
  315 TAU(I)=SIG(I)
      GO TO 370
C
C
C     .......WAS ELASTIC
C
C
C     DETERMINE PART OF STRAIN TAKEN ELASTICLY
C
C
  320 IPEL=2
C
      DUM=0.0
      CALL YIEL2(F0,SIG)
      RATIO1=-F0/(FT-F0)
      DO 1 I=1,4
    1 TAU(I)=SIG(I)+RATIO1*DELSIG(I)
      CALL YIEL2(F2,TAU)
```

```
      CALL GRAD2(GRAD,TAU)
      DO 2 I=1,4
    2 DUM=DUM+GRAD(I)*DELSIG(I)
      RATIO = RATIO1 - F2/DUM
C
      DO 350 I=1,IST
  350 TAU(I)=SIG(I)+RATIO*DELSIG(I)
      IF(ITYP2D.EQ.2) STRAIN(4)=EPS(4)-RATIO*(CE(4,1)*DELEPS(1)
     *                +CE(4,2)*DELEPS(2)+CE(4,3)*DELEPS(3))/CE(4,4)
C
C
C     *TAUM* NOW CONTAINS (PREVIOS STRESSES +
C     STRESSES DUE TO ELASTIC STRAIN INCREMENTS)
C
C
C        5. CALCULATE PLASTIC STRESSES
C
C
C     DETERMINE INCREMENT INTERVAL
C
C
  370 MU=20.0*DSQRT(FT)+1.
      IF (MU.GT.30) MU=30
      XN = (1.-RATIO)/FLOAT(MU)
C
C
      DO 380 I=1,ISR
  380 DEPS(I)=XN*DELEPS(I)
C
C
C     ..... CALCULATION OF ELASTOPLASTIC STRESSES ..... (START)
C
C
      DO 600 IN = 1,MU
C
      CALL ANIMAT(TAU,DEPS)
C
      DO 560 I=1,IST
      DO 560 J=1,ISR
  560 TAU(I)=TAU(I)+C(I,J)*DEPS(J)
C
C
C     CORRECTION
C
C
      DUM = 0.0
      CALL YIEL2(F1,TAU)
      CALL GRAD2(GRAD,TAU)
      DO 1211 I=1,4
 1211 DUM = DUM + GRAD(I)*GRAD(I)
      DUM = F1/DUM
```

```
      TAU(1)=TAU(1)-DUM*GRAD(1)
      TAU(2)=TAU(2)-DUM*GRAD(2)
      TAU(3)=TAU(3)-DUM*GRAD(3)
      IF (ITYP2D.NE.2) TAU(4)=TAU(4)-DUM*GRAD(4)
C
  600 CONTINUE
C
C
C ***** CALCULATION OF ELASTOPLASTIC STRESSES *****  (END)
C
C
  400 STRESS(4)=0.
      DO 390 I = 1,IST
      STRESS(I) =0.
      DO 390 J = 1,IST
  390 STRESS(I)=STRESS(I)+T(J,I)*TAU(J)
C
C
C        6. UPDATING STRESSES, STRAINS
C
C
      DO 410 I=1,IST
  410 SIG(I)=TAU(I)
      DO 420 I=1,ISR
  420 EPS(I)=STRAIN(I)
      IF (ITYP2D .EQ .2) EPS(4) = STRAIN(4)
      IF (KPRI.EQ.0) GO TO 700
C
C
      IF (ICOUNT.EQ.3) RETURN
C
C
C        7. FORM THE MATERIAL LAW
C
C
      IF (IPEL.EQ.1) GO TO 450
C
C     ELASTO-PLASTIC
      CALL ANIMAT(TAU,DEPS)
C
C
C   ROTATE THE STRESS STRAIN LAW TO THE GLOBAL COORDINATES
C
C
C     T(TRANSPOSE) * C(MATERIAL)
C
  461 ISS=4
      IF (ITYP2D . NE . 0) ISS = 3
      DO 61 IR=1,ISS
      DO 61 IC=1,ISS
      D(IR,IC) =0.0
```

```
      DO 51 IN=1,ISS
   51 D(IR,IC) = D(IR,IC) + T(IN,IR)* C(IN,IC)
   61 CONTINUE
C
C
C     T(TRANSPOSE) * C(MATERIAL) * T
C
C
      DO 81 IR=1,ISS
      DO 81 IC=IR,ISS
      C(IR,IC) =0.0
      DO 71 IN=1,ISS
   71 C(IR,IC) = C(IR,IC) + D(IR,IN)* T(IN,IC)
   81 C(IC,IR)=C(IR,IC)
C
C
C
  111 RETURN
C
C
C     ELASTIC
C
C
  450 ISS = 4
      IF (ITYP2D . NE . 0) ISS = 3
      DO 460 I=1,ISS
      DO 460 J=1,ISS
  460 C(I,J)=CEM(I,J)
      GO TO 461
C
C
C     P R I N T I N G  O F  S T R E S S E S
C
C
  700 IF (IPEL.EQ.1) GO TO 800
C
      CALL YIEL2(FT,TAU)
C
C
  800 IF (NG.NE.NGLAST) GO TO 802
      IF (NEL.GT.NELAST) GO TO 806
      IF (IPT-1) 810,808,810
C
  802 NGLAST = NG
  808 IF (ITYP2D) 803,805,803
  803 WRITE (6,2002)
      GO TO 806
  805 WRITE (6,2003)
C
  806 NELAST=NEL
      WRITE(6,2004) NEL
```

```
C
  810 CALL MAXMIN (STRESS,SX,SY,SM)
      IF (ITYP2D) 813,815,813
C
  813 WRITE (6,2005) IPT,STATE(IPEL),(STRESS(I),I=1,3),SX,SY,SM,FT
C
C
      RETURN
C
C
  815 WRITE (6,2007) IPT,STATE(IPEL),STRESS(4),(STRESS(I),I=1,3),
     1                SX,SY,SM,FT
C
C
      RETURN
C
C
 2002 FORMAT (90H ELEMENT STRESS
     1                                          ,21X,5HYIELD/99H NUM/IPT   STAT
     2E      STRESS-YY      STRESS-ZZ      STRESS-YZ          MAX STRESS     M
     3IN STRESS    ANGLE,9X,8HFUNCTION / )
 2003 FORMAT ( 104H ELEMENT STRESS
     1                                                      ,21X,5HYIELD /
     2 113H NUM/IPT    STATE       STRESS-XX      STRESS-YY     STRESS-ZZ
     3    STRESS-YZ       MAX STRESS    MIN STRESS     ANGLE,9X,8HFUNCTION
     4 / )
 2004 FORMAT (I4)
 2005 FORMAT (5X,I2,2X,A1,6HLAST IC,1X,3E14.6,3X,2E14.6,3X,F6.2,3X,E14.6)
 2007 FORMAT (5X,I2,2X,A1,6HLAST IC,1X,4E14.6,3X,2E14.6,3X,F6.2,3X,E14.6)
 2001 FORMAT (1H1,15H STOP PARISEAU )
 2000 FORMAT (10H0*** ERROR/
     1        43H ZERO LENGTH BETWEEN NODES 1-2 IN ELEMENT (,I4,1H))
 2010 FORMAT (45H0***ERROR  MATERIAL PROPERTIES NOT ADMISSABLE  )
C
C
      END
```

```
      SUBROUTINE YIEL2(FT,S)
C
C.....................................
C.
C.    S U B R O U T I N E
C.          TO CALCULATE THE PARISEAU YIELD FUNCTION
C.
C.....................................
C
      IMPLICIT REAL*8(A-H,O-Z)
      COMMON /PARI2/ H,F,G,U,V,W,L,M,N,IST,ISR,STRAIN(4)
      DIMENSION S(1)
      REAL*8 L,M,N
C
C
      S1 = (S(1) - S(2))*(S(1) - S(2))
      S2 = (S(2) - S(4))*(S(2) - S(4))
      S3 = (S(4) - S(1))*(S(4) - S(1))
      S4 = S(3)*S(3)
C
C
      FT=DSQRT(DABS(F*S1+G*S2+H*S3+L*S4))+U*S(4)+V*S(1)+W*S(2)-1.
C
C
      RETURN
C
C
      END
```

```
      SUBROUTINE TRAN (NEL,XX)
C
C.....................................................................
C.                                                                    .
C.    S U B R O U T I N E                                             .
C.          TO GENERATE THE MATRIX REQUIRED FOR TRANSFORMATION OF     .
C.          PROPERTIES FROM LOCAL SYSTEM(A,B,C)TO GLOBAL SYSTEM       .
C.                                                                    .
C.....................................................................
C
      IMPLICIT REAL*8(A-H,O-Z)
      COMMON /TODIN/ BET,THIC,DE,IEL,NNDS
      COMMON /TRANS/ T(4,4)
C
      DIMENSION XX(2,1)
C
      PI = 4.0*DATAN(1.0D0)
C
C
C     COMPUTE THE ANGLE BETWEEN EDGE 1-2 AND THE GLOBAL X-AXIS
C
C
      DX = XX(1,2) - XX(1,1)
      DY = XX(2,2) - XX(2,1)
      XL = DX**2 + DY**2
      IF(XL.GT.1.0E-12) GO TO 102
      WRITE (6,2000) NEL
      STOP
  102 XL=DSQRT(XL)
      SA=DABS(DY/XL)
      AL=DARSIN(SA)
      IF(DX.GE.0.0 .AND. DY.GE.0.0) P12 =          AL
      IF(DX.LT.0.0 .AND. DY.GE.0.0) P12 = PI     - AL
      IF(DX.LT.0.0 .AND. DY.LT.0.0) P12 = PI     + AL
      IF(DX.GE.0.0 .AND. DY.LT.0.0) P12 = PI*2.0 - AL
C
C
C     COMPUTE THE ANGLE BETWEEN THE MATERIAL A-AXIS AND GLOBAL X-AXIS
C
C
      PI2=PI*2.
      IF(DABS(P12).GT.PI2) STOP
      GAN=P12 + BET
      IF (GAN.GE.PI2) GAN=GAN-PI2
C
C
C     SET THE COORDINATE TRANSFORMATION FOR ROTATION OF PROPERTIES
C
C
      IF(DABS(GAN).LT.1.0D-8) GO TO 202
      IF (DABS(PI-GAN) .LT. 1.0D-8) GO TO 202
      IF (DABS(PI2-GAN) .LT. 1.0D-8) GO TO 202
```

```
      SG=DSIN(GAM)
      CG=DCOS(GAM)
      T(1,1) =  CG**2
      T(1,2) =  SG**2
      T(1,3) =  CG* SG
      T(1,4) =  0.0
      T(2,1) =  T(1,2)
      T(2,2) =  T(1,1)
      T(2,3) = -T(1,3)
      T(2,4) =  0.0
      T(3,1) =  T(2,3)* 2.0
      T(3,2) = -T(3,1)
      T(3,3) =  T(1,1)- T(1,2)
      T(3,4) =  0.0
      T(4,1) =  0.0
      T(4,2) =  0.0
      T(4,3) =  0.0
      T(4,4) =  1.0
C
C
      RETURN
C
C
  202 DO 203 I=1,4
      T(I,I) = 1.
      DO 203 J=1,4
      IF (I.EQ.J) GO TO 203
      T(I,J)=0.0
  203 CONTINUE
C
C
      RETURN
C
C
 2000 FORMAT (10H0**** ERROR./
     1        43H ZERO LENGTH BETWEEN NODES 1-2 IN ELEMENT (,I4,1H))
C
C
      END
```

```
      SUBROUTINE ANINAT(TAU,DEPS)
C
C.....................................................
C.                                                   .
C.   S U B R O U T I N E                             .
C.         TO FORM THE ELASTO-PLASTIC MATERIAL MATRIX .
C.                                                   .
C.....................................................
C
      IMPLICIT REAL*8(A-H,O-Z)
      COMMON /EL     / IND,ICOUNT,NPAR(20),NUMEG,NEGL,NEGNL,IMASS,IDAMP,
     1                 ISTAT,NDOF,KLIN,IEIG,IMASSN,IDAMPN
      COMMON /MATMOD/ STRESS(4),STRAIN(4),C(4,4),IPT,NEL
      COMMON /ORT2/ CE(4,4),CEN(4,4)
      COMMON /PARI2/ H,F,G,U,V,W,L,M,N,IST,ISR,STRAIN(4)
C
      EQUIVALENCE (NPAR(5),ITYP2D)
      DIMENSION TAU(1),DEPS(1)
      DIMENSION GRAD(4),AQ(4)
      REAL*8 L,M,N
C
C
      CALL GRAD2(GRAD,TAU)
      DO 10 I = 1,4
      AQ(I) = 0.0
      DO 10 J = 1,4
   10 AQ(I)=AQ(I)+CE(I,J)*GRAD(J)
      PHI = 0.0
      DLAMDA = 0.0
      DO 20 I = 1,4
   20 PHI = PHI + GRAD(I)*AQ(I)
      IF (ITYP2D .NE. 2) GO TO 80
      DEPS(4) = 0.
      DUM=CE(4,4)-AQ(4)*AQ(4)/PHI
      DO 70 I = 1,3
   70 DEPS(4)=DEPS(4)-(CE(4,I)-AQ(4)*AQ(I)/PHI)*DEPS(I)
      DEPS(4) = DEPS(4)/DUM
   80 ISS = 4
      IF (ITYP2D .EQ. 1) ISS = 3
      DO 30 I = 1,ISS
   30 DLAMDA = DLAMDA + AQ(I)*DEPS(I)
      DLAMDA = DLAMDA/PHI
      DO 35 I = 1,4
      DO 35 J = 1,4
   35 C(I,J) = 0.0
      IF (DLAMDA .LE. 0.0 ) GO TO 50
      DO 40 I = 1,4
      DO 40 J = 1,4
   40 C(I,J)=AQ(I)*AQ(J)/PHI
   50 DO 60 I = 1,4
      DO 60 J = 1,4
   60 C(I,J)=CE(I,J)-C(I,J)
```

```
      IF (ITYP2D .LT. 2) GO TO 100
C
C
C FOR PLANE STRESS CONDENSE STRESS-STRAIN MATRIX
C
C
      DO 95 I = 1,3
      A = C(I,4)/C(4,4)
      DO 95 J = I,3
      C(I,J) = C(I,J) - C(4,J)*A
   95 C(J,I) = C(I,J)
      DEPS(4) = - (C(4,1)*DEPS(1) + C(4,2)*DEPS(2) + C(4,3)*DEPS(3))/
     *          C(4,4)
      STRAIN(4) = STRAIN(4) + DEPS(4)
  100 CONTINUE
C
C
      RETURN
C
C
      END
```

```
      SUBROUTINE GRAD2 (GRAD,S)
C
C . . . . . . . . . . . . . . . . . . . . . . . . . . . . . . . . . . .
C .                                                                   .
C .   S U B R O U T I N E                                             .
C .          TO CALCULATE STRAIN-INCREMENT RELATIONS , REFERED TO THE.
C .                PRINCIPAL AXES OF ANISOTROPY                       .
C .                                                                   .
C . . . . . . . . . . . . . . . . . . . . . . . . . . . . . . . . . . .
C
      IMPLICIT REAL*8(A-H,O-Z)
      COMMON /PARI2/ H,F,G,U,V,W,L,M,N,IST,ISR,STRAIM(4)
      DIMENSION S(1),GRAD(1)
      REAL*8 L,M,N,I
C
C
      S1 = S(1) - S(2)
      S2 = S(2) - S(4)
      S3 = S(4) - S(1)
      S4 = S(3)
C
C
      I=DSQRT(DABS(F*S1*S1+G*S2*S2+H*S3*S3+L*S4*S4))
      I = 1./I
C
C
      GRAD(1) = I*(F*S1 - H*S3) + V
      GRAD(2) = I*(G*S2 - F*S1) + W
      GRAD(3) = I*L*S4
      GRAD(4) = I*(H*S3 - G*S2) + U
C
C
      RETURN
C
C
      END
```

BIBLIOGRAPHY

1. Adham, S., Bhaumic, A., and Isenberg, J., "Reinforced Concrete Constitutive Relations", Report No. AFWL-TR-74-72, Feb. 1975.

2. American Concrete Institute, "Criteria for Reinforced Concrete Nuclear Power Containment Structures", ACI Committee 349, 1971.

3. American Society of Civil Engineers, "Structural Analysis and Design of Nuclear Plant Facilities", Draft, Trial-Use and Comment, Editing Board and Task Groups of the Committee on Nuclear Structures and Materials, Structural Division of the ASCE, 1975.

4. Argyris, J.H., Faust, G., Szimmat, J., Warnke, E.P., and Willam, K.J., "Finite Element Ultimate Load Analysis of Three-Dimensional Concrete Structures", ISD-Report No. 174, Univ. of Stuttgart, 1974.

5. Argyris, J.H., Faust, G., and Willam, K.J., "Limit Load Analysis of Thick-Walled Concrete Structures", ISD-Report No. 166, Univ. of Stuttgart, 1975.

6. Augustin, W., Kafka, P., Bauer, J., Schveller, G.I., Zech, B., and Wittmann, F.H., "A Complex Study on the Reliability Assessment of the Containment of a BWR", Nuclear Eng. and Design, Vol. 48, pp. 563-593, 1978.

7. Balmer, G.G., "Shear Strength and Elastic Properties of Soil-Cement Mixtures Under Triaxial Loading", Proc. of the Sixty-First Annual Meeting of the ASTM, June 1958.

8. Bathe, K.J., "ADINA, A Finite Element Program for Automatic Dynamic Incremental Nonlinear Analysis", Report 82448-1, Acoustics and Vibration Laboratory, M.I.T., Cambridge, Massachusetts, May 1977.

9. Bathe, K.J., Bolourchi, S., Ramaswamy, S., and Snyder, M.D., "Some Computational Capabilities for Nonlinear Finite Element Analysis", Nuclear Eng. and Design, Vol. 46, pp. 429-455, 1978.

10. Bathe, K.J., Ozdemir, H., and Wilson, E.L., "Static and Dynamic Geometric and Material Nonlinear Analysis", Report No. UCSESM 74-4, Struct. Eng. Laboratory, Univ. of California, Berkeley, Feb. 1974.

11. Bathe, K.J., and Ramaswamy, S., "On Three-Dimensional Nonlinear Analysis of Concrete Structures", Nuclear Eng. and Design, Vol. 52, pp. 385-409, 1979.

12. Bathe, K.J., and Wilson, E.L., Numerical Methods in Finite Element Analysis, Prentice-Hall, INC., Englewood Cliffs, New Jersey, 1976.

13. Bathe, K.J., Wilson, E.L., and Iding, R.H., "NONSAP, A Structural Analysis Program for Static and Dynamic Response of Nonlinear Systems", Report No. UCSESM 74-3, Struc. Eng. Laboratory, Univ. of California, Berkeley, Feb. 1974.

14. Bažant, Z.P., and Bhat, P., "Endochronic Theory of Inelasticity and Failure of Concrete", Proc. ASCE, J. Eng. Mech., April 1976.

15. Bažant, P.Z., and Kim, S.S., "Plastic-Fracturing Theory for Concrete", Proc. ASCE, J. Eng. Mech., June 1979.

16. Bažant, Z.P., and Shieh, C.L., "Endochronic Model for Nonlinear Triaxial Behaviour of Concrete", Nuclear Eng. and Design, Vol. 47, pp. 305-315, 1978.

17. Bellamy, C.J., "Strength Under Combined Stress", ACI Journal, Proc. Vol. 58, No. 4, pp. 367-381, Oct. 1961.

18. Belytschko, T., "A Survey of Numerical Methods and Computer Programs for Dynamic Structural Analysis", Nuclear Eng. and Design, Vol. 37, pp. 23-34, 1976.

19. Bender, M., and Whitman, G.D., "Concrete Containment: A 1970 Assessment", Concrete for Nuclear Reactors, ACI Special Publication SP-34, Vol. 1, 1972.

20. Bergan, P.G., and Holand, I., "Nonlinear Finite Element Analysis of Concrete Structures", Proc. of the Intl. Conf. on Finite Elements in Nonlinear Mechanics, Stuttgart, Germany, Aug. - Sept. 1978.

21. Biggs, J.M., Introduction to Structural Dynamics, McGraw-Hill Book Company, New York, 1964.

22. Bresler, B., and Pister, K.S., "Strength of Concrete Under Combined Stresses", ACI Journal, Proc. Vol. 55, No. 3, pp. 321-345, Sept. 1958.

23. Buyukozturk, O., "Nonlinear Analysis of Reinforced Concrete Structures", Computers and Structures, Vol. 7, pp. 149 - 156, 1977.

24. Buyukozturk, O., and Conner, J.J., "Nonlinear Dynamic Response of Reinforced Concrete Under Impulsive Loading: Research Status and Needs", Nuclear Eng. and Design, Vol. 50, pp. 83-92, 1978.

25. Carbajo, J.J., and Munno, F.J., "TECAR, A New Program For LOCA Analysis", Nuclear Eng. and Design, Vol. 44, pp. 171-176, 1977.

26. Cedolin, L., Crutzen, Y.R.J., and Poli, S.D., "Triaxial Stress-

Strain Relationship for Concrete", Proc. ASCE, J. Eng. Mech., June 1977.

27. Chen, A.C.T., and Chen, W.F., "Constitutive Relations for Concrete", Proc. ASCE, J. Eng. Mech., Aug. 1975.

28. Clough, R.W., and Wilson, E.L., "Stress Analysis of Gravity Dam by the Finite Element Method", Rilem Bulletin No. 19, June 1963

29. Crawford, J., Murtha, R., and Thompson, R., "Soil Structure Calculations Pertinent to Strategic Structures", Proc. of the ADINA Conf., M.I.T., Cambridge, Aug. 1977.

30. Dahl, H.D., "A Finite Element Model for Anisotropic Yielding in Gravity Loaded Rock", Ph.D. Thesis, Penn. State Univ., 1969.

31. Dahl, D., and Voight, B., "Isotropic and Anisotropic Plastic Yield Associated With Cylindrical Underground Openings", Proc. of the Intl. Symp. on Large Permanent Underground Openings, Oslo, Sept. 1969.

32. Darwin, D., and Pecknold, D.A., "Nonlinear Biaxial Stress-Strain Law for Concrete", Proc. ASCE, J. Eng. Mech., April 1977.

33. Desai, C.S., and Abel, J.F., Introduction to the Finite Element Method, A Numerical Method for Engineering Analysis, Van Nostrand Reinhold Company, New York, 1972.

34. Eichholz, G.G., "Power Plant Siting", Nuclear Power Safety, Pergamon Press Inc., New York, pp. 33-55, 1976.

35. El-Tahan, H.W., "Dynamic Analysis of the 'Cut-and-Cover' Type Underground Nuclear Reactor Containment", M. Eng. Thesis, Memorial Univ., St. John's, Newfoundland, Aug. 1977.

36. El-Tahan, H., and Reddy, D.V., "Seismic Response to the 'Cut-and-Cover' Type Reactor Containments Considering Nonlinear Soil Behaviour", 5th Intl. Conf. on Struct. Mech. in Reactor Technology, Berlin, Germany, Aug. 1979.

37. Farhoomand, I., "Nonlinear Dynamic Stress Analysis of Two-Dimensional Solids", Ph.D. Thesis, Univ. of California, Berkeley, 1970.

38. Felippa, C.A., "Refined Finite Element Analysis of Linear and Nonlinear Two-Dimensional Structures", Ph.D. Thesis, University of California, Berkeley, 1966.

39. Franklin, H.A., "Nonlinear Analysis of Reinforced Concrete Frames and Panels", Ph.D. Thesis, Univ. of California, Berkeley, 1970.

40. Hadjian, A.H., "Engineering of Nuclear Power Facilities for Earthquake Loads", Nuclear Eng. and Design, Vol. 48, pp. 21-47, 1978.

41. Hannant, D.J., and Frederick, C.O., "Failure Criteria for Concrete in Compression", Magazine of Concrete Research, Vol. 20, No. 64, pp. 137-144, Sept, 1968.

42. Herrmann, L.R., "Finite Element Analysis of Contact Problems", Proc. ASCE, J. Eng. Mech., Oct. 1978.

43. Hill, R., The Mathematical Theory of Plasticity, Oxford at the Clarendon Press, 1950.

44. Hossain, Q.A., "Nonlinear Finite Element Analysis of Reinforced Concrete Frames", Ph.D. Thesis, Univ. of California, Davis, 1974.

45. Houde, J., "Study of Force-Displacement Relationships for the Finite Element Analysis of Reinforced Concrete", Ph.D. Thesis, McGill Univ., Montreal, 1973.

46. Huebner, K.H., The Finite Element Method for Engineers, John Wiley and Sons, New York, 1975.

47. Isenberg, J., and Adham, S., "Analysis of Orthotropic Reinforced Concrete Structures", Proc. ASCE, J. Struct., Dec. 1970.

48. Khan, M.H., and Saugy, B., "Evaluation of the Influence of Some Concrete Characteristics on Nonlinear Behaviour of a PCRV", Concrete for Nuclear Reactors, ACI Special Publication SP-34, Vol. 1, 1972.

49. Kotsovos, M.D., and Newman, J.B., "Generalized Stress-Strain Relations for Concrete", Proc. ASCE, J. Eng. Mech., Aug. 1978.

50. Kröger, W., Altes, J., and Escherich, K.H., "'Cut-and Cover' Design of a Commercial Nuclear Power Plant", 4th Intl. Conf. on Struct. Mech. in Reactor Technology, San Francisco, California, August 1977.

51. Kröger, W., Altes, J., and Schwarzer, K., "Underground Siting of Nuclear Power Plants with Emphasis on the 'Cut-and-Cover' Technique", Nuclear Eng. and Design, Vol. 38, pp. 207-227, 1976.

52. Kuhlemeyer, R.L., "Vertical Vibration of Footings Embedded in Layered Media", Ph.D. Thesis, Univ. of California, Berkeley, 1969.

53. Kupfer, D., Hilsdorf, H.K., and Rusch, H., "Behaviour of Concrete Under Biaxial Stresses", ACI Journal, Proc. Vol. 66, No. 8, pp. 656-666, Aug. 1969.

54. Launay, P., and Gachon, H., "Strain and Ultimate Strength of Concrete Under Triaxial Stress", Concrete for Nuclear Reactors, ACI Special Publication SP-34, Vol. 1, 1972.

55. Lindbo, T., "The Swedish Underground Containment Studies: State of Art", Nuclear Eng. and Design, Vol. 50, pp. 431-442, 1978.

56. Liu, T.C.Y., Nilson, A.H., and Slate, F.O., "Biaxial Stress-Strain Relations for Concrete", Proc. ASCE, J. Struct., May 1972.

57. Lysmer, T., and Kuhlemeyer, R.L., "Finite Dynamic Model for Infinite Media", ASCE Proc., J. Eng. Mech., Aug. 1969.

58. Lysmer, T., and Waas, G., "Shear Waves in Plane Infinite Structures", Proc. ASCE, J. Eng. Mech., Feb. 1972.

59. Mahrenholtz, O., Reddy, D.V., and Bobby, W., "Limit Analysis of Internally Pressurized 'Cut-and-Cover' Type Underground Reactor Containments", Submitted for publication.

60. Marcal, P.V., "Comparative Study of Numerical Methods of Elastic-Plastic Analysis", AIAA Journal, Vol. 6, No. 1, 1968.

61. Marr, W.A., and Christian, J.T., "Finite Element Analysis of Elasto-Plastic Soils", Soils Publication No. 301, Research Report R72-21, M.I.T., Cambridge, Massachusetts, April 1972.

62. McHenry, D., and Karni, J., "Strength of Combined Tensile and Compressive Stress", ACI Journal, Proc. Vol. 54, No. 10, pp. 829-839, April 1958.

63. Mikkola, M.J., and Schnobrich, W.C., "Material Behaviour Characteristics for Reinforced Concrete Shells Stressed Beyond the Elastic Range", UILU-ENG-70-103, Tech. Report, Univ. of Illinois, Urbana, Aug. 1970.

64. Mirza, M.S., and Mufti, A.A., "Nonlinear Finite Element Analysis of Reinforced Concrete Structures", Proc. of the Intl. Conf. on Finite Element Methods in Eng., Univ. of New South Wales, Australia, Aug. 1974.

65. Mondkar, D.P., and Powell, G.H., "Static and Dynamic Analysis of Nonlinear Structures", Report No. EERC 75-10, Earthquake Eng. Research Center, Univ. of California, Berkeley, March 1975.

66. Mondkar, D.P., and Powell, G.H., "ANSR-I, General Purpose Program for Analysis of Nonlinear Structural Response", Report No. EERC 75-37, Earthquake Eng. Research Center, Univ. of California, Berkeley, Dec. 1975.

67. Moselhi, O.E., "Finite Element Analysis of Dynamic Structure-

Medium Interaction with some Reference to Undergound Nuclear Reactor Containment", M. Eng. Thesis, Memorial Univ., St. John's, Newfoundland, August 1975.

68. Ngo, D., and Scordelis, A.C., "Finite Element Analysis of Reinforced Concrete Beams", ACI Journal, Proc. Vol. 64, No. 3, pp. 152-163, March 1967.

69. Ngo, D., Scordelis, A.C., and Franklin, H.A., "Finite Element Study of Reinforced Concrete Beams With Diagonal Tension Cracks", Report No. UCSESM 70-19, Univ. of California, Berkeley, Dec. 1970.

70. Nilson, A.H., Nonlinear Analysis of Reinforced Concrete by the Finite Element Method", ACI Journal, Proc. Vol. 65, No. 9, pp. 757-766, Sept. 1968.

71. Oden, J.T., "Finite Element Applications in Nonlinear Structural Analysis", Proc. of the Symp. on Application of Finite Element Methods in Civil Eng., Nashville, Tennessee, Nov. 1969.

72. Oden, J.T., Finite Element of Nonlinear Continua, McGraw-Hill Book Company, New York, 1972.

73. Ottosen, N.S., "A Failure Criterion for Concrete", Proc. ASCE, J. Eng. Mech., Aug. 1977.

74. Pariseau, W.G., "Plasticity Theory for Anisotropic Rocks and Soils", Proc. 10th Symp. on Rock Mech., Univ. of Texas, Austin, May 1968.

75. Reddy, D.V., and Kierans, T.W., "Dynamic Analysis for Design Criteria for Underground Nuclear Reactor Containments", Nuclear Eng. and Design, Vol. 38, pp. 177-205, 1976.

76. Reddy, D.V., Bobby, W., and Mahrenholtz, O., "Ultimate Load Behaviour of 'Cut-and-Cover' Underground Nuclear Reactor Containments with Reinforced Earth Backfill", Proc. Intl. Conf. on Soil Reinforcement, Paris, France, March 1979.

77. Reddy, D.V., Moselhi, O.E., and Sheha, S.A.E., "Dynamic Structure-Medium Interaction of Underground Nuclear Reactor Containments", Proc. Sixth World Conf. on Earthquake Eng., New Delhi, India, Jan. 1977.

78. Reyes, S.F., and Deere, D.U., "Elasto-plastic Analysis of Underground Openings by the Finite Element Method", Proc., 1st Intl. Congress on Rock Mech., Lisbon, 1966.

79. Robinson, G.S., "Behaviour of Concrete Under Biaxial Compression", Proc. ASCE, J. Struct., Vol. 93, Feb. 1967.

80. Sarne, Y., "Material Nonlinear Time Dependent Three-Dimensional

Finite Element Analysis for Reinforced and Prestressed Concrete Structures", Ph.D. Thesis, MIT, Cambridge, Massachusetts, Jan. 1975.

81. Schäfer, H., "A Contribution to the Solution of Contact Problems with the Aid of Bond Elements", Computer Methods in Applied Mech. and Eng., Vol. 6, pp. 335-354, 1975.

82. Schnobrich, W.C., "Behaviour of Reinforced Concrete Structures Predicted by the Finite Element Method", Computers and Structures, Vol. 7, pp. 365-376, 1977.

83. Scordelis, A.C., "Finite Element Analysis of Reinforced Concrete Structures", Proc. of the McGill-EIC Specialty Conf. on Finite Element Methods in Civil Eng., McGill Univ., Montreal, 1972.

84. Seed, H.B., and Lysmer, J., "Soil-Structure Interaction Analysis for Seismic Response", Proc. ASCE, J. Geotechnical Eng., May 1975.

85. Sheha, S.A., "Static and Dynamic Analysis of Underground Cavities with some Reference to Nuclear Reactor Containments", M. Eng. Thesis, Memorial Univ., St. John's, Newfoundland, August 1975.

86. Sims, F.W., Rhodes, J.H., and Clough, R.W., "Cracking in Norfolk Dam", ACI Journal, Proc. Vol. 61, No. 3, pp. 265-285, March 1964.

87. Smith, P.D., Cook, W.A., and Anderson, C.A., "Finite Element Analysis of Prestressed Concrete Reactor Vessels", 4th Intl. Conf. on Struct. Mech. in Reactor Technology, San Francisco, California, 1977.

88. Sorensen, S.I., Arnesen, A., and Bergan, P.G., "Nonlinear Finite Element Analysis of Reinforced Concrete Using Endochronic Theory", Proc. Intl. Conf. on Finite Elements in Nonlinear Solid and Struct. Mech., Geilo, Norway, Aug. 1977.

89. Spokowski, R.W., "Finite Element Analysis of Reinforced Concrete Members", M. Eng. Thesis, McGill Univ., Montreal, 1972.

90. Stanton, J.F., "An Investigation of the Dowel Action of the Reinforcement of Nuclear Containment Vessels and their Nonlinear Dynamic Response to Earthquake Loads", M.Sc. Thesis, Cornell Univ., Ithaca, New York, Jan. 1977.

91. Stevenson, J.D., "Overview of Concrete Containment Design Practice in the U.S.A.", Proc. Conf. Experience in the Design, Construction, and Operation of Prestressed Concrete Pressure Vessels and Containments for Nuclear Reactors, Univ. York, England, Sept. 1975.

92. Stevenson, J.D., "Current Development of Nuclear Standards", Civil Eng. and Nuclear Power, ASCE National Convention, Boston, Massachusetts, April 1979.

93. Suidan, M., and Schnobrich, W.C., "Finite Element Analysis of Reinforced Concrete", Proc. ASCE, J. Struct., Oct. 1973.

94. Tan, C.P., "Concrete Containments for Reactors - State of Art", Proc. ASCE, J. Struct., July 1970.

95. United Engineers and Acres American, "Review of Underground Siting of Nuclear Power Plants", UEC-AEC-740/07, Jan. 1974.

96. Valanis, K.C., "A Theory of Viscoplasticity Without a Yield Surface", Archiwum Mechaniki Stosowanej, Vol. 3, pp. 517-551, Warzawa, 1971.

97. Valliappan, S., and Doolan, T., "Nonlinear Stress Analysis of Reinforced Concrete", Proc. ASCE, J. Struct., April 1972.

98. Waas, G., "Linear Two-Dimensional Analysis of Soil Dynamics Problems in Semi-infinite Layered Media", Ph.D. Thesis, Univ. of California, Berkeley, 1973.

99. Watson, M.B., Kammer, W.A., Langley, N.P., Selzer, L.A., and Beck, R.L., "Underground Nuclear Power Plant Siting", Report No. 6, Environmental Quality Laboratory, California Inst. of Tech., Pasadena, Calif., Sept. 1972.

100. Wegner, R., "Finite Element Models for Reinforced Concrete", Proc. U.S.-Germany Symp. on Finite Element Methods, M.I.T., Cambridge, Massachusetts, Aug. 1976.

101. Wilson, E.L., "Finite Element Analysis of Two-Dimensional Structures", Ph.D. Thesis, Univ. of California, Berkeley, 1963.

102. Wilson, E.L., "A Computer Program for the Dynamic Stress Analysis of Underground Structures", Report No. 68-1, Univ. of California, Berkeley, Jan. 1968.

103. Yuzugullu, O., and Schnobrich, W.C., "A Numerical Procedure for the Determination of the Behaviour of a Shear Wall Frame System", ACI Journal, July 1973.

104. Zienkiewicz, O.C., The Finite Element Method, McGraw-Hill Book Company (UK) Limited, London, 1977.

105. Zienkiewicz, O.C., Valliappan, S., and King, I.P., "Elasto-Plastic Solutions of Engineering Problems, 'Initial Stress' Finite Element Approach", Intl. J. Numer. Methods Eng., Vol. 1, pp. 75-100, 1969.